

THE UNIVERSITY OF ALBERTA

NON-NEWTONIAN FLOW DISTRIBUTION IN A POROUS BED

by

SHAPOUR VOSSOUGH

C

A THESIS

SUBMITTED TO THE FACULTY OF GRADUATE STUDIES AND RESEARCH IN
PARTIAL FULFILMENT OF THE REQUIREMENTS FOR THE DEGREE OF
MASTER OF SCIENCE

in

CHEMICAL ENGINEERING

DEPARTMENT OF CHEMICAL ENGINEERING

EDMONTON, ALBERTA

FALL, 1973

To Ziba
whom I love most

ABSTRACT

Fluid flow of both Newtonian and viscoelastic fluid was studied in a model porous medium composed of a matrix of small glass cylinders. Local velocity profiles and flow distribution were determined by a streak photomicrography technique. Measurements were obtained for average interstitial velocities of the bed ranging from $V/\epsilon = 0.0568$ cm/sec to 0.568 cm/sec. The major effect focused on was the variation in flow between pores owing to small inhomogeneities in the bed.

Compared to the Newtonian fluid, the effect of viscoelastic fluid is found to be a suppression of the velocity and also flow distribution variations with pore opening. The effect of elasticity on flow distribution was observed to occur before its influence in pressure drop measurement.

Qualitative visual observations also revealed that the number of dead zones, or nearly dead zones and recirculation regions for viscoelastic fluid were reduced relative to the Newtonian case.

ACKNOWLEDGEMENTS.

In compiling the present thesis the author wishes to acknowledge the aid and assistance given by the following:

Dr. F. A. Seyer, research supervisor, for his generous help and constructive criticism.

The staff of the Workshop and the Instrument Shop for their assistance in building the equipment.

The Petroleum Aid to Education fund which provided partial support for the research.

Dow Chemical Co. who donated the Polymer used in the research, and

Mrs. Beth Scott who typed the manuscript.

TABLE OF CONTENTS

Chapter	Page
I. INTRODUCTION AND BACKGROUND	1
I.1 General.	1
I.2 Mobility Ratio Concept	4
I.3 Polymer Flooding	9
II. THEORY	19
II.1 Introduction	19
II.2 Parallel-Plates Capillary Model-- Pressure Drop.	20
II.3 Power-Law Model.	27
II.4 Modified Friction Factor and Reynolds Number.	28
II.5 Application of Theory.	28
III. EXPERIMENTAL EQUIPMENT AND PROCEDURE.	30
III.1 Multi-Cylinder Matrix.	30
III.2 Experimental Fluids.	35
III.3 Pumping.	36
III.4 Streak Photography Technique	37
III.4-1 Optical System.	37
a. Light Source	37
b. Chopper Disk	39
c. Photomicrography Assembly.	40
III.4-2 Measurement of the Streak Length	40

Chapter	Page
III.5 Pressure Drop Measurement	44
IV. RESULTS	45
IV.1 Pressure Drop	45
IV.2 Streamlines	49
IV.3 Local Velocity Profiles	49
V. DISCUSSION OF THE RESULTS	65
V.1 Pressure Drop	65
V.2 Streamlines	72
V.3 Visual Observation	75
V.4 Local Velocity Profiles and Flow Distribution	76
IV. CONCLUSION AND RECOMMENDATIONS	100
VI.1 Conclusions	100
VI.2 Recommendations	101
BIBLIOGRAPHY	102
APPENDIX A RHEOLOGICAL PROPERTIES OF THE SOLUTIONS	107
I. Rheogoniometer Parameters	108
II. Evaporation Correction	111
APPENDIX B PRESSURE DROP AND RELATED CORRELATIONS	123
APPENDIX C CONSTRUCTION OF VELOCITY PROFILE FROM STREAK LENGTH	139
APPENDIX D FLOW THROUGH PARALLEL PLATES-- POWER LAW MODEL	144

Chapter

Page

APPENDIX E EXPERIMENTAL DATA POINTS 147

LIST OF TABLES

Table		Page
V-1	FLOW PARAMETERS OF 0.2% SEPARAN SOLUTION	70
V-2	MAXIMUM VELOCITIES AT CENTER LINE OPENING	82
V-3	CORRECTED FRACTIONAL FLOW RATES.	91
A-1	CALIBRATION OF NORMAL FORCE TRANSDUCER	116
A-2	VISCOMETRIC MEASUREMENTS FOR STANDARD OIL, GLYCEROL, AND POLYMER SOLUTION.	116
B-1	FLOW BEHAVIOR PARAMETERS OF 96% GLYCEROL SOLUTION.	131
B-2	FLOW BEHAVIOR PARAMETERS OF 0.2% SEPARAN	135
B-3	PREDICTED PRESSURE DROPS BY BERGELIN'S CORRELATION-- 0.2% SEPARAN.	137
C-1	OPENINGS, d , AREA UNDER THE DIMENSIONLESS VELOCITY PROFILES A_v , AND FRACTIONAL FLOW RATES, q_v	142
E-1	STREAK LENGTH DATA OF GLYCEROL	149
E-2	STREAK LENGTH DATA OF SEPARAN.	167

LIST OF FIGURES

Figure		Page
II-1	PARALLEL-PLATE CAPILLARY MODEL	21
II-2	RECTILINEAR FLOW THROUGH PARALLEL PLATES	22
III-1	TRIANGULAR-PITCH ISOCELL	31
III-2	MULTI-CYLINDER MATRIX	31
III-3	TOP VIEW OF GLASS RODS	34
III-4	SCHEMATIC PLAN VIEW OF OPTICAL SYSTEM	38
III-5	PHOTOMICROGRAPHY ASSEMBLY	41
IV-1	PRESSURE DROP V.S. FLOW RATE-- GLYCEROL	46
IV-2	PRESSURE DROP V.S. FLOW RATE-- SEPARAN	47
IV-3	FRICTION FACTOR V.S. REYNOLDS NUMBER	48
IV-4	PHOTOGRAPH NO. 1: FLOW PAST SINGLE CYLINDER	50
IV-5	PHOTOGRAPHS NO.'S 2, 3, 4: NEWTONIAN FLOW PAST MULTI CYLINDERS.	51
IV-6	PHOTOGRAPHS NO.'S 5, 6, 7: VISCO- ELASTIC FLOW PAST MULTI CYLINDERS.	52
IV-7	LOCAL VELOCITY PROFILES OF POSITION NO. 2--GLYCEROL.	55
IV-8	LOCAL VELOCITY PROFILES OF POSITION NO. 2--SEPARAN	56
IV-9	LOCAL VELOCITY PROFILES OF POSITION NO. 17--GLYCEROL	57

IV-10	LOCAL VELOCITY PROFILES OF POSITION NO. 17--SEPARAN	58
IV-11	LOCAL VELOCITY PROFILES OF POSITION NO. 27--GLYCEROL	59
IV-12	LOCAL VELOCITY PROFILES OF POSITION, NO. 27--SEPARAN	60
IV-13	CENTERLINE VELOCITY PROFILE	64
V-1	ESTIMATION OF ELONGATIONAL RATE	69
V-2	DEPENDENCE OF ELASTICITY EFFECT UPON THE DEBORAH NUMBER OF THE FLOW PROCESS.	73
V-3	VISUAL OBSERVATION--GLYCEROL.	78
V-4	VISUAL OBSERVATION--SEPARAN	80
V-5	MAXIMUM CENTER LINE VELOCITIES-- ROW NO. 20.	84
V-6	MAXIMUM CENTER LINE VELOCITIES-- ROW NO. 21.	85
V-7	MAXIMUM CENTER LINE VELOCITIES-- ROW NO. 22.	86
V-8	RESULTANT OF MAXIMUM CENTER LINE VELOCITIES OF THREE ROWS-- GLYCEROL.	88
V-9	RESULTANT OF MAXIMUM CENTER LINE VELOCITIES OF THREE ROWS-- SEPARAN	89
V-10	FLOW DISTRIBUTION WITH OPENING-- GLYCEROL.	94
V-11	FLOW DISTRIBUTION WITH OPENING-- SEPARAN	95
V-12	FLOW DISTRIBUTION WITH OPENING-- GLYCEROL.	96
V-13	FLOW DISTRIBUTION WITH OPENING-- SEPARAN	97

Figure

Page

A-1	NORMAL FORCE TRANSDUCER CALIBRATION	112
A-2	VISCOMETRIC BEHAVIOR OF NEWTONIAN FLUIDS.	113
A-3	VISCOMETRIC BEHAVIOR OF SEPARAN AP-273, 0.2% (BY WEIGHT).	114
A-4	RELAXATION TIME OF SEPARAN AP-273, 0.2% (BY WEIGHT)	115
E-1	DIRECTION OF X AND THE ORIGIN WITH RESPECT TO THE LIGHT AND FLOW DIRECTION.	148

NOMENCLATURE

A	Cross-sectional area of the bed, cm^2
A_i	Area under the dimensionless velocity profile, cm.
A_V	Area under the velocity profiles, cm^2/sec .
b_1	Constant, cm.
C	Solute concentration, gr/cm^3
$C_1 - C_6$	Constants
C_D	Dispersion coefficient, cm^2/sec .
d	Minimum opening between two adjacent cylinders of the same row, cm.
d_M	Minimum opening between two adjacent cylinders of the same row, in.
d_C	Diameter of the constriction, cm.
d_{Pl}	Diameter of the platen, cm.
D	Diameter of the cylinders, cm.
D_p	Diameter of the particles, cm.
f	Corrected fractional flow rate, dimensionless.
f_B	Friction factor defined by Eq. (B-6), dimensionless.
f_K	Friction factor defined by Eq. (II-38), dimensionless.
F	Normal force, dyne
F()	Function of.

g	Acceleration of gravity, cm/sec^2 .
H	Viscosity parameter defined by Equation (I-5), $\text{gr cm}^{-n} \text{sec}^{n-2}$.
K	Effective permeability, cm^2
K_1	Constant, defined by Equation B-3, dimensionless.
K_t	Torsion bar constant, dyne/micron
ℓ	Exposed length of the cylinders, cm.
L	Length of the bed, cm
L'	Tortuous length of particle path, cm.
m	Mobility ratio, dimensionless
m_1	Power-law parameter, $\text{gr cm}^{-1} \text{sec}^{n-2}$.
n	Power-law parameter, dimensionless.
N	Number of major restrictions encountered in flow through the bank.
N_{Deb}	Deborah number defined by Equation (I-12), dimensionless.
N_m	Number of the minimum openings in one row.
N_{Re}	Reynolds number defined by Equation (II-40), dimensionless.
N_T	Total number of cylinders, dimensionless.
N_{We}	Weissenberg number defined by Equation (I-11), dimensionless.
P	Pressure, dyne/cm^2
P_t	Pitch ratio, dimensionless.
$P_{11} - P_{22}$	Primary normal stress difference, dyne/cm^2

q	Total volumetric flow rate, cm^3/sec .
q_i	volumetric flow rate passing through each opening, cm^3/sec .
R	One half the gap between two parallel plates, cm.
Re_C	Reynolds number defined by Equation (V-9), dimensionless.
Re_T	Reynolds number defined by Equation (B-4), dimensionless.
R_g	Gas constant, $\text{gr cm}^2/\text{sec}^2 \text{ g-mole } ^\circ\text{K}$
R_H	Hydraulic radius, cm.
R_{pl}	Radius of the platen, cm.
RPM	Revolutions per minute.
s	length of the streaks, cm.
S	Length of the streaks, in.
S_1	Sensitivity of the torque transducer, micron/volt.
S_2	Sensitivity of the normal force transducer, gr/volt.
S_B	Minimum free flow area, cm^2 .
S_L	Longitudinal pitch, cm.
S_s	Specific surface, cm^{-1} .
S_T	Transverse pitch, cm.
S_v	Wetted surface per volume of bed, cm^{-1} .
t	Duration of one revolution, second/rev
Δt	Movement of torsion head transducer, volt.

T	Absolute temperature, °K
t_p	Time of period of opening or closing the light, sec.
T_r	Torque, dyne cm.
u	Interstitial velocity, cm/sec.
U	Approach velocity, cm/sec.
u_m	Average interstitial velocity from center line openings, cm/sec.
\bar{u}_{max}	Average value of the maximum velocities at center line openings of two consecutive rows, cm/sec.
u_z	velocity in the z-direction, cm/sec.
V	Superficial velocity, cm/sec.
\bar{V}	Average velocity of the flow through parallel plates, cm/sec.
V_C	Volume occupied by cylinders, cm ³ .
v_t	Output of transducer, volt.
V_T	Total volume, cm ³ .
V_v	Void volume, cm ³ .
V_w	Volume of the water, cm ³ .
W_B	Mass flow rate, gr/sec.
x	x-coordinate, cm.
X	X-coordinate, in.
y	y-coordinate, cm.
z	z-coordinate, cm.

Greek Symbols

α	Angle of cone, degrees
β	Angular rotation of the platen, rad./sec.
Δ	Delta operator.
ϵ	Volumetric porosity, dimensionless.
ϵ_s	Surface porosity, dimensionless.
$\bar{\gamma}$	Average nominal shear rate, sec^{-1} .
λ	Mobility, $\text{cm}^3 \text{sec/gr}$
μ	Viscosity, poise.
μ_0	Limiting viscosity at low shear rate, poise.
μ_s	Viscosity of the solvent, poise.
ρ	Density, gr/cm^3 .
τ	Shear stress, dyne/cm^2
τ_0	Limit of the relaxation time at low shear rate, sec.
τ_f	Relaxation time of fluid, sec.
τ_{pr}	Duration of a process, sec.
$\dot{\gamma}$	Shear rate, sec^{-1} .

Subscripts

B	indicate an ideal bundle of tubes.
e	elastic
G	Glycerol
o	oil
S	Separan
w	water
w	wall
c	modified for the porous bed.

CHAPTER I

INTRODUCTION AND BACKGROUND

I.1 General

Increasing demands for petroleum supply and the limited number of the oil reservoirs make it inevitable not only to use the produced oil efficiently but also to increase the ultimate recovery of reservoirs. Investigation of the many fields revealed (1) that more than 50 per cent and in the case of heavy oil reservoir, even 80 per cent of the original oil in the reservoir remained unrecovered after primary recovery; i.e., when the production rate became so low as to make economical operation impracticable.

Oil production requires energy to expell the oil trapped in the interstices of the porous rock into the production well. This energy may be available in the reservoir initially in different forms. The major forms of natural energy in the oil reservoirs are:

1. Compression energy of the oil or water within the field or contiguous to the oil-bearing rock.
2. Compression energy of the gas dissolved in the oil or free-gas zones overlying the oil layer.
3. Gravitational energy due to the difference in hydrostatic level of producing well and upper part of the

reservoir.

If no natural energy is available in the reservoir or if the existing energy is not sufficient, the external energy should be applied to exceed the economical rate of production. Even in the case of high pressure reservoirs, the initial content of energy would be depleted after a long period of production and, therefore, external energy would be required.

Fluid injection as an external energy supply to the reservoir may be applied for two different purposes; (a) during the period of the operation of the well to compensate for the pressure decline created due to the oil withdrawals from the space voidage. The fluid injection will help to keep the rate of production almost constant and above the limit of economical rate, (b) after the production well reaches a state of substantially complete depletion of its initial content of energy. In reservoir engineering terminology the former is called "Pressure Maintenance" or "Pressure Regulation" and the latter "Secondary Recovery." In secondary recovery operations the pressure required for the fluid injection is often lower than that which would be required for injection under primary pressure maintenance.

Fluid injection as a method of oil recovery is indeed more than one century old. The first accidental or perhaps intentional water flooding occurred in 1865 in the Pithole City of Pennsylvania (2) Since then a great variety

of fluids such as gas, liquids, even slurries, and also different additives to the fluids to achieve better performance have been tried.

Of the different methods of the secondary oil recovery, water flooding is the most advanced method. Gas-injection operations, usually termed "gas repressuring," are less common than water flooding. Secondary recovery by water flooding has been carried on, as a common practice, in regular patterns. Historically, the first type of regular network was the alternating-line-drive pattern(3). Next followed the five-spot pattern which is most commonly employed. The mechanisms of the fluid displacement for various patterns of injection and production wells have been extensively investigated (4-12). The injected water pushes the oil in a somehow piston-like behavior from the vicinity of the injection wells and ahead of the advancing water, a zone of high oil saturation is formed which moves toward the producing well. The clean oil is produced until the oil-water bank reaches the producing well at which point breakthrough occurs. After breakthrough, increasing amounts of water are produced with the oil.

Development of the oil bank and its stability governs the success of the operation. In some projects the high oil saturation zone does not develop at all and breakthrough takes place from the start. The rate of the production of water may reach a limit such that the production

of oil becomes too low to support continued operation.

It is intuitively understood that if the conditions at the start of the flood are such that the water can move more readily than oil, the displacement front will spread into the oil and early breakthrough occurs. Water intrusion into the frontal oil bank is termed "fingering."

I. 2 Mobility Ratio Concept

Whether or not a stable oil bank develops depends largely on the relative permeability characteristics of the formation, on the viscosity of the displacing and displaced fluids, on the saturations of water and oil at the time the water injection is started and also on the inhomogeneities of the rock itself. The first two conditions can be regrouped in mobility ratio (13) which is defined as the ratio between the mobilities of the displacing and displaced fluids, where

$$m = \frac{\lambda_w}{\lambda_o}, \quad (I-1)$$

m represents mobility ratio and λ_w and λ_o are mobilities of water and oil respectively.

Definition of the mobility is better understood by studying Darcy's law. The theory of flow through porous media originated by Darcy's experiment in 1856 (14a). Darcy found that the flow rate is proportional to the pressure drop along the bed, or in terms of superficial velocity,

$$V = \lambda \frac{\Delta P}{L} \quad (I-2)$$

where V is superficial velocity, ΔP , pressure drop, L , length of the porous medium and λ , constant which by definition is the mobility of the fluid. Later, in 1930, Nutting elucidated (14a) the physical significance of λ and stated that,

$$\lambda = \frac{K}{\mu} \quad (I-3)$$

where μ is the viscosity of the fluid and K the specific permeability of the porous medium. Substituting (I-3) into (I-2), one obtains,

$$V = \frac{K}{\mu} \frac{\Delta P}{L} \quad (I-4)$$

Equation (I-4) is known as Darcy's law which holds for the laminar flow of Newtonian fluids through homogeneous porous media.

Darcy's law was modified by Christopher, et al. (15) for the flow of power-law model fluids through porous media. Using a modified Blake-Kozeny equation, they obtained,

$$V = \left(\frac{K}{H} \frac{\Delta P}{L} \right)^{1/n} \quad (I-5)$$

where n is power-law parameter and H , viscosity level parameter, a factor which accounts for the additional dependence of V on K and porosity due to non-Newtonian behavior.

The first theoretical attempt to show the role of the mobility ratio in fluid displacement was carried on by Leverett, who published his fractional flow formula in 1940. On neglecting capillary pressure gradient and gravity effects

his equation takes on the following simple form (16a)

$$f_w = \frac{1}{1 + \frac{K_o \mu_w}{K_w \mu_o}} \quad (I-6)$$

or, using the mobilities of two fluids,

$$f_w = \frac{1}{1 + \frac{\lambda_o}{\lambda_w}} \quad (I-7)$$

where,

$$f_w = \frac{q_w}{q_w + q_o} \quad (I-8)$$

q_w and q_o are volumetric flow rates of water and oil respectively. In an attempt to calculate the oil recovery, Welge (17), Aronofsky (4,5) and other investigators (8,12,18) also recognized that through decreased mobility ratio an improvement in displacement efficiency could be obtained. Mungan (19) amongst others showed qualitatively the conditions of stability at a displacement front in a simplified model. He considered the incompressible horizontal linear displacement of oil by water in a piston-like manner and neglected capillary effects. In a system of length L the displacement front is at position x where $x < L$. Writing Darcy's law for the positions filled with water and oil,

$$\frac{q}{A} = -\lambda_w \frac{P_i - P_x}{x} \quad (I-8)$$

$$\frac{q}{A} = -\lambda_o \frac{P_x - P_L}{L - x} \quad (I-9)$$

where q is volumetric flow rate, A , cross-sectional area, $\frac{q}{A}$, velocity of the displacement front, P_i , P_x , P_L pressure at inlet, displacement front and outlet respectively. Eliminating P_x between Equations (I-8, 9),

$$\frac{q}{A} = (P_i - P_L) \frac{\lambda_o}{\lambda_w} \frac{1}{L\lambda_w + x(\lambda_o - \lambda_w)} \quad (I-10)$$

The Equation (I-10) shows, qualitatively, the role of the mobility ratio in stability of oil sweeping. When $\lambda_o/\lambda_w > 1$, i.e. $\lambda_o > \lambda_w$, for any increment increase of x , say dx , which physically is indicated by forming a tiny finger or kink of water into the oil-filled segment the velocity of displacement front, i.e. q/A , will decrease. Therefore, the finger or kink of water can not proceed into the oil-filled segment. That is the tendency for early breakthrough will be suppressed. For the case when $\lambda_o/\lambda_w < 1$, i.e. $\lambda_o < \lambda_w$, any incremental increase of x will increase the velocity of the displacement front which leads eventually to complete breakthrough.

Slobod, et al (10, 11) studied fingering in miscible-phase displacement by an X-ray shadowgraph technique. Their photographs showed that at high flow rate (i.e. 29 ft/day) a large number of very thin fingers was developed; whereas, the slow flowrate (i.e. 1.6 ft/day) showed a gradual blending of fluids with no fingering. Both had an unfavorable mobility ratio of 3. Photographs taken for mobility ratio of unity

r vealed no fingering. One interesting effect was the complete elimination of fingering when they used a continuous gradation in viscosity of flooding fluid. It is worthwhile to note that the overall viscosity ratio had the unfavorable value of $\mu_o/\mu_w = 3$. This can well be in support of Mungan's modification in polymer slug process (20).

Since the mobility of the oil is a fixed parameter--depending on the kind of reservoir and oil--the only possibility to maintain stability in water flooding is to reduce the water mobility.

An improved mobility ratio would also increase recovery efficiency by correcting permeability distribution problems as discussed by Stiles (21), Dyskstra, et al. (22), and Pye (23).

Mobility reduction may be achieved by one or a combination of the following two ways:

1. Permeability reduction of the porous media.
2. Increasing the viscosity of the injected water.

Materials such as Glycerol, sugar, starch, etc. have been used to increase the water viscosity. However, due to the large amount of the materials to be used, the method is not economically feasible. The concept of using natural high molecular weight polymers to increase the water viscosity is not new. The first patent appeared in 1944 by Detting (Shell Development Co.). The reader is referred to 27 different patents mentioned in reference (1). These patents were

granted during 1944 to 1961.

I. 3 Polymer Flooding

The use of synthetic polymers in the injected water of the water flood, as compared to the former mentioned additives, is a fairly new technique. Polyacrylamide was first introduced in 1964 by Pye (23) and Sandiford (1). Their experiments showed that the presence of this kind of polymer in dilute concentrations decreases the water mobility 5 to 20 times more than would be expected from measurement of the solution viscosity. Since then it has become of increasing interest to study and investigate the flow behavior and mechanism of polymer flooding and recovery (20, 24-28). In addition to the laboratory experiments, the polymer water flood has also been successful in the majority of the small or even large scale field projects where it has been employed (29-33).

In polymer water flooding a water-soluble high molecular weight polymer which is partially hydrolyzed is desirable. The polymer solutions, at the concentrations generally used in polymer floods, are non-Newtonian and show pseudoplastic behavior in viscosity measurement and elastic effects in normal force measurement. The pseudoplasticity is suppressed greatly in the presence of the strong electrolytes (20, 24, 34).

The main preference of the polymer water flooding over the conventional method is that a greater fraction of

the reservoir volume may be swept at water breakthrough. In other words, the sweep efficiency increases by introducing a small amount of polymer into the injected water. In addition to the increased macroscopic sweep efficiency, improved microscopic displacement at a given amount of fluid injected has also been observed (1), i.e. the residual oil saturation would be less in swept areas compared with that of conventional flooding. The surprising ability of the polymer to lower the mobility of flooding water may be attributed to the adsorption of the polymer molecules on the pore surface, to the plugging of the very fine pores by polymers, to the viscoelastic effect of the polymer solution, or to a combination of all of these.

Lee, et al. (27) studied the behavior of the polymer solution in oil recovery by looking at pseudoplasticity effect. They concluded that provided the polymer concentration in the flood water is such that the average mobility ratio is favorable or unfavorable, the oil-water contact may exhibit a stable or unstable situation during the course of the flood. Their visual study on a Hele-Shaw model verified their qualitative prediction of the fingering based on pseudoplasticity effect. However, there is considerable evidence to doubt that the power-law model is sufficient to predict the flow behavior of polymer solution in real porous media under all conditions of interest.

Burcik (35-38) attributed the mobility control of

the polymer solution not only to the viscosity improvement but also to the reduction of the effective permeability due to adsorption of polymer molecules on the surface of pores. He observed dilatant behavior of polymer solution flow through a disc of Berea Sandstone which, presumably, was a result of the bound polymer molecules within the pore structure reducing the effective permeability. To distinguish this behavior from true dilatancy, the author suggested that the phenomenon observed be designated as pseudo-dilatancy. Plugging effects, as well as adsorption have also been noticed by other investigators (20, 24, 28, 29, 31). In another paper, Burcik and Walrond (39) proposed that small particles of microgel might be primarily responsible for the permeability reduction; however, Lynch and MacWilliams (40) in response to Burcik's claim showed that gel particles need not be present to have polymer units of the order of one micron and single polymer molecules of that size can be reasonably expected in the ranges of 3 million molecular weight. Patton, et al. (41) revealed that the polymers with less adsorption affinity on the pore surface are more effective at the flood front and also on the oil recovery. They found that the quantity of adsorption varied widely from one polymer to another. For one specific kind of polymer the adsorption varied from one type of mineral surface to another and increased with salt concentration (28). Reduction in relative permeability observed by Patton, et al. (41) was attributed largely to the tight connate water-saturated

pores. These colloidal particles could physically block the smaller capillaries and inhibit the displacement of the connate water.

The relative permeability becomes insensitive to the concentration of the polymer solution above a minimum value of concentration. The dependency of the relative permeability on the polymer concentration has been discussed by Jennings, et al. (34).

At this stage it is felt fruitful to define two factors namely "Resistance Factor" and "Residual Resistance Factor." Both are descriptive of polymer behavior but in different situations. Resistance factor, as defined by Pye (23), is the ratio of the brine mobility to the polymer solution mobility. Resistance factor is indeed a measure of adsorption together with entrapment of the large molecules in the small size pores and also elasticity which mostly has been ignored. Jennings, et al. (34) showed that resistance factor decreases as K/ϵ increases; where K is permeability and ϵ , the porosity of bed. Residual Resistance Factor called "Permeability Reduction" by Smith (28) is defined as the ratio of the brine mobility in a rock, not previously contacted by polymer, to the brine mobility in the same rock after being swept by polymer solution. Smith (28) pointed out that permeability reduction is due to the immobile polymer retained within the porous medium. It is greater in less permeable rocks and increases with the

polymer molecular weight and also with the flow rate.

According to Jewett, et al. (32), the oil recovery increases with both factors which is inconsistent with Patton, et al. (41).

In flows which are non-steady from a Lagrangian point of view, the flow behavior of polymer solutions is often surprisingly different from that of Newtonian fluids and is very dependent upon exact details of velocity field; e.g. flow around submerged objects or flow in converging-diverging channels. Ultman, et al. (42), studied the flow of polymer solution around a submerged single cylinder and sphere using Polyacrylamide and high molecular weight Cellulose Gum as polymers. They introduced Weissenberg number and studied the effect of the magnitude of the Weissenberg number on the effect of viscoelasticity. Weissenberg number was defined (42) as,

$$N_{we} = \frac{\theta_0 U}{D}, \quad (I-11)$$

where θ_0 is the limit of relaxation time at low shear rate, U , the approach velocity, and D , diameter of the cylinder or sphere. They noticed a significant difference in the shape of the streamlines. For instance the streamlines of the flow of viscoelastic fluid across a submerged cylinder responded to the presence of the cylinder earlier than those of the Newtonian fluids and returned to the undisturbed motion sooner. The position of the separation point at the aft portion of the cylinder was noticed to be dependent upon

the magnitude of the Weissenberg number.

The effects of elasticity of polymer solutions in porous media have been completely or partially ignored in a great number of papers published in this field. Some authors such as Jennings, et al. (34), Smith (38), and Harvey (43) believed that the effect of elasticity of the low polymer concentrations of polymer solutions in porous media is insignificant. Sadowski and Bird (44), to justify their capillary-hydraulic radius model based on three-parameter Ellis model which suffered from lack of the time-dependent elastic phenomena, reasoned that no significant elastic effect would be observed provided the fluid relaxation time is small with respect to the transit time.

By the same reasoning one can conclude that the effect of elasticity could be significant if the geometry of the media is such that the transit time of the fluid flow through a contraction or expansion in a tortuous channel is comparable with the relaxation time of the fluid. This expectation has been theoretically shown and experimentally verified by Marshall and Metzner (45). They gave a correlation of the effect with Deborah number for Polyisobutylene and partially hydrolyzed Polyacrylamide solutions. Deborah number was defined as,

$$N_{\text{Deb}} = \frac{\theta_f}{\theta_{\text{Pr}}}, \quad (\text{I-12})$$

where θ_f is the relaxation time of the fluid, and θ_{Pr} , the

duration of a process which represents either the duration of a given deformation state or, equivalently, the reciprocal of the rate at which the deformation process changes (46, 47). In their analysis, Marshall and Metzner (45) used the convected Maxwell model to approximate the behavior of the viscoelastic fluid and thus could estimate the fluid relaxation time from steady shear flow measurements of the normal stresses. By assuming the porous media to be a series of converging sections in the flow direction Z, they showed that the appropriate measure of the process time in a packed bed of spheres is the reciprocal of the deformation or stretch rate in the flow direction, i.e. $(\frac{\partial u}{\partial z})^{-1}$ which in turn is approximately D_p/u_m where u_m is average interstitial velocity and D_p the particle diameter. With this choice of θ_{pr} , Equation (I-12) becomes,

$$N_{Deb} = \theta_f \frac{\partial u}{\partial z} \approx \theta_f \frac{u_m}{D_p} \tag{I-13}$$

The quantity u_m/D_p may also be viewed as a measure of the deformation rate or so called elongation rate in the flow direction. In pure steady elongation flows, the Maxwell model they used predicts infinite stresses must occur when the N_{Deb} , defined by (I-13), approaches 1/4. Intuitively then, they suggested that the pressure drop required to pump a viscoelastic fluid through porous medium would rise to infinity as N_{Deb} defined by (I-13) approaches a value of 1/4. The experimental pressure drop measurements presented by Marshall and Metzner indicated that appreciable influences

of the fluid elasticity were felt when N_{Deb} , as defined by Equation (I-13), was approximately 0.05-0.06 and at the very low values of the Deborah number the effect of elasticity were negligible. It is worthwhile to mention that some investigators (15, 48) have failed to see the viscoelastic deviation in friction factor--Reynolds number plot even at higher values of Deborah number than that from Marshal and Metzner (45) or Sadowski (44).

Elasticity has no effect on flow behavior in Lagrangian steady flows. Therefore, the increase in pressure drop due to elasticity can only be observed in an elongational flow experiment; i.e. a converging-diverging strata which is very much likely to appear in porous media. The failure of the capillary tube model of porous media to predict this phenomenon is, therefore, evident.

Pye (23) seems to be the first one who observed the increase in resistance factor with advance rate which appeared to be noticeable only in tortuous passages not straight capillaries. Similar observations and statements have been brought up by Gogarty (24), Dauben and Menzie (25), Smith (28), Jennings, et al. (34) and Harrington, et al. (49). It is interesting to mention that Jones and Maddock (50) observed this behavior of viscoelastic fluid in porous media, but they considered it disadvantageous rather than advantageous for oil displacement.

The effect of elasticity of the viscoelastic fluids, contrary to what Jennings, et al. (34) stated, need not,

necessarily, be expected to happen only at high flow rates. Jennings, et al. (34) tried to include the relaxation time into the flow resistance correlation. They considered the total pressure drop, P , across a system to be the sum of the viscous, kinetic energy, and an elastic term, ΔP_e , i.e.,

$$\Delta P = C_1 \mu L u_m + C_2 \rho u_m^2 + \Delta P_e, \quad (I-14)$$

where C_1 and C_2 are constants and ρ , density. They made a further assumption that the elastic pressure drop be proportional to the normal stress difference. The final correlation appeared to be,

$$\frac{\Delta P}{u_m} = C_1 \mu L + C_2 \rho u_m + C_3 \mu \theta_f \frac{u_m}{d_c^2}, \quad (I-15)$$

where, C_3 is constant and d_c , the diameter of the constriction. They plotted $\frac{\Delta P}{u_m}$ v.s. u_m for two different molecular weight polymer solutions passing through a core specimen of rock and noticed a significant difference in the slope which was presumed to be due to the sensitivity of θ_f --not viscosity--with molecular weight, and quantitative justification was avoided.

To conclude, this entire section can be summarized as follows. Addition of polymers to water has been shown to be effective in enhancing behavior of water floods in porous media. The mechanism and therefore controlling factors, however, are poorly understood. In a number of experiments increases in pressure drop, much above what would be expected

from a consideration of viscosity, have been observed. This effect has been variously attributed to pore blockage, adsorption and viscoelasticity. In the case of viscoelasticity, theoretical considerations, although only semi quantitative, suggest significant changes can occur in flow distribution and in pressure drop. It is significant that the predictions and resultant dimensionless groups are very dependent on the velocity field of the fluid. As pointed out, in steady flow in a capillary tube, elasticity has nothing to do with either pressure drop or velocity distribution.

Since experimental data and an analysis are available for flow around a single cylinder, it was decided appropriate to study the flow of a viscoelastic fluid in a porous bed composed of closely spaced cylinders. The scale of the experiments is such that any effects of blockage, etc. can be safely ignored and attention can be focused on any changes in flow field that might occur as a result of continuum properties of the polymer.

CHAPTER II

THEORY

II. 1 Introduction

Solving the equations of change to predict the velocity field and pressure drop with the exact boundary conditions of the present model would be extremely tedious--if at all possible. However, as a first approximation, for slow flow the opening between two parallel cylinders--especially when the gap between is small compared to the diameter--can be simulated by two parallel plates with an unknown equivalent length. The unknown equivalent length for the entire bed can be obtained experimentally by experiments with a Newtonian fluid. The procedure would be the same as for the capillary tube model commonly used in porous media.

The capillary tube model, in spite of its lack of ability to portray time-dependency, has been successfully applied in porous media to predict the pressure drop or friction factor--Reynolds number relation of purely viscous flow (15, 51). The model is based on cylindrical Poiseuille flow using hydraulic radius of the medium instead of radius of the cylinder. Then, a correction factor, due to the tortuosity of the bed is considered. A similar approach but with parallel-plates approximating the capillary pores will be followed for the present bed. It is worthwhile to

mention that the pores of the present bed are actually rectangular channels with dimensions d and ℓ , where d is the opening between two rods and ℓ , the exposed length of rods. However, since $\ell \gg d$ the channel can be fairly taken as a two infinite parallel plates.

To achieve a more comprehensive feeling concerning the above approach, consider the plane perpendicular to the paper along the line A-A in Figure (II-1). The space between the glass rods along the line A-A are simulated as parallel plates and at the rear side of the rods, say along the line B-B, the plates are discontinued. Since the gaps are very small most of the pressure drop will result from the flow between adjacent cylinders in a given row rather than flow from one row to the next.

The shape of the interstitial velocity profiles of the assumed model is the same as that of flow through parallel plates. The equations of the velocity profiles for the flow of Newtonian and power-law model fluids through parallel plates, which can be found elsewhere (52a, 53) and are presented in Appendix D, will not be discussed in this chapter.

II. 2 Parallel-Plates Capillary Model--Pressure Drop

Consider the flow of a fluid through two parallel plates in the z -direction as shown in Figure (II-2). One can write,

$$q_1 = 2 \int_0^{\ell} \int_0^R u_z dy dx, \quad (\text{II-1})$$

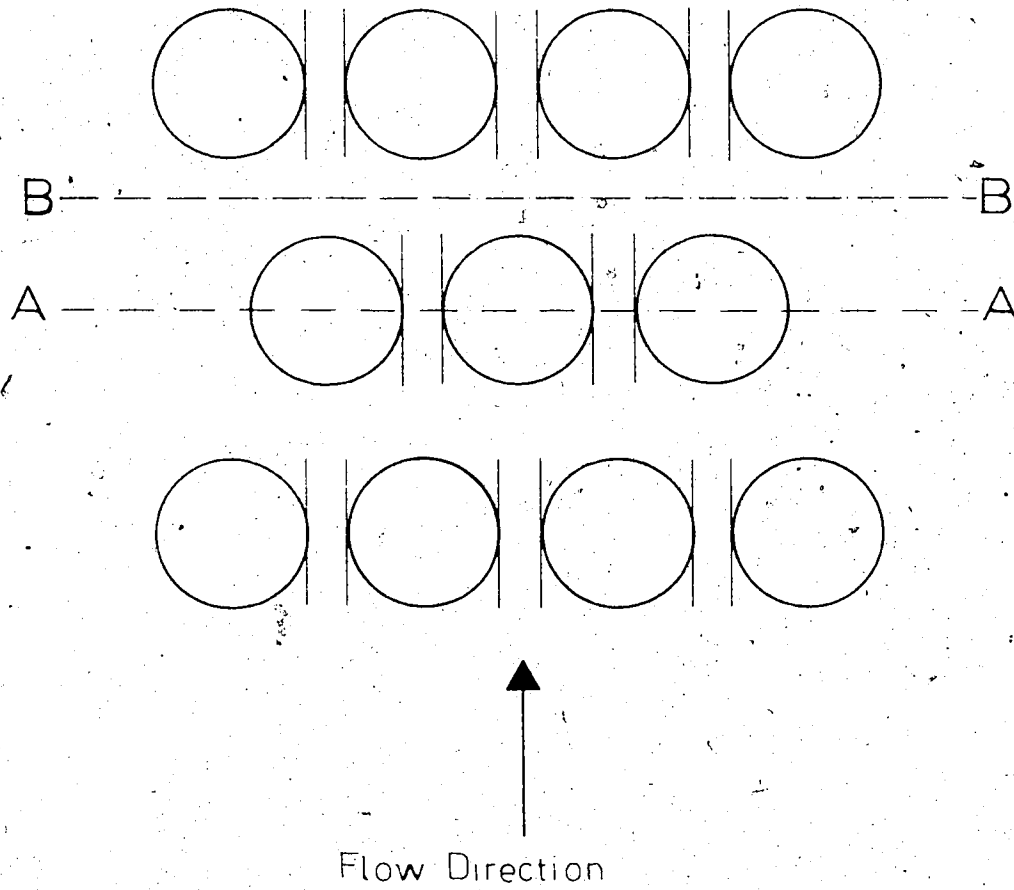


FIGURE II-1 PARALLEL-PLATE
CAPILLARY MODEL

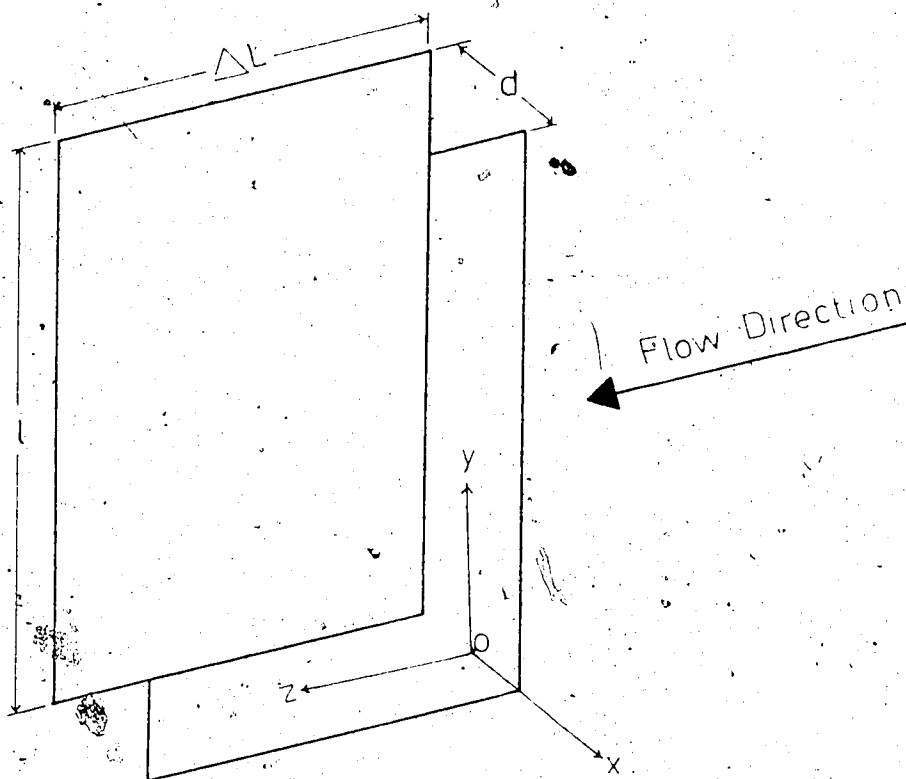


FIGURE II-2 RECTILINEAR FLOW THROUGH
PARALLEL PLATES

where, q_i is volumetric flow rate, u_z , velocity in the z-direction, l , the length of the channel in transverse direction and R , half the gap between the plates, i.e.,

$$R = d/2. \quad (\text{II-2})$$

Since flow is assumed rectilinear, u_z is a function of x only, i.e.,

$$\frac{q_i}{2l} = \int_0^R u_z dx. \quad (\text{II-3})$$

Integrating Equation (II-3) by parts,

$$\int_0^R u_z dx = u_z x \Big|_0^R - \int_0^R x du_z. \quad (\text{II-4})$$

Assuming no slip at the wall,

$$u_z x \Big|_0^R = 0. \quad (\text{II-5})$$

From Equation (II-4) and (II-5), Equation (II-3) can be written,

$$\frac{q_i}{2l} = - \int_0^R x du_z, \quad (\text{II-6})$$

or,

$$\frac{q_i}{2l} = - \int_0^R x \left(\frac{du_z}{dx} \right) dx. \quad (\text{II-7})$$

The equation of motion (52b) for the laminar flow of Figure (II-2) takes the following simple form,

$$\nabla P = - \nabla \cdot \tau, \quad (\text{II-8})$$

where P is pressure and τ , stress tensor. Integrating Equation (II-8) for the present case,

$$\tau = \left(\frac{P_i - P_L}{\Delta L} \right) x = \frac{\Delta P}{\Delta L} x. \quad (\text{II-9})$$

τ represents τ_{xz} . From Equation (II-9) the wall shear stress, τ_W , is obtained,

$$\tau_W = \frac{\Delta P}{\Delta L} R. \quad (\text{II-10})$$

Dividing Equation (II-9) by (II-10) and solving for x ,

$$x = \frac{R}{\tau_W} \tau, \quad (\text{II-11})$$

and,

$$dx = \frac{R}{\tau_W} d\tau. \quad (\text{II-12})$$

If we substitute (II-11, 12) into (II-7), we get,

$$\frac{q_i}{2L} = - \frac{R^2}{\tau_W^2} \int_0^{\tau_W} \tau \left(\frac{du_z}{dx} \right) d\tau, \quad (\text{II-13})$$

or,

$$\frac{q_i}{2LR} = u_m = - \frac{R}{\tau_W^2} \int_0^{\tau_W} \tau \left(\frac{du_z}{dx} \right) d\tau, \quad (\text{II-14})$$

where u_m is average velocity and du_z/dx is shear rate and will be designated by σ , so that,

$$u_m = - \frac{R}{\tau_W^2} \int_0^{\tau_W} \tau \sigma d\tau. \quad (\text{II-15})$$

For the assumed steady flow σ is a function only of τ . For Newtonian fluids,

$$\sigma = -\frac{\tau}{\mu}, \quad (\text{II-16})$$

and for a fluid approximated by the power-law model,

$$\tau = m_1 |\sigma|^n, \quad (\text{II-17})$$

where $|\sigma|$ is the absolute value of σ , m_1 and n are rheological parameters. By defining Γ as an average nominal Shear rate,

$$\Gamma = \frac{u_m}{R}, \quad (\text{II-18})$$

Equation (II-15) can be written in the following form,

$$\Gamma = -\frac{1}{\tau_W} \int_0^{\tau_W} \tau \sigma d\tau. \quad (\text{II-19})$$

To modify Equation (II-19) for the multicylinder box, it is sufficient to introduce V/ϵ_s in place of u_m , i.e.

$$u_m \equiv \frac{V}{\epsilon_s}, \quad (\text{II-20})$$

where ϵ_s is surface porosity. Surface porosity is calculated as follows,

$$\epsilon_s = \frac{\Sigma d}{\Sigma d + \Sigma D} \quad (\text{II-21})$$

Therefore, Equations (II-18) and (II-19) become,

$$\Gamma_\epsilon = \frac{V}{\epsilon_s R} = -\frac{1}{\tau_\epsilon} \int_0^{\tau_\epsilon} \tau \sigma d\tau \quad (\text{II-22})$$

where the subscript ϵ indicates that the equation has been modified for the porous bed. Also, Equation (II-10) can be modified for the porous bed as follows,

$$\tau_\epsilon = \frac{\Delta P}{L'} R, \quad (\text{II-23})$$

where L' is written instead of L , the length of the bed to include tortuosity, i.e.

$$L' = C_4 L. \quad (\text{II-24})$$

C_4 is geometric constant which accounts for tortuosity of the path of the fluid particles. The magnitude of C_4 is estimated from Figure (II-1) to be approximately equal to,

$$C_4 \approx \frac{(\pi D/2) N}{L} = 1.5, \quad (\text{II-25})$$

where $(\pi D/2)$ is half the circumference of the cylinder and N the number of rows. A more accurate value of C_4 which will be presented later, should be determined experimentally. Substituting (II-24) into (II-23),

$$\tau_\epsilon = \frac{\Delta P}{C_4 L} R. \quad (\text{II-26})$$

For a Newtonian fluid, Equation (II-22) by using Equation (II-16) becomes,

$$\Gamma_\epsilon = \frac{\tau_\epsilon}{3\mu} \quad (\text{II-27})$$

Solving for μ ,

$$\mu = \frac{\tau_\epsilon}{3\Gamma_\epsilon}. \quad (\text{II-28})$$

The expression found for μ is defined as Darcy's viscosity.

Substituting (II-22, 26) into (II-28),

$$\mu = \frac{\epsilon_s R^2}{3C_4} \frac{\Delta P}{LV} \quad (\text{II-29})$$

By comparing Equation (II-29) with Darcy's law, Equation (I-4), the expression for the permeability of a Newtonian fluid in the parallel-plates capillary model bed is obtained as,

$$K = \frac{\epsilon_s R^2}{3C_4}, \quad (\text{II-30})$$

in which C_4 , as stated earlier, has to be evaluated experimentally.

II. 3 Power-Law Model

Assuming fluid flow is purely viscous, the power-law model can be used to approximate the properties of the polymer solution. Solving for σ from Equation (II-17),

$$\sigma = - \left(\frac{\tau}{m_1} \right)^{1/n}, \quad (\text{II-31})$$

where the minus sign is chosen because of the choice of coordinates. Substituting (II-31) into (II-22) and integrating,

$$\Gamma_\epsilon = \frac{n}{1+2n} \left(\frac{\tau_\epsilon}{m_1} \right)^{1/n}, \quad (\text{II-32})$$

or,

$$\tau_\epsilon = m_1 \left[\frac{1+2n}{n} \Gamma_\epsilon \right]^n. \quad (\text{II-33})$$

Further, we write τ_ϵ and Γ_ϵ in terms of K and C_4 using Equations (II-22, 26, 30),

$$\tau_\epsilon = \sqrt{3K/C_4} \epsilon_s \frac{\Delta P}{L}, \quad (\text{II-34})$$

$$\Gamma_\epsilon = V/\sqrt{3C_4 K} \epsilon_s. \quad (\text{II-35})$$

If we substitute (II-34, 35) into (II-33) and solve for V^n ,

$$V^n = \frac{(3K/C_4 \epsilon_s)^{1/n} (3C_4 K \epsilon_s)^{n/2}}{m_1 \left(\frac{1+n}{n} \right)^n} \frac{\Delta P}{L}. \quad (\text{II-36})$$

Comparing Equation (II-36) with the modified Darcy's law, i.e. Equation (I-5), H can be obtained,

$$H = \frac{m_1}{3} \left(\frac{1+2n}{n} \right)^n (3C_4 K \epsilon_s)^{(1-n)/2} \quad (\text{II-37})$$

From (II-37), it is evident that $H = m = \mu$ when $n = 1$ as for a Newtonian fluid.

II. 4 Modified Friction Factor and Reynolds Number

If we use Ergun's definition of the friction factor (54), we obtain,

$$f_K = \frac{2d \epsilon_s^2 \Delta P}{\rho V^2 L} \quad (\text{II-38})$$

The Reynolds number is arbitrarily defined so that,

$$f_K = 1/N_{Re} \quad (\text{II-39})$$

After straight forward algebraic manipulation, it follows from Equations (II-2, 30, 38) and (I-5),

$$N_{Re} = \frac{\rho d V^{2-n}}{2^4 C_4 \epsilon_s H} \quad (\text{II-40})$$

For a Newtonian fluid, we set $n = 1$ and therefore,

$$N_{Re} = \frac{\rho d V}{2^4 C_4 \epsilon_s \mu} \quad (\text{II-41})$$

II. 5 Application of Theory

The permeability, K , of the bed can be determined from Equation (I-4) by a Newtonian fluid flow experiment. Then, from Equation (II-30) the tortuosity factor, C_4 , can be predicted. Therefore, H from Equation (II-37), and consequently, ΔP from Equation (I-5) for the polymer solution runs are calculated.

Equation (I-5) predicts that a plot of ΔP v.s. V on log-log scale is a straight line with slope n in the absence of inertia and elastic effects. Upward deviation of experimental points from this straight line might be due to the inertia effect, elastic effect or both. Effect of elasticity would be confirmed by showing the absence of inertia effect with a Newtonian fluid of similar viscosity. An equivalent verification can be obtained by plotting friction factor v.s. Reynolds number which according to (II-39) would give a straight line with slope -1 on log-log scale.

CHAPTER III

EXPERIMENTAL EQUIPMENT AND PROCEDURE

III. 1 Multi-Cylinder Matrix

To simulate flow in porous media a regularly spaced matrix of 6mm diameter glass rods in a triangular arrangement was used. Figure (III-1) illustrates a unit cell of triangular pitch. The cylinders were contained in a rectangular channel of inside cross section 5.2 cm x 6.5 cm--Figure (III-2). The top and side walls of the channel were made of 1/2" Plexiglass sheets and the bottom, inlet and outlet, of stainless steel. On the bottom plate a 1mm brass sheet was set to keep the cylinders fixed in their positions. The inside surface of the rear side wall was painted black by "Wrought Iron Black" paint to eliminate reflection. The front side of the box (i.e. the side facing the light source) was covered with a black hard paper which had an approximately 1mm horizontal slit at the middle to provide a narrow slit of light from the broader slit coming from the light source.

To minimize the inlet and outlet disturbances, two distributors, 26 cm apart, were used; one before the first row and the other after the last row. The distance between the distributors and the inlet/outlet plates was 1.5 cm. The length of the model was 40 rows of cylinders, each

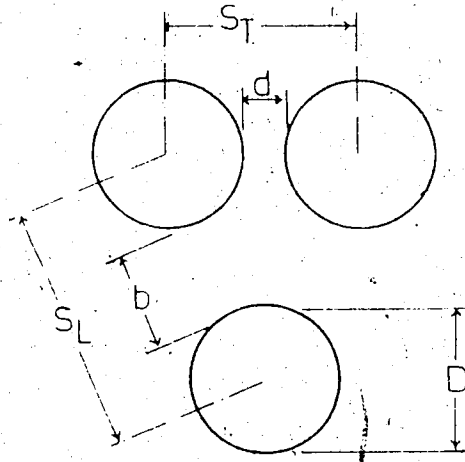


FIGURE III-1 TRIANGULAR-PITCH ISOCELL

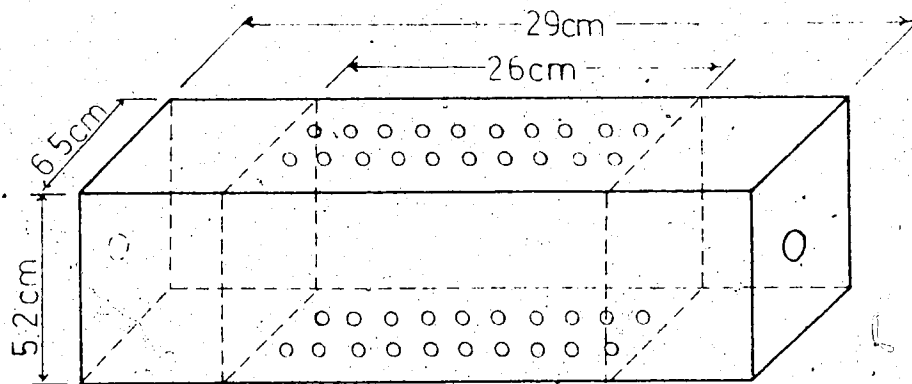


FIGURE III-2 MULTI-CYLINDER MATRIX

row alternatively 9 or 10 cylinders across. The minimum and maximum pore openings, shown as d and b in Figure III-1, were approximately 0.5 and 1mm, respectively. The volumetric porosity, ϵ , of the bed was 0.357. Measurement of ϵ was performed by measuring the void volumes, V_V . The box was filled with water, then the volume of the water, V_W , was measured. Knowing the total volume of the box, V_T , porosity was obtained by,

$$\epsilon = \frac{V_V}{V_T} = \frac{V_W}{V_T} \quad (\text{III-1})$$

Void volume can also be approximated by,

$$V_V = V_T - V_C \quad (\text{III-2})$$

where V_C is the volume occupied by cylinders and is equal to,

$$V_C = \frac{\pi D^2}{4} \times N_T \quad (\text{III-3})$$

where N_T is the total number of cylinders.

A similar model with cylinders of shorter length and larger diameter was used by Kyle, et al. (55). A smaller diameter was chosen for the present study to achieve larger elongational rates (i.e. $\partial u_z / \partial z$ in Equation V-3) which is required to observe any significant elastic effect.

The model was constructed to represent a uniform homogeneous bed, but it was found that some inhomogeneity in the microscopic scale existed. Specifically, the minimum opening, which was nominally to be 0.5mm, varied between 0.46 to 0.787mm--excluding the openings next to the walls. These

openings are given in Table (C-1) for three rows. And the diameter of rods which were nominally 6mm circular cross-section varied from 5.9 to 6.2mm. The cylinders were not perfectly circular and the maximum to minimum diameter ratio was as large as 1.03.

The twentieth, twenty first and twenty second rows--numbered from the inlet--were chosen to represent the bed. The positions are numbered from 1 to 32 as shown, schematically, in Figure (III-3). A complete map of these rows, measured at a total magnification 100 was prepared to define the spacings of the cylinders. This was performed by projecting the pictures taken of the different positions which covered the whole area of interest.

An attempt was made to obtain velocity profiles at the minimum openings, where the maximum pressure drop and the maximum deformation rates occur. These positions are along the line A-A in Figure (III-3). However, due to the difficulties involved in photography--e.g. not having enough light at some center line positions--it was not possible to have photographs of usable quality at these positions for all the 32 openings. As a result of this the complete distribution of the flow across a row had to be determined indirectly. Thus some of the pictures had to be taken from the positions below or above the line A-A, say B-B. The center line openings (i.e. the openings along the line A-A such as

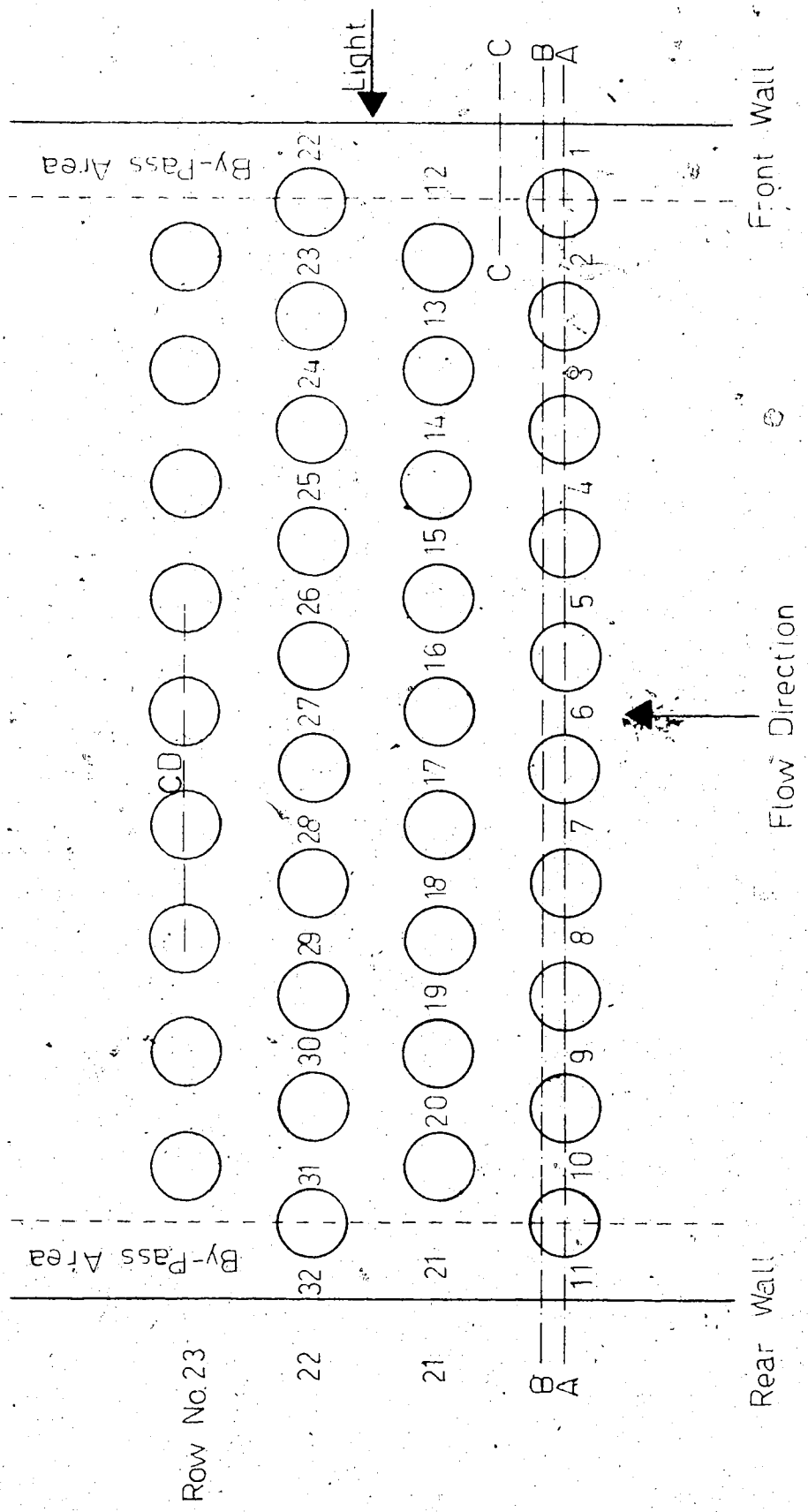


FIGURE III-3 TOP VIEW OF GLASS RODS

CD in Figure III-3 are designated by d ; and the openings above or below A-A are called NCL, implying "Not Center Line." The relative magnitude of NCL with respect to d is an indication of the relative position of the line B-B with respect to the line A-A. In the case of NCL, the orthogonal component of the streaks length was taken; but for the center line openings this need not be considered, because all the streaks are perpendicular to A-A. For the positions 1, 11, 22, and 3 2 the "Not Center Line," NCL, was taken even farther than B-B, say C-C, and those streamlines, crossing C-C, which passed through these positions were chosen.

Every alternate row of the matrix had two large openings next to walls. These openings were in the order of magnitude of the radius of cylinders, i.e. 3mm, while the minimum openings between two cylinders as was already mentioned, were designed to be 0.5mm. These large openings caused by-pass channels near the walls. That is a larger fraction of fluid passed from the openings next to walls. The by-pass area is shown in Figure (III-3) by dashed-line.

III. 2 Experimental Fluids

A partially hydrolized Polyacrylamide product of Dow Chemical Co., trade name SEPARAN AP-273 was used as polymer. This white granular powder is soluble in water and has a molecular weight of approximately three million. Its solution in water shows effects of elasticity and the rheological properties of 0.2% (by weight) solution, which

was used for the entire experiment, are given in Appendix A. Domestic tap water was used for preparation of polymer solutions and care was taken to avoid mechanical degradation of the polymer molecules by stirring the solution very gently during preparation. The solutions were protected from bacterial degradation by approximately 1cc of Sodium Benzoate powder in 10^6 cc solution. The specific gravity of the polymer solutions, determined for every new solution, was 0.9965 gr/cc.

To provide a wide range of friction-factor Reynolds number for Newtonian fluids, Glycerol solutions ranging from 96 to 58% Glycerol by volume in tap water were used.

Aluminum metal dust, manufactured by J. T. Baker Chemical Co., Lot No. 2347, was used to visualize the flow pattern. The volumetric concentration of Aluminum dust was approximately 2cc of the bulk dust in 10^6 cc solution.

III. 3 Pumping

Fluid flow at a desired rate was obtained by a ZENITH gear pump driven by a variable speed transmission. For low flow rates (i.e. 0.685 to 6.85 cc/sec), one pump was used but for higher flow rates, which were required to increase the range of flow rate for pressure drop measurement, two pumps were used. The pumps were calibrated by weighing the polymer solution collected over a known period of time. Since the Glycerol solutions (i.e. more than 85% Glycerol by volume) are highly hygroscopic a complete closed recycle system was used. For the polymer solution, to avoid

degradation of the polymer molecules, recycling was avoided. Rheological properties were measured before and after running and consistency was checked to assure absence of any degradation.

III. 4 Streak Photography Technique

Streak photography not only gives the streamlines but also the velocity profile can be established by measuring the length of the streaks of known duration. These were provided by placing a chopping disk perpendicular to the light beam to interrupt the light for known duration of time. In the present work the streak photography using a photomicrography technique was applied to obtain the local velocity profile.

III. 4.1 Optical System

The main features of the optical system are shown in Figure (III-4) which are briefly reviewed below.

a. Light Source

The light source used in the present study was the same as the one used by Rollin (56) and Catania (57). It was a CHRISTIE Xenon arc lamp which operated from a three phase CHRISTIE transformer of D.C. maximum output of 3300 Watts at 100 amps. The necessary optical alignment and adjustments of the lamphouse No. BSF 50 were made to achieve the maximum brightness and light uniformity. Immediately in front of the lamphouse lens an adjustable horizontal slit, then a converging lens were placed. Therefore a narrow beam

8

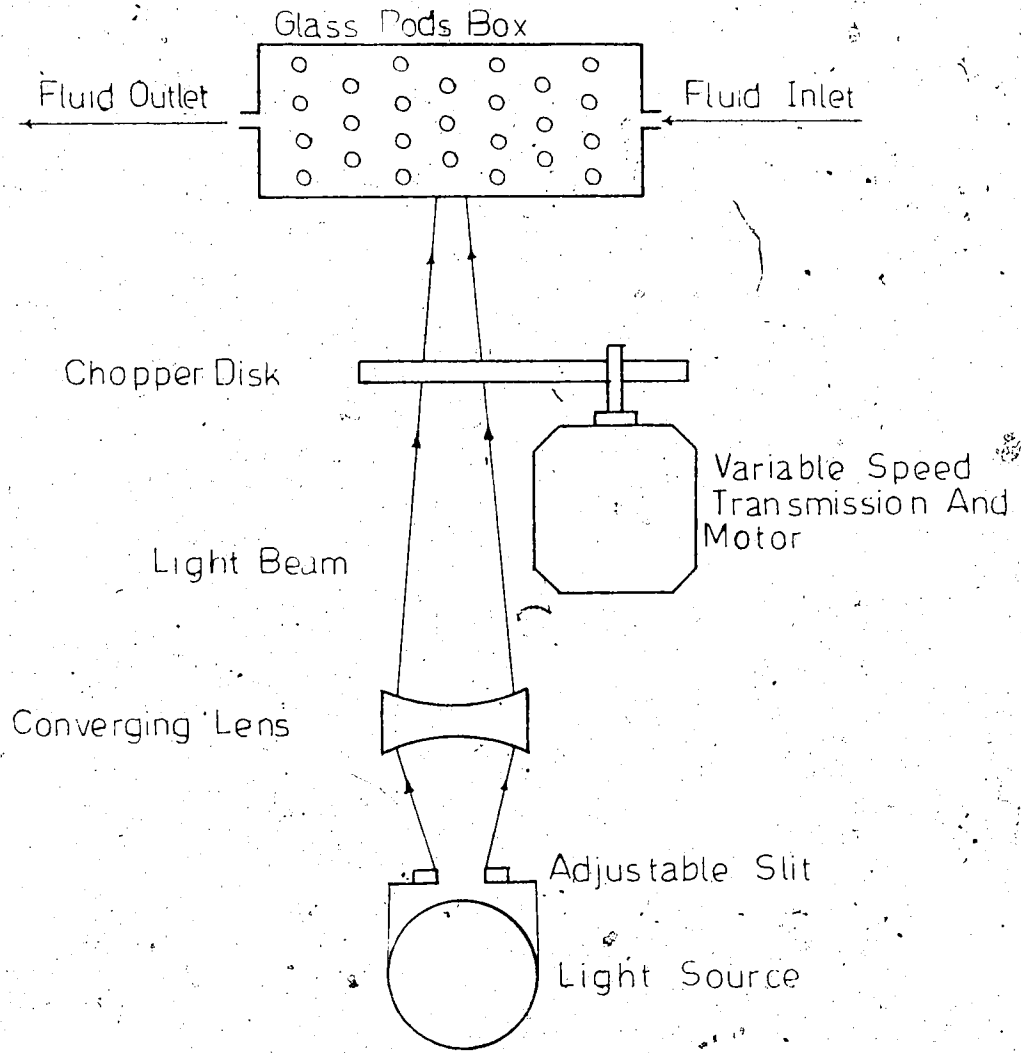


FIGURE III-4 SCHEMATIC PLAN VIEW OF OPTICAL SYSTEM

to a thickness of, approximately, 2mm, less than the slits on the chopper disk but broader than the slit on the box was produced. The light slit was set horizontal so that the plane of light beam was perpendicular to the rods.

b. Chopper Disk

Two transparent lucite disks were assembled on a variable speed transmission through a pulley connection with a ratio of diameter of disk pulley to transmission pulley 2.7:1. In order to interrupt the light and provide streaks of known duration, a paper wheel with 8 equal radial slits and spokes was placed between the lucite disks and fastened together. The chopper disk was placed perpendicular to the light beam with the axis of rotation in the plane of the light slit.

The rotational speed of the motor was set in order to obtain reasonable length of streaks. In an accelerating flow long streaks are not representative of the local velocity; on the other hand, uncertainty in the length measurement of very short streaks is more than that of longer ones. It is evident that higher flow rates require higher rotational speed. The rotational speed of the chopper above 100 RPM was measured by a Stroboscope Type 1531-A STROBOSCOPIC. Below 100 RPM, speed was determined using a stop watch.

After the experiment was finished a disagreement was noticed between the actual and experimental total flow rates. The actual total flow rate was measured by the formerly calibrated pump, while the experimental flow rate

was calculated from the area under the velocity profiles. This disagreement appeared only for the two high flow rates where the rotational speed of the chopper was above 100 RPM. By checking the stroboscope, it was found that the stroboscope was not calibrated and the measured RPM's were 10.4 per cent less than the actual RPM's which was indeed equal to the inconsistency of the flow rates.

C. Photomicrography Assembly

As illustrated in Figure (III-5), a Miranda 35mm camera was positioned at the top of a phototube of a Wild M5 microscope. The phototube was perpendicular to the light and the camera film parallel. Magnification on the microscope was 12X, but the real magnification on the film was 4X. Thirty-five mm Tri-X film with ASA speed of 400 was used. The exposure times were determined after a set of trials and were approximately 15 to 20 seconds. The exposure times were different according to the brightness of the position. For the positions where the light was not sufficient the exposure time was extended even to one minute in order to increase the probability of having a bright particle passing that position.

III. 4-2 Measurement of the Streak Length

A Bell & Howell projector was used to project the negatives on a large sheet of graph paper. Total magnification of the streaks on the graph paper was 100 in all cases. The distance between the projector and graph paper was adjusted so as to obtain the final magnification of 100. The graph

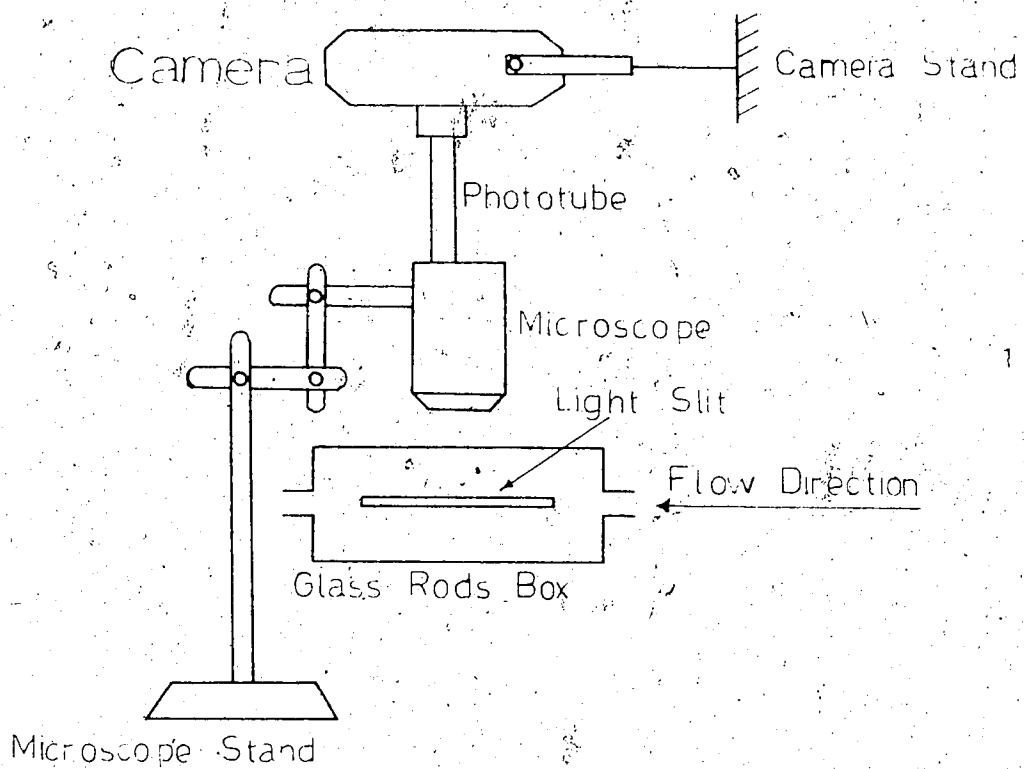


FIGURE III-5 PHOTOMICROGRAPHY ASSEMBLY

paper had 0.1" divisions and the length of the streaks were read directly from the graph paper at the total magnification of 100. Therefore all the reported lengths in Tables (E-1, 2) are in units of 10^{-3} inches.

The system was calibrated by projecting photographs of a precision steel ruler with 0.5mm division.

To eliminate the error due to the half-shadow at the beginning and the end of every light period of the chopper's opening, all measurements of streak length were performed on head-to-head or tail-to-tail basis. That is the length 'a' was measured not 'b'.



Some typical photographs are given for Glycerol and Separan in Figures (IV-5, 6).

Two major sources of error which caused the data points to be scattered in Figures (IV-7 to 12) or (IV-13) are how accurately the streaks could be located with respect to the edge of the rods and the hazy beginning and end of the streaks.

By observing several photographs, points on the circumference of the rods were located and the cross sections of the rods were drawn onto the graph paper. In pictures which did not provide sharp edges, uncertainty in determining the points on the circumference is in the range of a few tenths of an inch in the magnified scale. This uncertainty

is, approximately, 10 per cent the nominal center line opening, $d = 0.5\text{mm}$. Noting that the slope of the local velocity profiles near the walls is high, the uncertainty in the location of the streaks causes significant scattering. For instance, the velocity profile of position No. 13 of Separan in Figure (IV-13) is a good example. In this profile, two groups of data points which belonged to two different photographs are observed at the left side of the mid-point of the opening. By shifting the upper group 0.05mm to the right, the scattering could be minimized significantly. This effect is more severe near the cylinders where the slope of the velocity profiles is high, but is zero at the mid-point of the opening where the slope is almost zero.

The formerly mentioned second source of error is the measurement of the length of the streaks which is due to the hazy beginning and end of the streaks. This could reach two-tenths of an inch in the magnified scale for good pictures. The percentage contribution of this error is negligible for long streaks, say 3 inches in magnified scale, but is significant for the short ones which are near the cylinders; e.g. for a 0.4 inches long streak in magnified scale, the percentage of the error in measurement is 50 per cent.

Position No. 13 of Glycerol in Figure IV-13 is a good example of this kind of scattering. For the pictures of poor quality, the hazy part of streaks was much larger than what was reported above. This could reach to even half an

inch in magnified scale. Some of the data points of positions No. 15 and 16 of Separan in Figure (IV-13) belong to this kind of picture.

The "Not Center Line" positions were chosen so that both of these two sources of error were minimized. That is, they were chosen along a line where sharp image of the cylinder allowed accurate positioning and also where sharp streaks images occurred.

III. 5 Pressure Drop Measurement

Mercury and also two colored manometer liquids, MERIAN No. D-2883 and D-8325 with specific gravity of 2.95 and 1.75 respectively, were used to measure the pressure drop. Pressure taps were located on the rear side of the box, 22.2 cm apart, between row No. 3 and row No. 38. Pressure drop was measured for pure, 96% (by volume), 81% (by volume), 58% (by volume) Glycerol, tap water, and 0.2% (by weight) Separan solutions. The range of flow rates for the different fluids is given below,

<u>Fluid</u>	<u>Range of Flow Rates</u>
Pure Glycerol	0.431 - 3.42 cc/sec
96% Glycerol	0.835 - 17.06 cc/sec
81% Glycerol	0.835 - 10.76 cc/sec
58% Glycerol	2.13 - 34.35 cc/sec
tap water	10.76 - 34.35 cc/sec
0.2% Separan	0.431 - 34.35 cc/sec

CHAPTER IV

RESULTS

IV. 1 Pressure Drop

Figure (IV-1) is a plot of the measured pressure drop v.s. superficial velocity for the several Newtonian fluids. In this plot the empirical correlation of Bergelin, et al. (58) for the flow across banks of cylinders has been shown. This empirical correlation is discussed in Appendix B. The data points of this plot, together with the calculated permeability, are recorded in Table (B-1). The permeability of the bed has been calculated for individual runs using Darcy's law, i.e. Equation (I-4). The arithmetic average permeability of the runs number 1 to 41 in Table (B-1) has been chosen to approximate the permeability of the bed, i.e.

$$K = 1.3 \times 10^{-4} \text{ cm}^2 \quad (\text{IV-1})$$

Figure (IV-2) shows the pressure drop measurement v.s. superficial velocity for polymer solution. In this plot the predicted curve of pressure drop by Equation (I-5) based on the parallel-plates capillary model is presented. The empirical correlation of Bergelin which gave a good prediction for Glycerol solutions was modified for the polymer solution and the predicted curve is also given in Figure (IV-2).

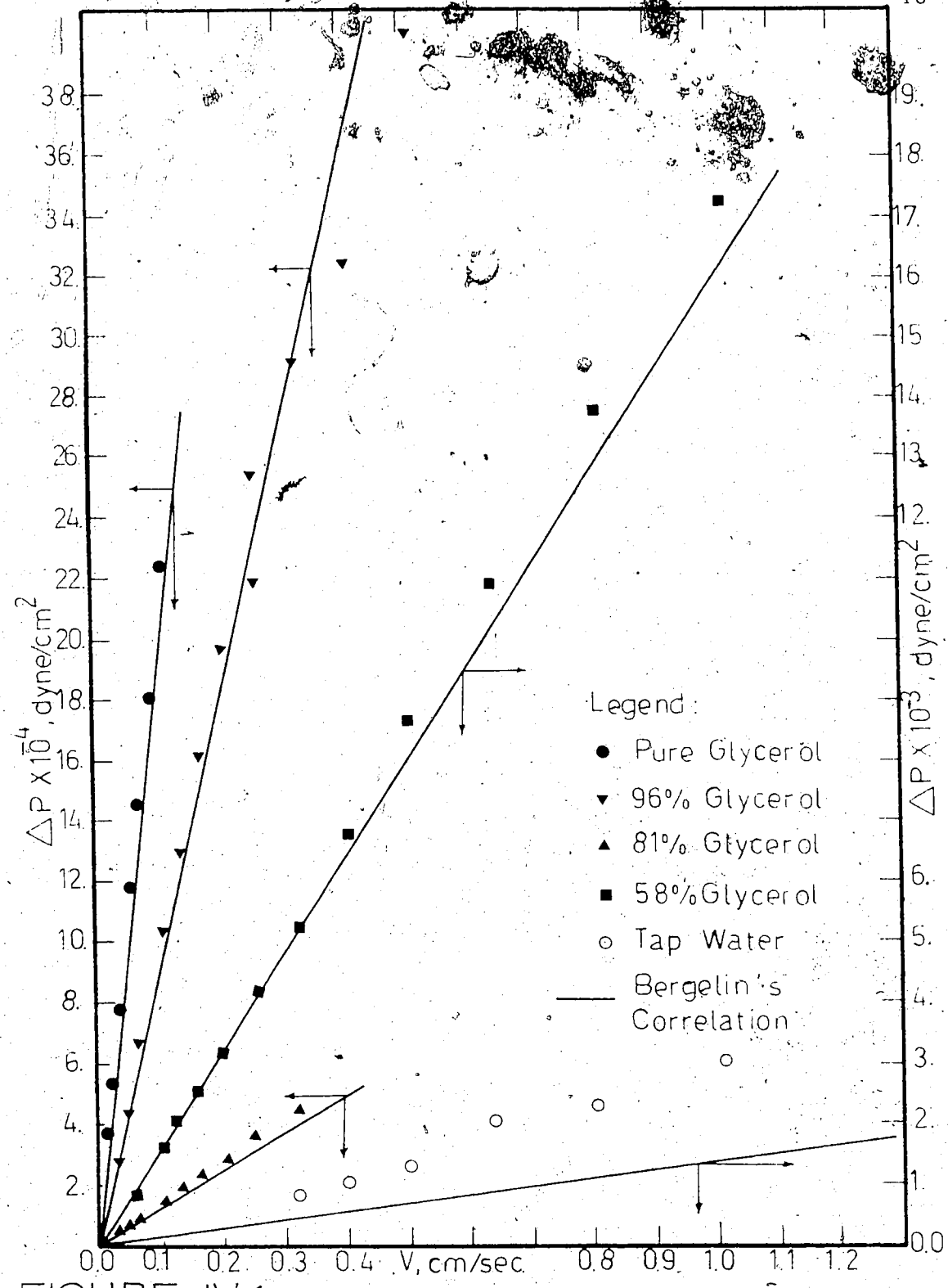


FIGURE IV-1 PRESSURE DROP VS. FLOW RATE
GLYCEROL

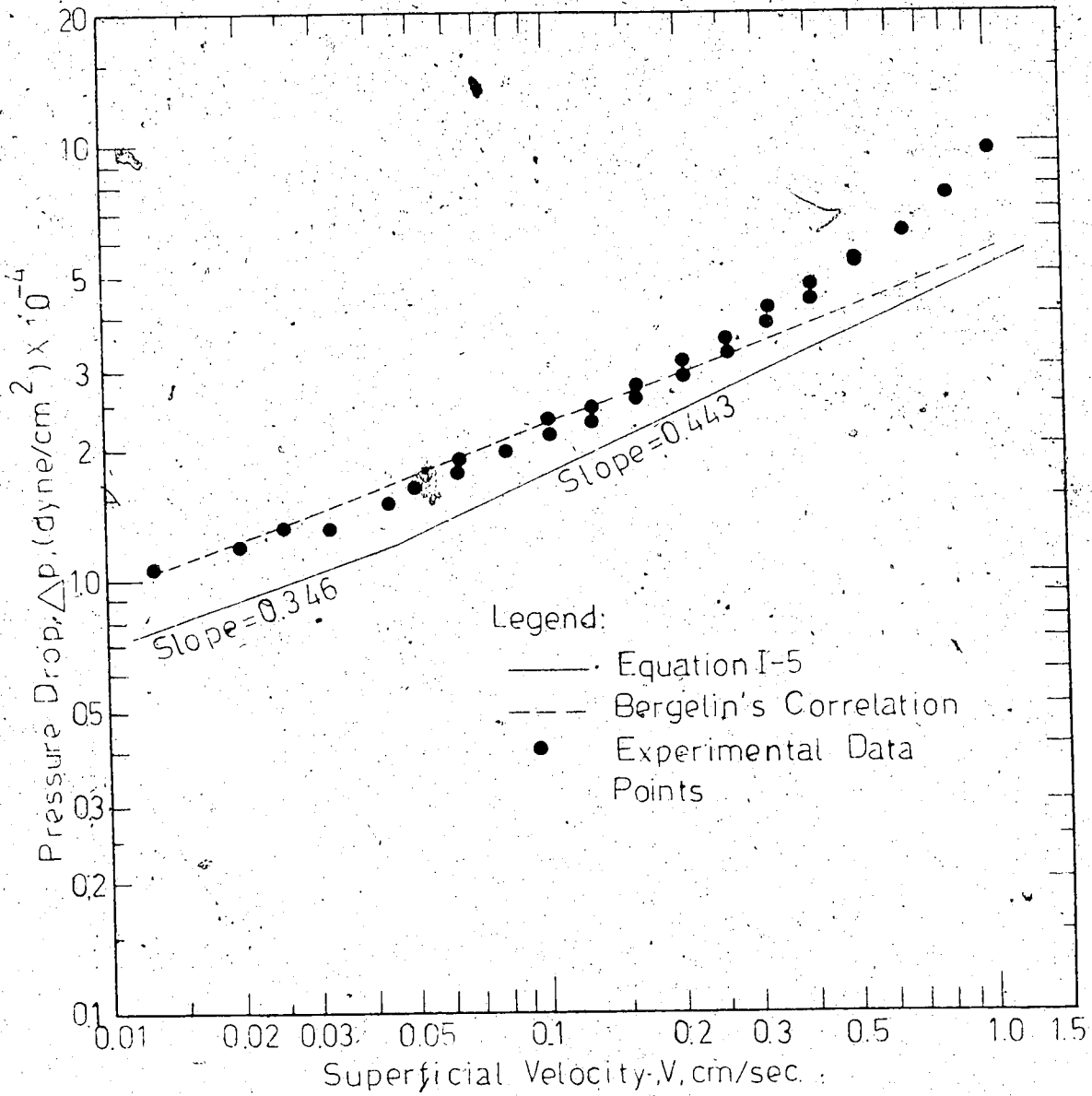


FIGURE IV-2 PRESSURE DROP VS FLOW RATE SEPARAN

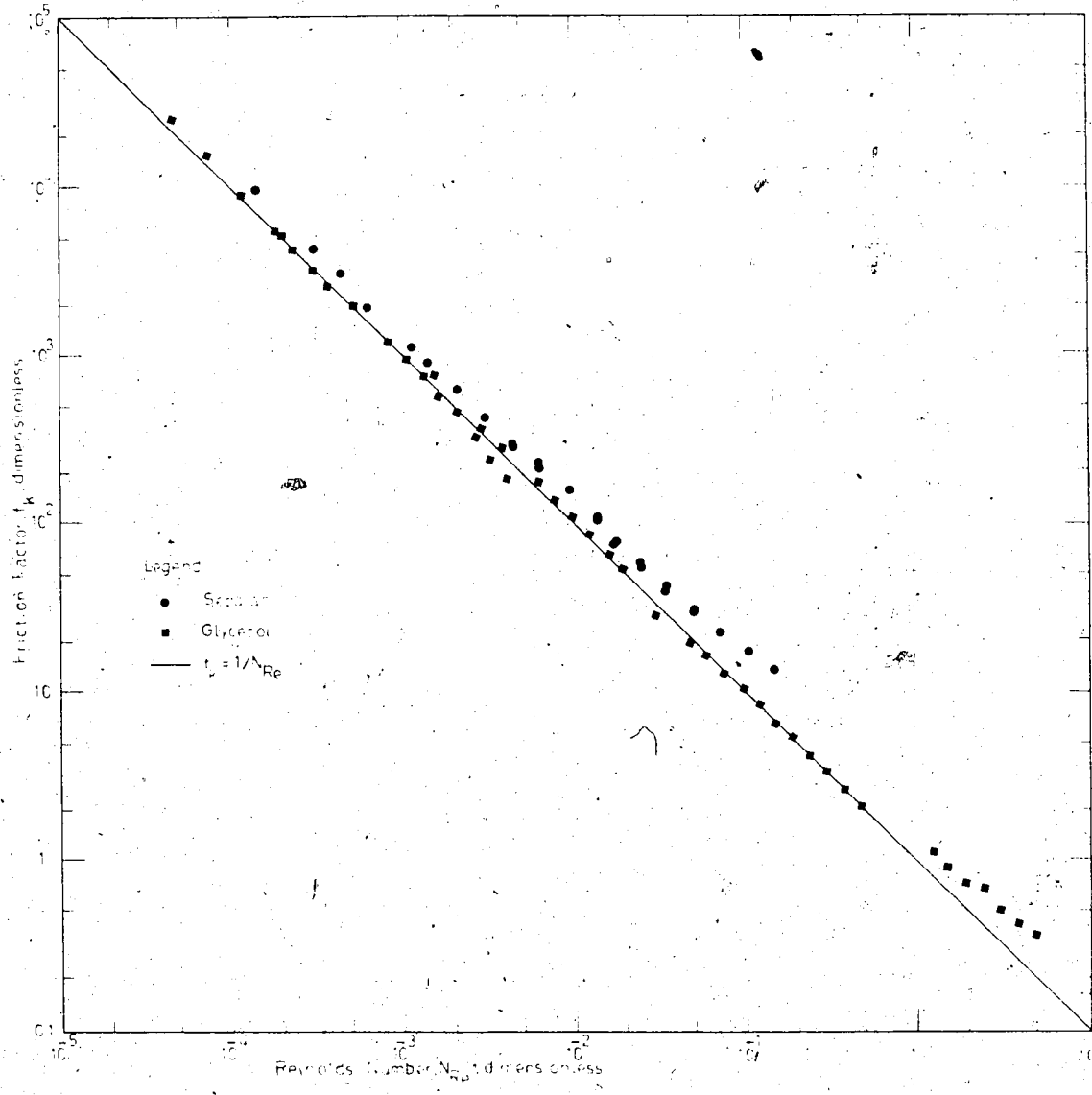


FIGURE IV-3 FRICTION FACTOR VS. REYNOLDS NUMBER

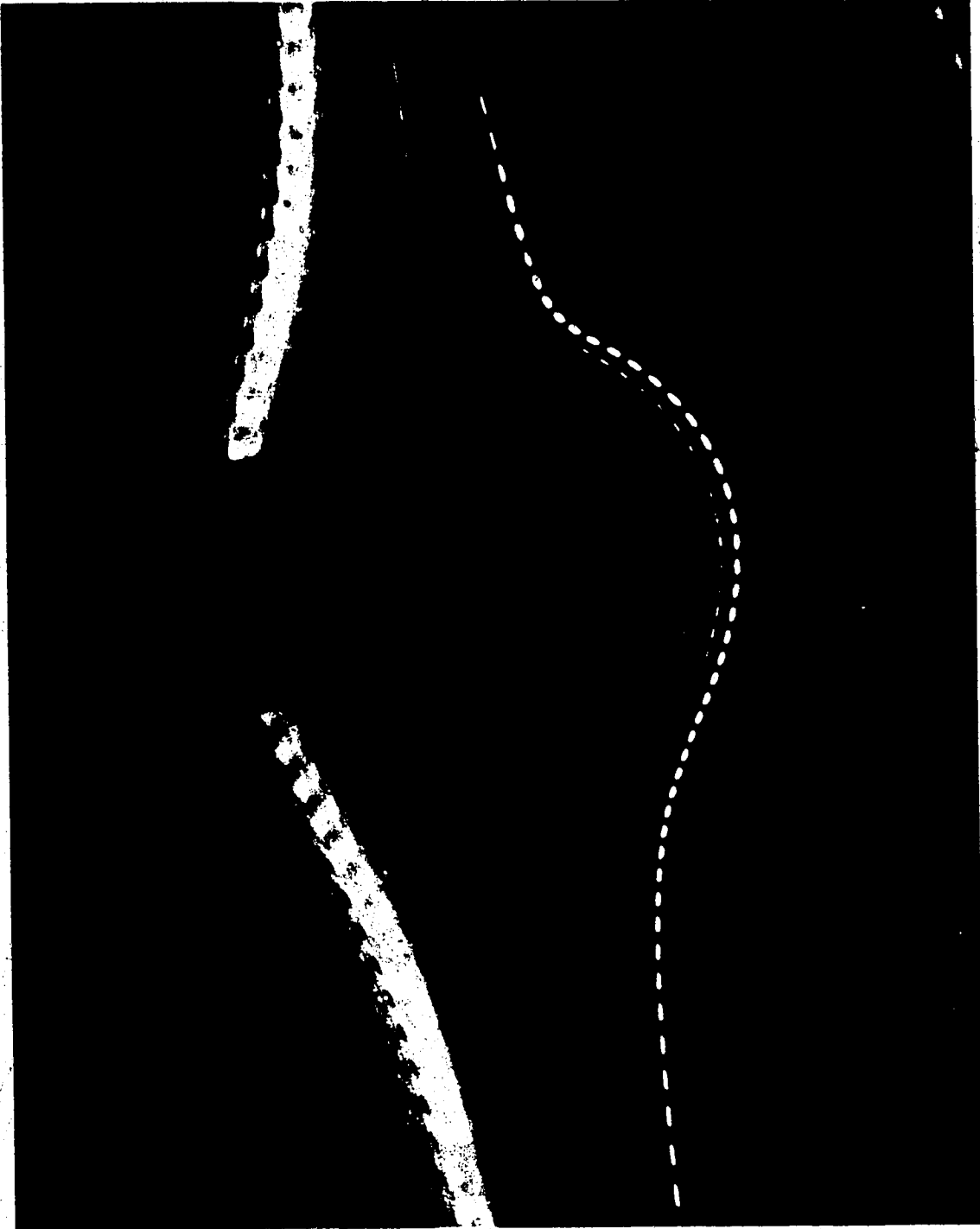
Figure (IV-3) shows the behavior of friction factor v.s. Reynolds number for Glycerol and polymer solutions. The correlations used in this plot are Equations (II-38, 40, 41). The Separan data points of this plot and also those from Figure (IV-2) are recorded in Table (B-2). The Glycerol data points of Figure (IV-3) are presented in Table (B-1).

IV. 2 Streamlines

Photograph No. 1 in Figure (IV-4) presents the shape of the streamlines of 0.2% polymer solution across a single submerged cylinder. The diameter of the cylinder was 3mm and the exposed length, 5.2 cm. The photograph has been taken in a plane perpendicular to the cylinder at its mid-point. The approach or free stream velocity was 0.437 cm/sec. Photographs No. 2, 3, and 4 in Figure (IV-5), taken from position No. 25, present typical streamlines of pure Glycerol through the bank of glass rods. The flow rates were 0.685, 1.717, and 3.42 cc/sec respectively. Photographs No. 5, 6, and 7 in Figure (IV-6) have been taken from the same position and the same flow rates as Glycerol but with the 0.2% polymer solution.

IV. 3 Local Velocity Profiles

Local velocity profiles have been studied for three rows, namely row numbers 20, 21 and 22, and were established for total flow rates of 0.685, 1.717, 3.42 and 6.84 cc/sec. It was noticed that the percentage of the total flow rate



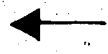
Photograph No.1
 $U = 0.437 \text{ cm/sec}$

Flow Direction

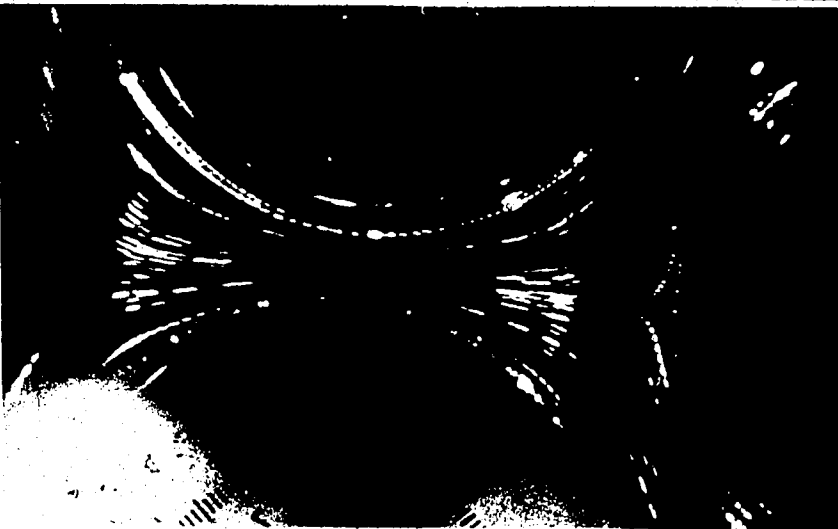
FIGURE IV-4 VISCOELASTIC FLOW PAST SINGLE
CYLINDER



Photograph No. 2
 $q=0.68$ cc/sec



Flow Direction



Photograph No. 3
 $q=1.71$ cc/sec



Flow Direction

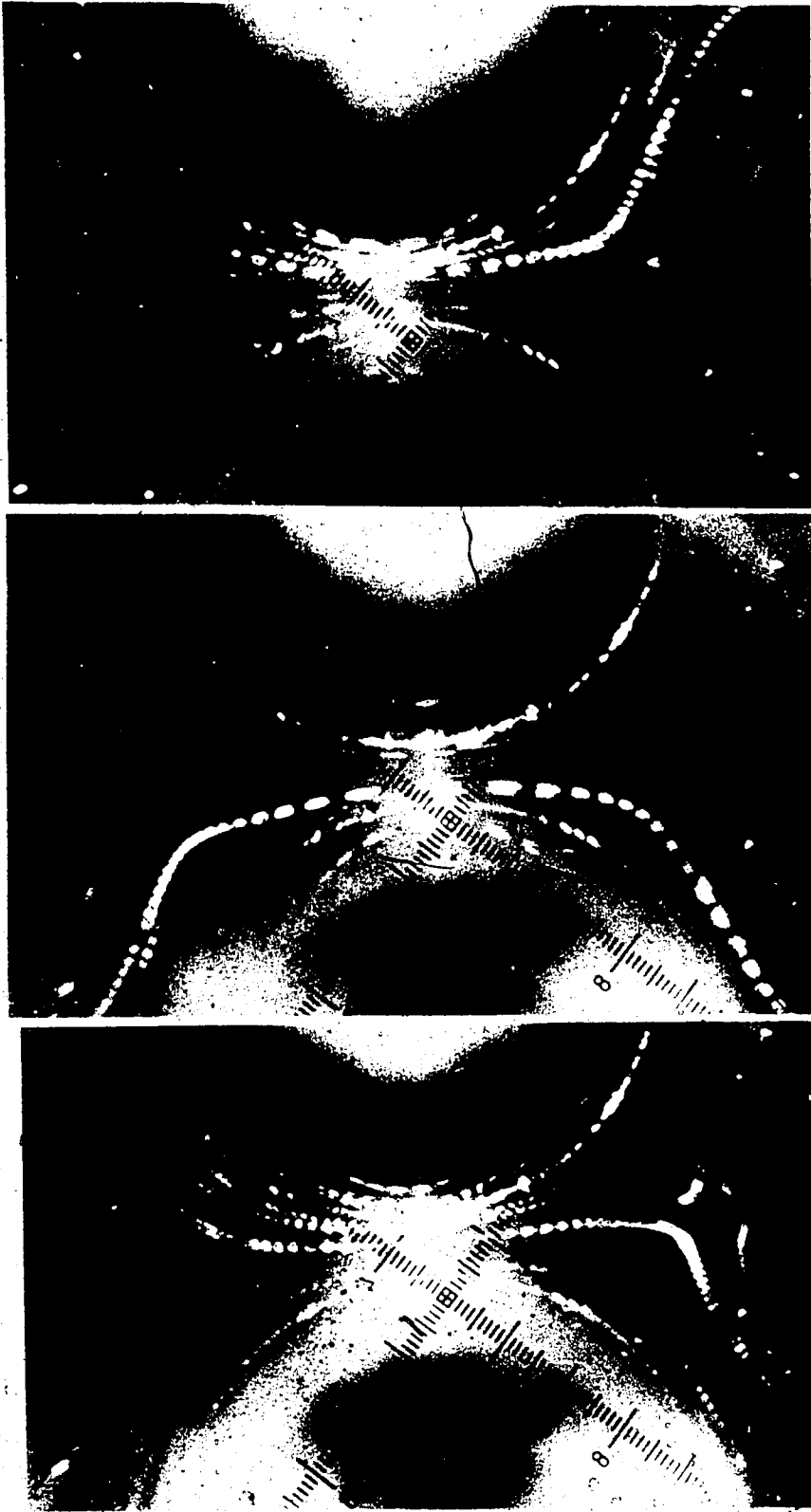


Photograph No. 4
 $q=3.42$ cc/sec



Flow Direction

FIGURE IV-5. NEWTON'S FLOW PAST BULBHEADS— $q=0.68, 1.71, 3.42$ cc/sec



Photograph No. 6
 $q = 1.717 \text{ cc/sec}$

Flow Direction

FIGURE IV-6 VISCOUS FLOW PAST MULTICHANNELS $Re = 100$

passing through each opening was independent of the total flow rate through the bed. In other words, flow distribution remained the same for all sets of data. This suggests that by choosing a proper factor, the four sets of local velocity profiles could be superimposed. The data points of different flow rates are shown in the same plot in the Figures (IV-7) to (IV-12) by different symbols. For the sake of brevity, this has been performed only for one position of each row, namely positions No. 2, 17, and 27, and the velocity profiles of the other positions are not presented here.* In these plots projected streak length as measured directly from graph paper at the total magnification of 100 are plotted v.s. the position between two cylinders. However, the scale given in the plots has been chosen so that the profiles present the dimensionless interstitial velocity, i.e. u/V , v.s. position. The procedure to obtain the scale factor is discussed in Appendix C.

The total data points obtained in the present study was over 5000, but the complete set of data points are presented only for row No. 21 and minimum flow rate, i.e. $q = 0.685$ cc/sec and for one position of each row, namely positions 2, 17, and 27. Again, for the sake of brevity, only some of the data points are presented for the other positions and flow rates. These data points are recorded

* The complete set of plotted local velocity profiles is available from the Chemical Engineering Department, University of Alberta, Edmonton 7, Alberta, Canada.

Legend for Figures IV-7 To IV-12

△ $q = 0.685 \text{ cc/sec.}$

□ $q = 1.717 \text{ cc/sec.}$

○ $q = 3.42 \text{ cc/sec.}$

▼ $q = 6.82 \text{ cc/sec.}$

----- Eye-Fit Curve

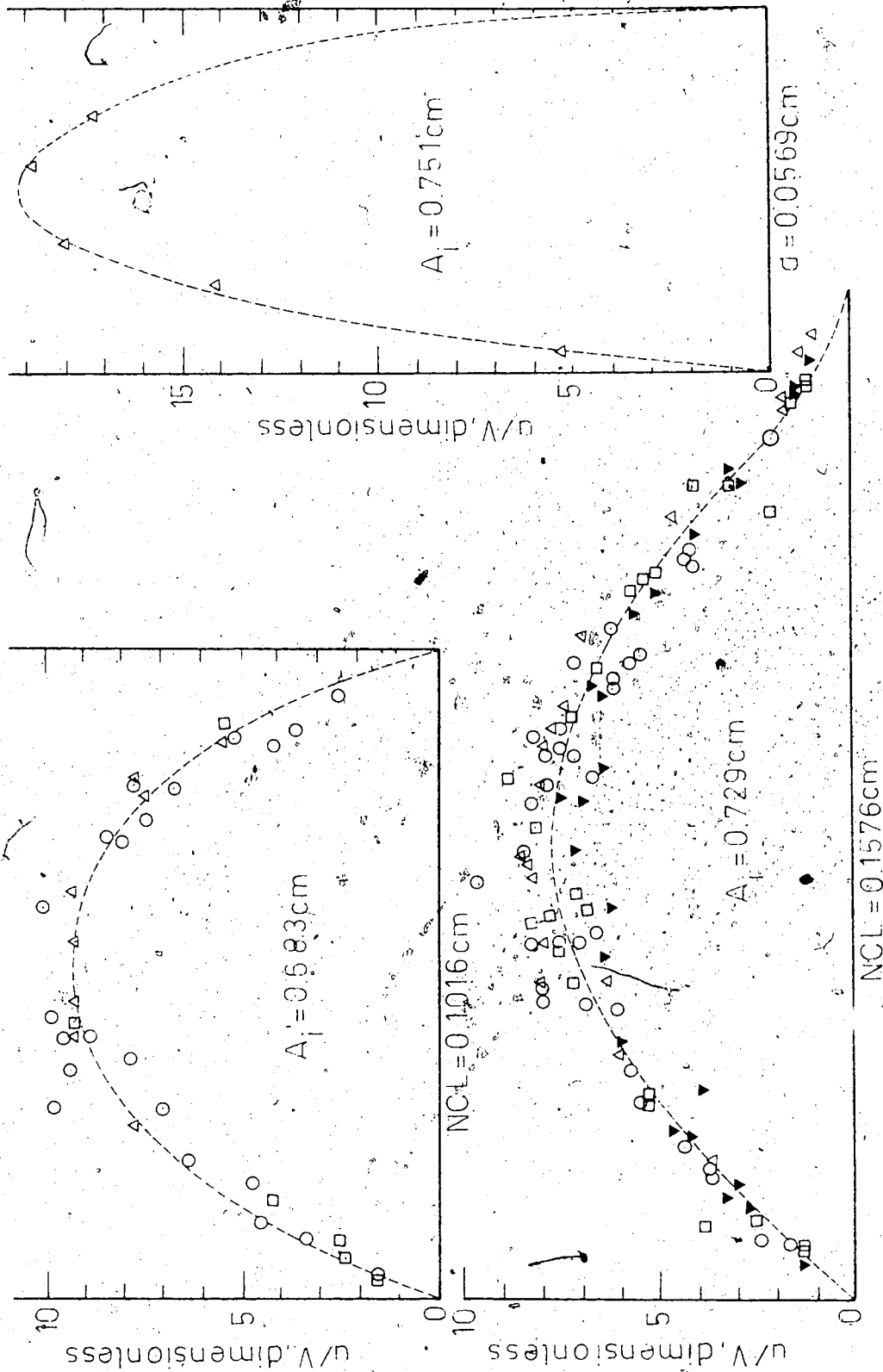


FIGURE IV-7. LOCAL VELOCITY PROFILES OF POSITION NO.2 — GLYCEROL

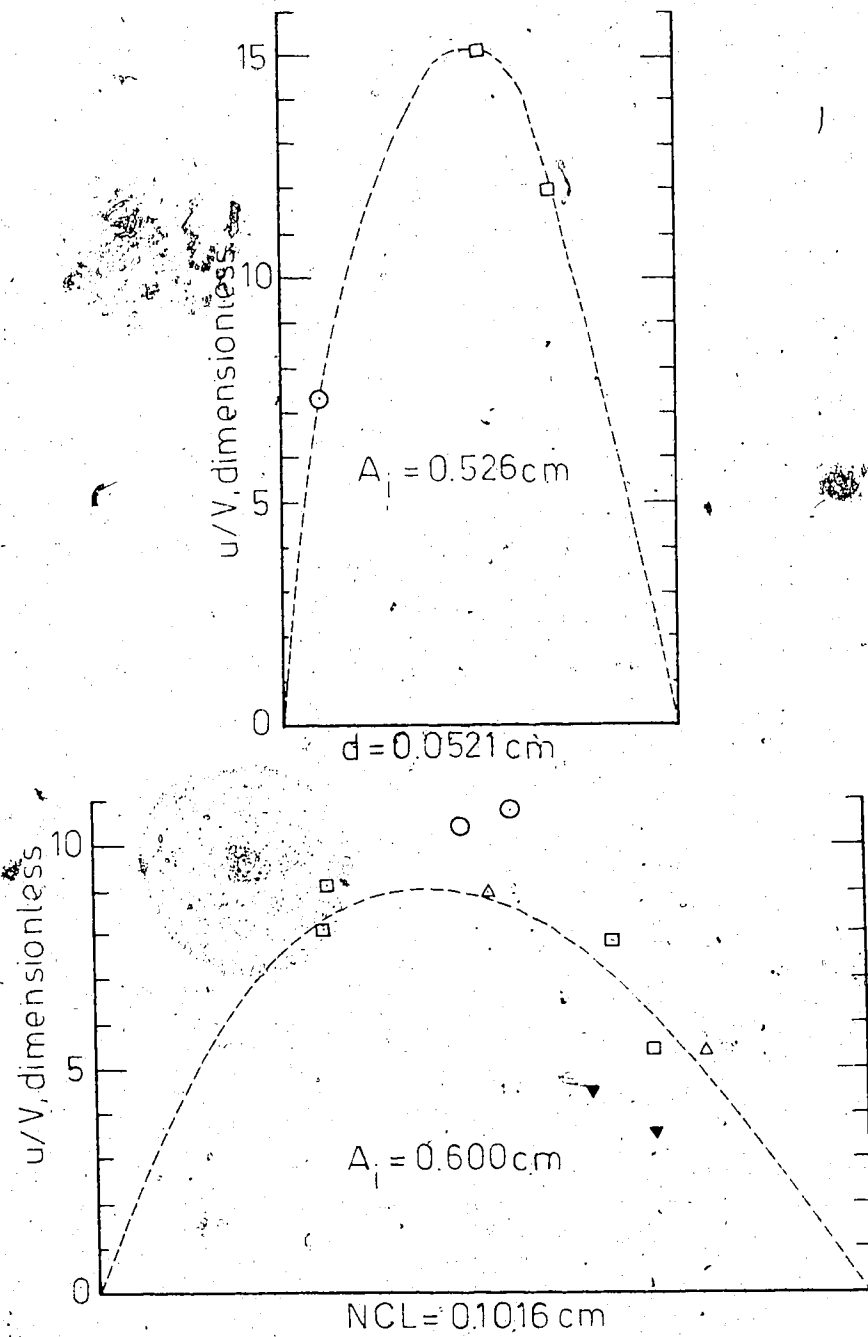


FIGURE IV-8 LOCAL VELOCITY PROFILES OF POSITION NO. 2 — SEPARAN

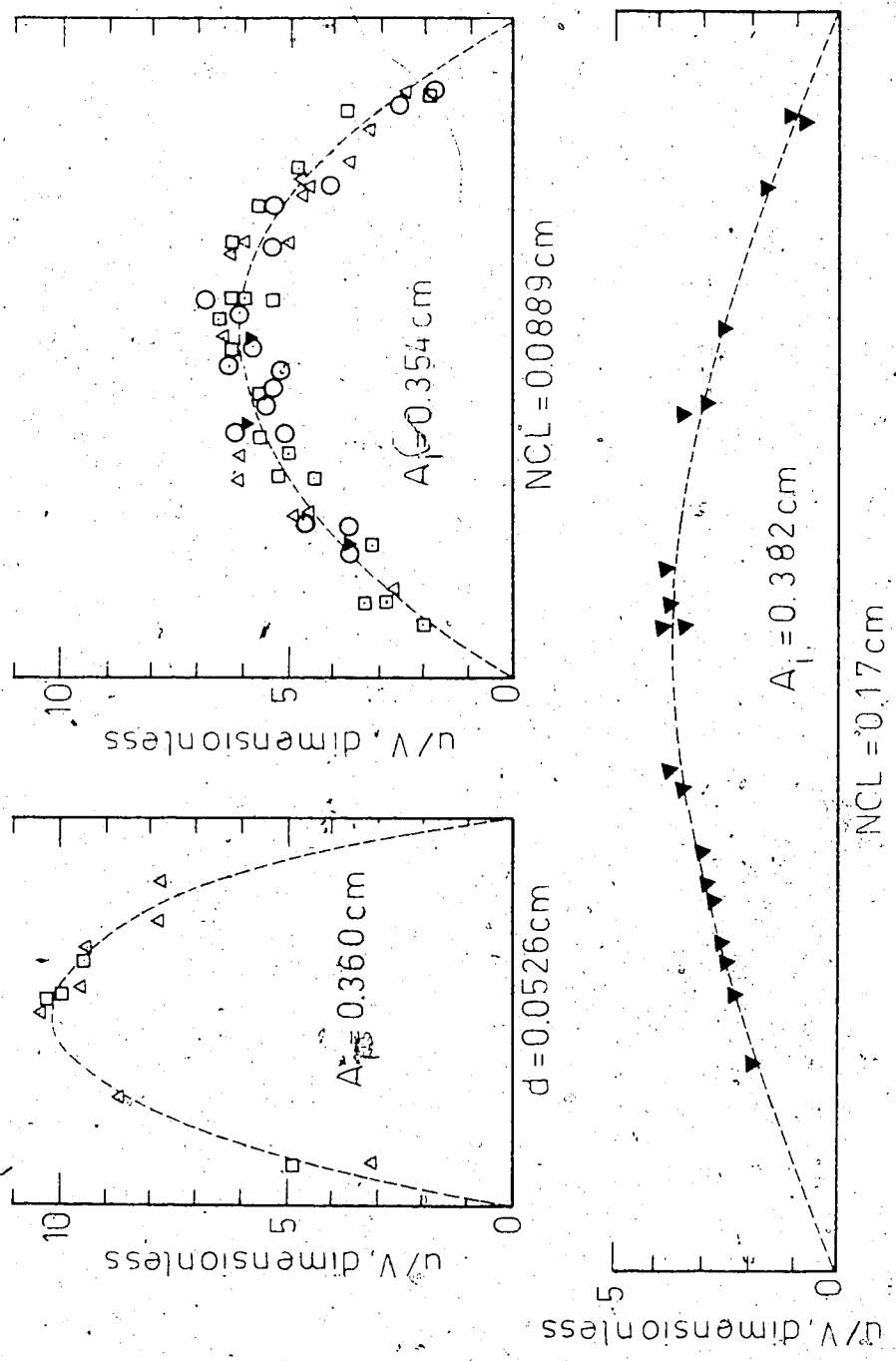


FIGURE IV-9 LOCAL VELOCITY PROFILES OF POSITION NO.17 — GLYCEROL

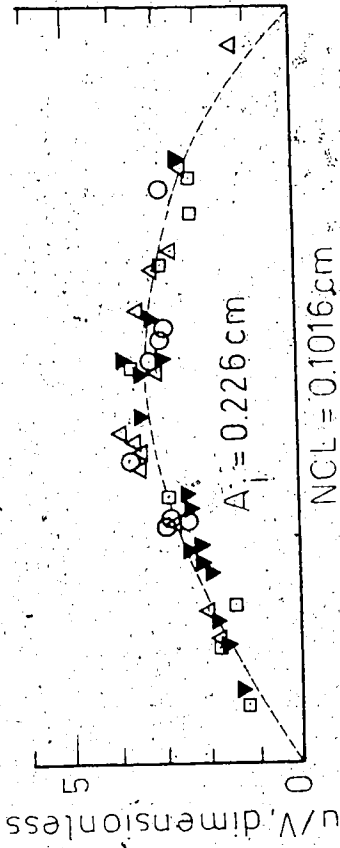
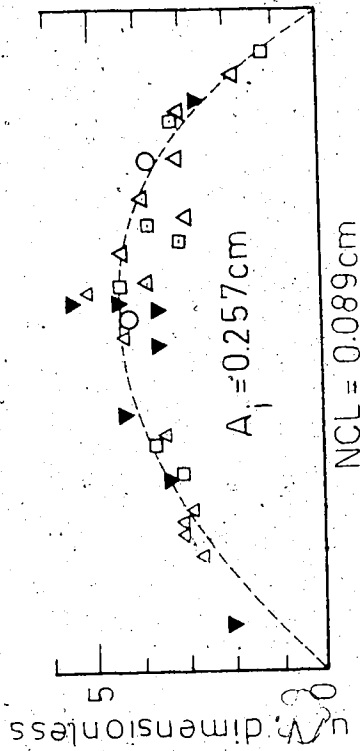
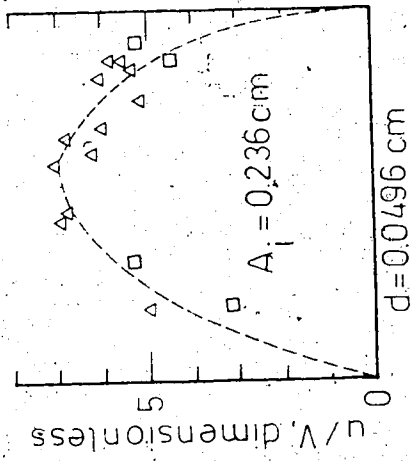


FIGURE IV-10 LOCAL VELOCITY PROFILES OF POSITION NO.17 -- SEPARAN

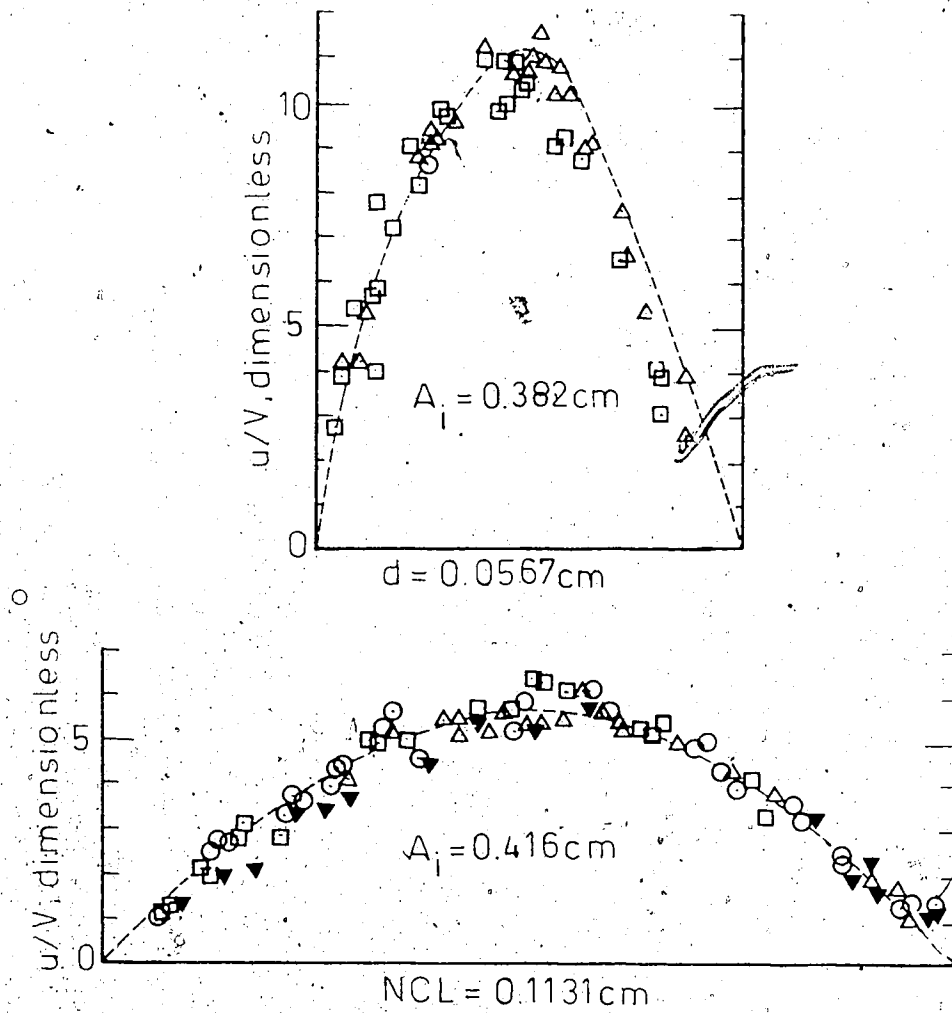


FIGURE IV-11 LOCAL VELOCITY PROFILES OF
POSITION NO. 27 — GLYCEROL

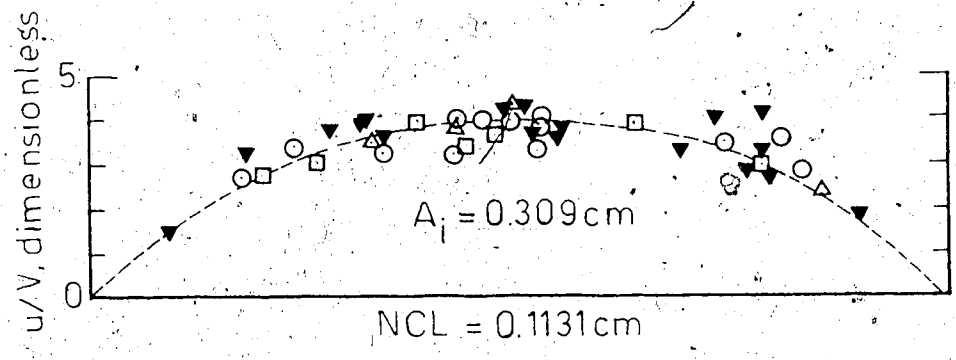
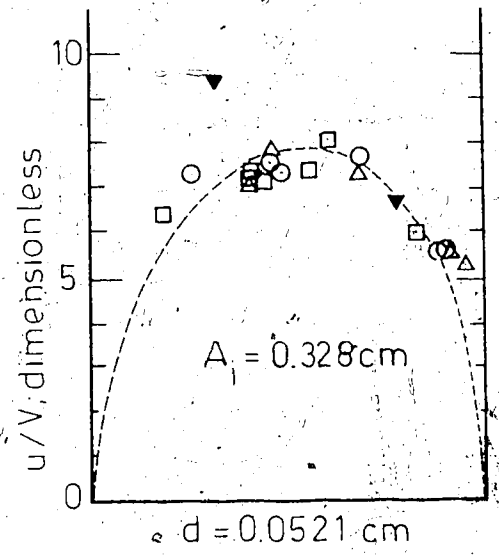


FIGURE IV-12 LOCAL VELOCITY PROFILES OF POSITION NO. 27 — SEPARAN.

in Tables (E-1, 2).

The area under the local velocity profiles as well as the d 's (i.e. center line openings) are given in Table (C-1). It is evident that the area under the velocity profile--in appropriate units--multiplied by the length of the cylinder gives the portion of the flow passing through that specific opening, no matter whether the velocity profile is chosen at d or NCL. This flow rate will be designated by q_i .

It should be noted from Table (C-1) that some of the values of d 's of Glycerol solution runs are different from those of the polymer solution runs, although they were from the same positions. The reason is that, after the runs with polymer solution were completed, the system was taken apart and washed. Therefore, those glass rods which were not perfectly tight in their positions did not return to the same place as before. Also, as was mentioned in Section (III-1), the glass rods were not perfectly uniform; therefore, their relative positions could cause an increase or decrease in d . This, of course, occurred only for a few positions.

The maximum interstitial velocity occurs at the mid-point of d --assuming symmetry in local velocity profile which is not exactly so. Non-symmetry in experimental velocity profiles, which is evident from Figures (IV-7) to (IV-12), is due to nonhomogeneity of the bed. For the positions that the center line local velocity profile could not be obtained, the maximum velocities were calculated by

Equations (D-15,17). The calculated and also experimental values are presented in Table (V-3).

In Figure (IV-13) theoretical parabolic velocity profiles for the flow of Newtonian fluids through parallel plates are compared with experimental data points for three positions. To compare with experimental data points of polymer solution, the velocity profiles predicted from flow of a power-law fluid through parallel plates are also presented in Figure (IV-13). The Equations of these profiles are derived in Appendix D.

Legend:

○ Position No.13

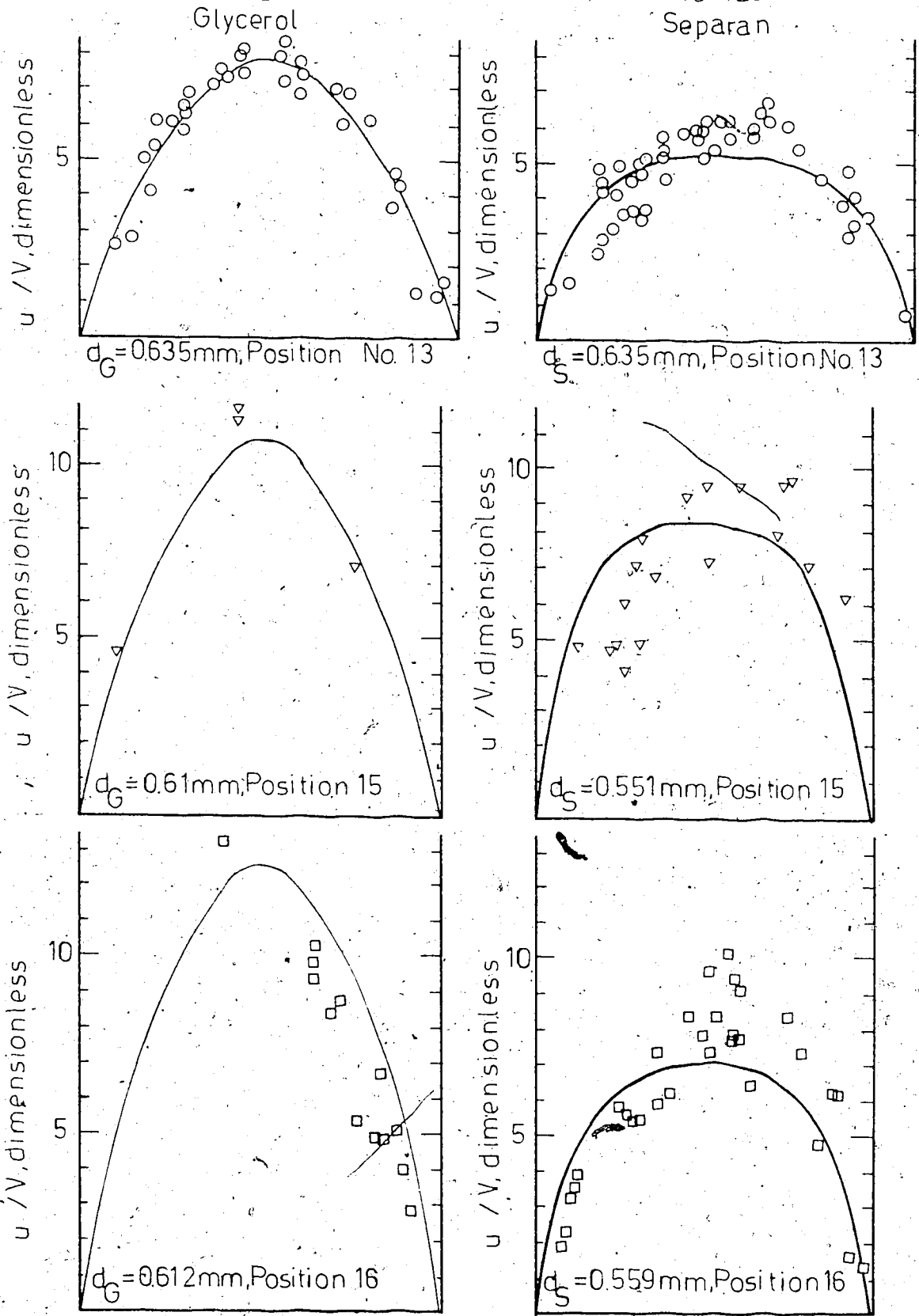
▽ Position No.15

□ Position No.16

— Equation D-14

— Equation D-16

FIGURE IV-13 CENTERLINE VELOCITY PROFILE



CHAPTER V

DISCUSSION OF THE RESULTS

V. 1 Pressure Drop

The linearity of the pressure drop with superficial velocity is evident from Figure (IV-1) which suggests the applicability of Darcy's law, i.e. Equation (I-4). Except for the water data, the empirical correlation of Bergelin, et al. (58) to predict the pressure drop across an ideal bank of tubes is in excellent agreement with the data. The calculations and use of this equation are given in detail in Appendix B. The water data are significantly higher than the predicted line. Since this is simply a Newtonian fluid it is expected inertial effects cause the discrepancy. Although the value of Reynolds number at which inertial effects become important cannot be uniquely defined for different porous media (14b), the particular value for a given media can be determined by experiments over a sufficiently large range of flow rates. Thus the Newtonian data as plotted on Figure IV-3 show that inertial effects become significant at a Reynolds number (defined by Equation II-41) of order unity.

Assuming the flow of the polymer solution is pure viscous, Equation (I-5) which is equivalent to (II-36) can be applied. That is the slope of ΔP v.s. V on log-log coordinates is equal to the power-law parameter, n . The pressure drop

measurement v.s. flow rate for the polymer solution in Figure IV-2 indicates the pseudoplastic nature of the polymer solution. However, the slope varied from approximately 0.35 to 0.92 over the range of flow rates while the slope of the viscometric data ranges from 0.35 to 0.44 in Figure A-3. Note in Figure A-3 the best fit lines have been taken over two portions of the curve to define power-law parameters used in the calculations. This is of little consequence in that calculated parameters, such as Reynolds number are not very sensitive to the exact value of the slope. The large slope at high flow rates and the fact that the Reynolds number is significantly below that at which inertial effects are expected suggest elasticity effects are occurring. Thus predictions for the pressure drop of the polymer solution need to be limited to the lower flow rates.

Different approaches were tried to predict the pressure drop of polymer solution in the bed. First the modified capillary model discussed in Chapter II, then, the empirical correlation of Bergelin, et al. (58) with apparent viscosity was applied. For estimation of apparent viscosity Equation (B-38) was assumed to define the shear rate--refer to Appendix B. To predict P from Equation (I-5), one needs to estimate the viscosity level parameter, H . H for the present model is given by Equation (II-37) in which C_4 and K must be determined, experimentally, by a Newtonian fluid. In Section (IV-1) K was reported to be equal to $1.3 \times 10^{-4} \text{ cm}^2$

and surface porosity for the present model is calculated from (II-21) to be,

$$\epsilon_s = 0.134. \quad (V-1)$$

This value is the arithmetic average of two consecutive rows, one without by-pass channel and the other with two by-pass channels near the walls. The values of K and ϵ_s were used in Equation (II-30) to calculate C_4 .

$$C_4 = 0.682. \quad (V-2)$$

The calculated pressure drop together with H are recorded in Table (B-2) and the complete predicted curve of ΔP v.s. V is shown in Figure (IV-2).

In this approach the openings of parallel plates are taken equal to the minimum center line openings, d . This gives the highest possible value for a characteristic shear rate, therefore, smallest value for viscosity. In view of Equation (I-5), which is equivalent to (II-36), this gives the lowest possible value for ΔP . In fact, in the bed, there is a range of values of viscosity which occur and, therefore, the bed would have a somewhat higher value of average viscosity, and consequently ΔP , than the minimum which comes from the analysis. This problem does not occur for Newtonian; because, μ is constant. In terms of $f_K - N_{Re}$, the low value of viscosity causes higher N_{Re} which makes the data points of Separan systematically shift to the right of Newtonian in Figure (IV-3).

To further show the possibility of elasticity effect,

Deborah number was calculated. Deborah number was defined in Section (I-3) and is rewritten in the following form,

$$N_{\text{Deb}} = 20 \theta_f \frac{\partial u_z}{\partial z} \quad (\text{V-3})$$

Referring to the geometry of the bed $\partial u_z / \partial z$ can be estimated via maximum velocity at center line openings. According to Figure (V-1),

$$\frac{\partial u_z}{\partial z} = \frac{\bar{u}_{\text{max}} - 0}{\Delta z} = \frac{\bar{u}_{\text{max}}}{\Delta z} \quad (\text{V-4})$$

Δz is approximately 0.33 cm for the present model and \bar{u}_{max} is the average value of the maximum velocities at center line openings for two consecutive rows. To be on the conservative side, the shear dependent relaxation time was used for θ_f which was read from Figure (A-4). This required shear rate to estimate θ_f . The value of shear rate occurring at the minimum opening is of the order of,

$$\sigma = \frac{u_m}{d/2} = \frac{2u_m}{d} \quad (\text{V-5})$$

and,

$$u_m = \frac{q_i}{d} \quad (\text{V-6})$$

Therefore,

$$\sigma = \frac{2q_i}{d^2} \quad (\text{V-7})$$

Recorded values of σ in Table (V-1) are the arithmetic average value of two consecutive rows. That is q_i/d^2 at a given flow in the bed has been averaged for opening in

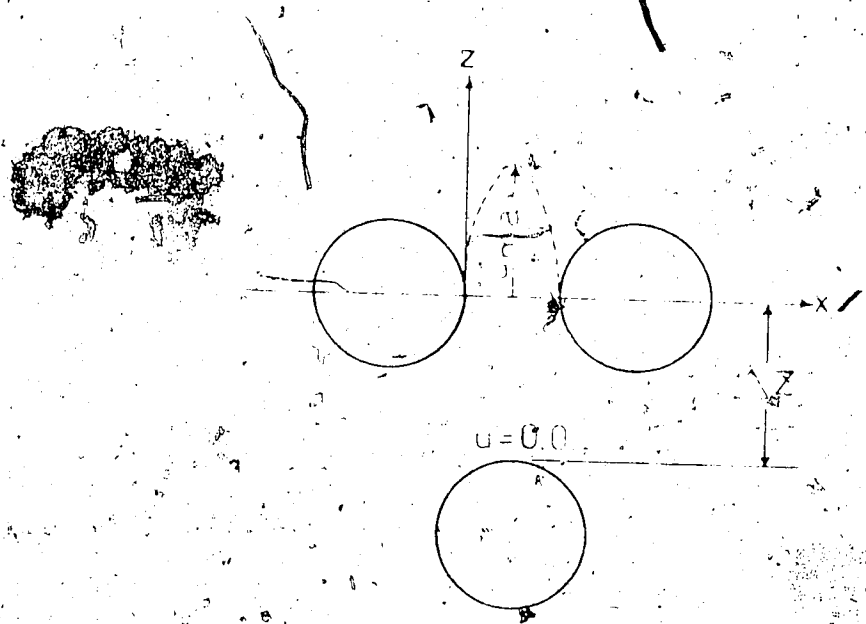


FIGURE V-1 ESTIMATION OF ELONGATIONAL RATE

TABLE (V-1)

FLOW PARAMETERS OF 0.2% SEPAKAN SOLUTION

BUN NO.	q cc/sec	\bar{u} sec ⁻¹	\bar{u} sec	\bar{u}_{max} cm/sec	$\partial u_z / \partial z$ sec ⁻¹	N_{Deb} Dimensionless	$f_{KN} Re$ Dimensionless
1	0.431	3.09	0.68	0.113	0.337	0.458	1.33
2	0.685	4.91	0.47	0.18	0.537	0.505	1.31
3	0.835	6	0.4	0.219	0.654	0.523	1.31
4	1.07	7.68	0.33	0.281	0.839	0.554	1.16
5	1.49	10.7	0.25	0.392	1.17	0.585	1.228
6	1.717	12.3	0.24	0.451	1.343	0.645	1.262
7	2.13	15.28	0.19	0.56	1.67	0.634	1.278
8	2.17	15.58	0.18	0.57	1.7	0.612	1.317
9	2.725	19.55	0.15	0.716	2.137	0.64	1.29
10	3.39	24.3	0.13	0.899	2.68	0.697	1.3
11	3.42	24.55	0.13	0.899	2.68	0.697	1.31
12	4.27	30.6	0.11	1.122	3.35	0.737	1.41
13	4.28	30.6	0.11	1.122	3.35	0.737	1.336
14	5.38	38.55	0.089	1.422	4.24	0.755	1.388

TABLE (V-1) (continued)

RUN NO.	q cc/sec	sec-l	u _{max} cm/sec	u _z /az sec-l	N _{Deb} Dimensionless	f _K x N _{Re} Dimensionless
15	5.41	38.8	1.422	4.24	0.755	1.388
16	5.76	48.4	1.8	5.37	0.785	1.418
17	6.84	49.1	1.8	5.37	0.785	1.51
18	8.53	61.1	2.255	6.72	0.82	1.267
19	8.58	61.6	2.255	6.72	0.82	1.35
20	10.76	77.1	2.85	8.5	0.897	1.31
21	10.84	77.7	2.85	8.5	0.897	1.41
22	13.6	97.7	3.58	10.69	0.897	1.34
23	13.62	97.7	3.58	10.69	0.897	1.445
24	17.06	122.2	4.51	13.43	0.94	1.476
25	17.19	123	4.51	13.43	0.94	1.517
26	21.52	154	5.65	16.85	0.976	1.586
27	27.25	195.8	7.16	21.37	1.023	1.76
28	34.35	246	9.02	26.9	1.076	1.968

the two rows.

Calculated Deborah numbers are presented in Table (V-1). According to Marshall and Metzner (45), the magnitude of Deborah number is high enough to expect significant elasticity effect. As mentioned in Section (I-3), Marshall and Metzner revealed that appreciable influences of the fluid elasticity were observed when Deborah number, defined by Equation (I-13), reached 0.05-0.06 or, defined by Equation (V-3), reached 0.2-0.24. It is noted that Deborah number defined by Equation (V-3) is four times as large as that of Equation (I-13).

In Figure (V-2), $f_{K, Re} N_{De}$ was plotted v.s. Deborah number for polymer solution. The upward deviation of the data points at high flow rates, is similar to that observed by Marshall and Metzner (45), although the analysis is not sufficient to indicate when this might occur in the figure.

V. 2 Streamlines

The elasticity effect predicted by Ultman, et al. (42) in the flow past a submerged cylinder is obviously present in photograph No. 1 in Figure (IV-4). The early bulge of the upstream streamlines, the earlier return to undisturbed flow downstream of the rod and the non-symmetry of the flow are characteristic behavior of viscoelastic fluid flow past a submerged cylinder. The approach velocity which was calculated from the length of streaks was $U=0.437$ cm/sec.

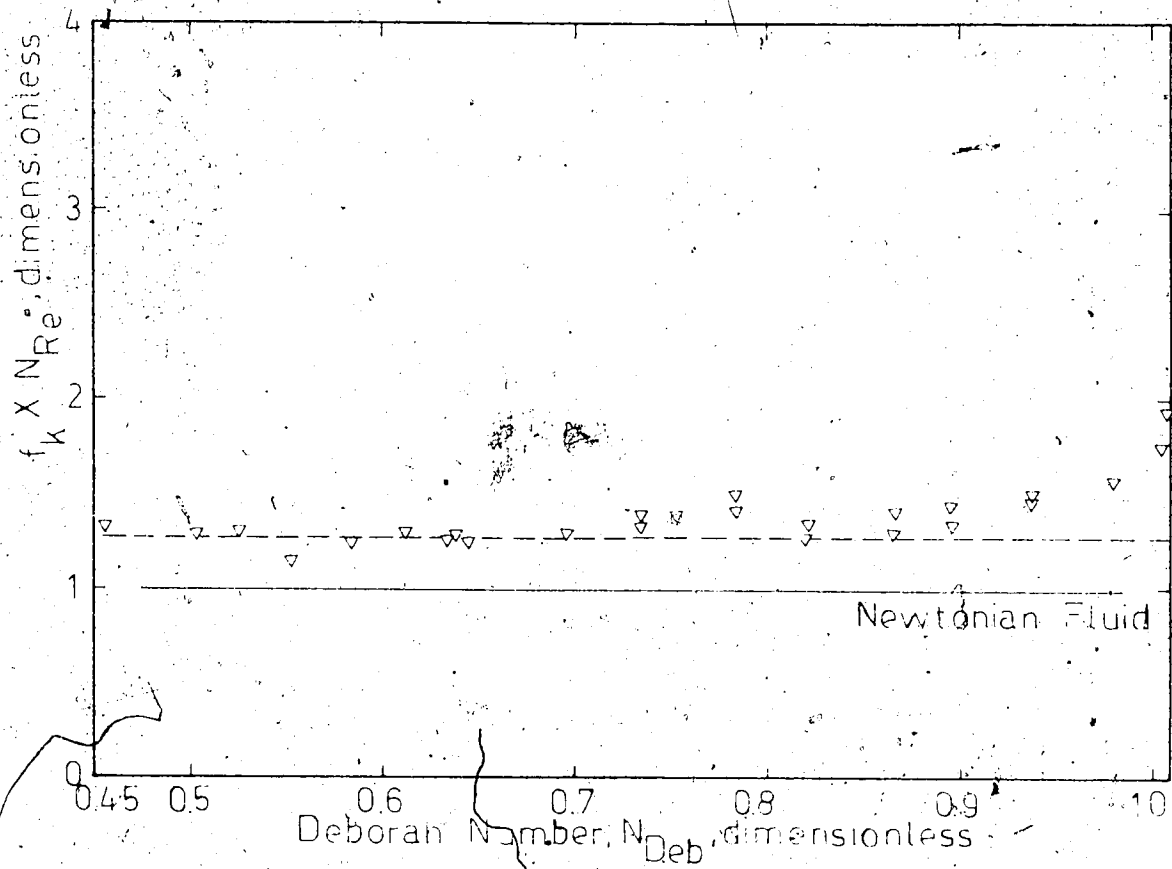


FIGURE V-2 DEPENDENCE OF ELASTICITY EFFECT UPON THE DEBORAH NUMBER OF THE FLOW PROCESS

Reynolds number is defined as,

$$Re_c = \frac{\rho U D}{\mu_0} \quad (V-9)$$

where density, $\rho = 1$, diameter of the rod, $D = 0.326$ cm, and $\mu_0 = 42$ poise is the limit of viscosity at low shear rate.

Therefore,

$$Re_c = 0.00339. \quad (V-10)$$

also, Weissenberg number is calculated by Equation (I-11) in which to be consistent with Ultman, et al. (42), $\theta_0 = 3.126$ sec was estimated from Bueche's theory, i.e. Equation (A-6). Therefore,

$$N_{we} = 4.19. \quad (V-11)$$

To compare the situation prevailing in the submerged bank of rods with that of single submerged rod, the following justification is made. The average velocity at the center line opening is taken as the approach velocity,

$$U \equiv u_m = \frac{Q}{A c_s} \quad (V-12)$$

The flow rates studied varied from 0.685 to 6.85 cc/sec, therefore, approach velocities varied from $U = 0.151$ cm/sec to 1.51 cm/sec. The other parameters remained the same.

Therefore,

$$Re_c = 0.00216 \text{ to } 0.0216, \quad (V-13)$$

$$N_{we} = 0.787 \text{ to } 7.87. \quad (V-14)$$

By comparing the Reynolds and Weissenberg numbers of bank of glass rods with those of single rod, it was felt that the range of flow rates studied was broad enough to cover any elasticity effects observable in the shape of the streamlines.

The initial goal of photographic study was to seek if the bulge effect for the polymer solution would be intensified by the presence of the other rods. The behavior could be, hopefully, related to the increased microscopic sweep efficiency in polymer flooding. However, on observation of streamlines in the bed it was apparent that simple determination of the streamlines would not clearly show the major differences in flow field of the two fluids. Therefore, the direction of study was changed and focused on local velocity profiles and flow distribution.

V. 3 Visual Observations:

Visual observations were limited to the positions along rows 19 to 23 for Glycerol and Separan. The flow rates studied were $q = 0.685, 1.717, 3.42$ and 6.85 cc/sec. The observations at points where the flow was anomalous revealed some significant differences between Newtonian and polymer solution. The positions where anomalous behavior

occurred with the description of the peculiarity are given in Figures (V-3, 4). These positions are where no flow exists, i.e. dead zones, flow is slow compared to the normal neighborhood openings, or the flow is in the opposite direction of the normal flow direction. It is noticed from Figures (V-3, 4) that the number of anomalous points for Newtonian fluid are 15 while those from polymer solution are only 5. The observed difference, especially the number of dead zones or nearly dead zones, might be a good qualitative explanation of the increased microscopic sweep efficiency in polymer flooding. These points were usually near the walls where by-pass flow existed, however, this situation is not unexpected in the oil reservoir fields.

The above observed distinguished difference imply that the streamlines are not the same for Glycerol and Separan solutions. This is also revealed in section (V. 4) by observing the difference in flow distribution.

V. 4 Local Velocity Profiles and Flow Distribution

It is clearly observed from Figures (IV-7) to (IV-12) that the local velocity profiles were not the same in the different openings. That is the small

DESCRIPTION OF ANOMALOUS BEHAVIOR

1. Very small flow, in the opposite direction of the normal flow direction at $q=0.685, 1.717, 3.42, \text{ and } 6.85$ cc/sec.
2. Very small flow at $q=0.685$ cc/sec.
3. Same as (1).
4. Same as (1).
5. Same as (1).
6. Almost no flow at $q=0.685, 1.717$ cc/sec. and same as (1) at $q=3.42, 6.34$ cc/sec.
7. Almost no flow at all four flow rates.
8. Same as (7).
9. Same as (1).
10. Very small flow at all four flow rates.
11. Same as (10).
12. Same as (2).
13. Same as (1).
14. Same as (10).
15. Same as (10).

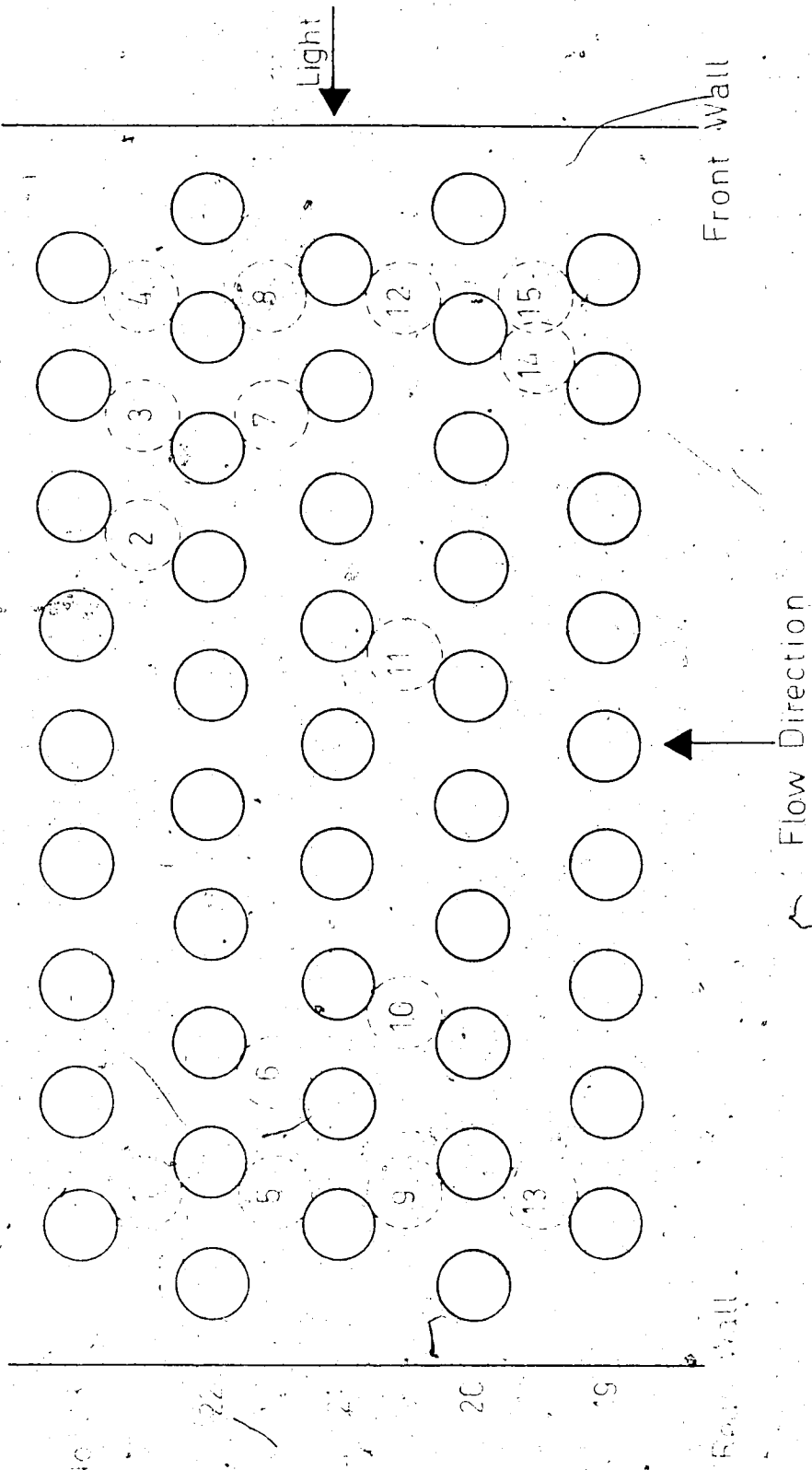


FIGURE V-3 VISUAL OBSERVATION - GLYCEROL

DESCRIPTION OF ANOMALOUS BEHAVIOR

1. Almost no flow at $q=0.685$ cc/sec. and very small flow at $q=1.717$, 3.42 , and 6.85 cc/sec.

Very small flow in the opposite direction of the normal flow direction at $q=0.685$, 1.717 , 3.42 and 6.85 cc/sec.

Almost no flow at $q=0.685$, 1.717 cc/sec. and very small flow at $q=3.42$, 6.85 cc/sec.

Very small flow at $q=0.685$, 1.717 , 3.42 , and 6.85 cc/sec.

Almost no flow at $q=0.685$, 1.717 , and 3.42 cc/sec. and very small flow at $q=6.85$ cc/sec.

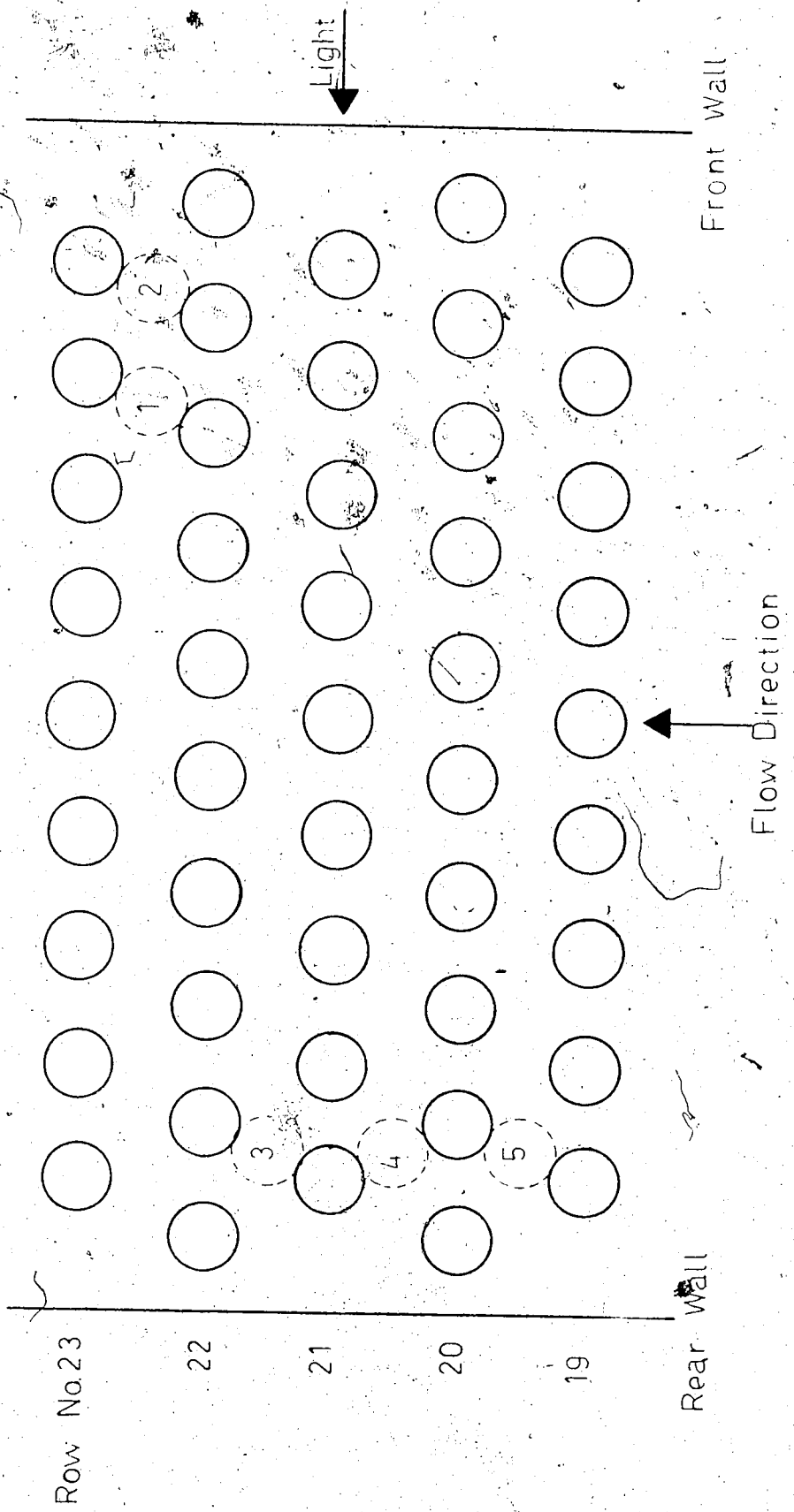


FIGURE V-4 VISUAL OBSERVATION - SEPARAN

inhomogeneity of the bed caused significant differences in velocity profiles. Also, the local velocity profiles of glycerol show larger differences between positions than those of Separan. This shows that the nonhomogeneity has less effect on polymer solution than Newtonian. To emphasize the differences in flow distribution, the maximum velocities at the center line openings of rows 20, 21 and 22 are plotted against position for Glycerol and Separan solutions in Figures (V-5) to (V-7). The maximum velocities of the positions which could not be determined directly--due to the difficulty involved in photography at the center line positions--were calculated by Equations (D-15, 17). The justification for this can be found in Table (V-2) where the predicted and experimental maximum velocities are compared. In all cases, except one or two, quantitative agreement was obtained. No usable pictures could be taken from position No. 3 of polymer solution runs--neither at center line nor at NCL. The flow rate through this position was calculated by subtracting the sum of the flow rates passing the other openings of row No. 20 from the total flow rate.

From Figures (V-5) to (V-7) it is clear that there is a greater variation in velocity at the center of the openings of glycerol than with Separan. It should be noticed that the value of u_{\max}/V for position No. 3 in Figure (V-5) as

TABLE V-2
 MAXIMUM VELOCITIES AT CENTER LINE OPENINGS
 u_{\max}/V , DIMENSIONLESS

Position No.	Glycerol		Separan	
	Calc.	Exp.	Calc.	Exp.
1	23.5	?	31.1	?
2	18.65	18.5	14.2	14.66
3	14.16	?	5.42	?
4	12.7	?	10.76	?
5	11.4	?	8.64	?
6	14.8	?	8.3	9.16
7	10.56	10.28	8.14	8.63
8	12.1	12.32	7.27	8.05
9	16.9	17.1	9.82	10.28
10	13.4	13.14	12.9	?
11	16.93	?	10.7	?
12	6.92	6.57	7.9	8.64
13	7.62	7.6	5.06	6.16
14	10.56	?	7.52	?
15	10.28	11.1	8.35	9.25
16	12.1	12.33	6.57	8.22
17	10.02	9.86	6.29	6.57
18	15.53	14.8	8.06	9.45
19	7.56	?	6.82	7.97
20	6.9	?	6.82	7.4

TABLE V-2 (continued)

Position No.	Glycerol		Separan	
	Calc.	Exp.	Calc.	Exp.
21	4.89	4.11	3.8	3.9
22	24.5	?	34.6	?
23	21	?	25	?
24	10	10	6.95	8.85
25	16.55	16.24	8.85	9.87
26	11.36	10.78	6.42	7.82
27	10.4	10.7	7.53	7.82
28	10.7	10.28	6.79	8.1
29	16.03	?	8.24	9.17
30	15.06	?	8.64	10.17
31	13.54	13.6	12.7	?
32	17.5	?	17.4	?

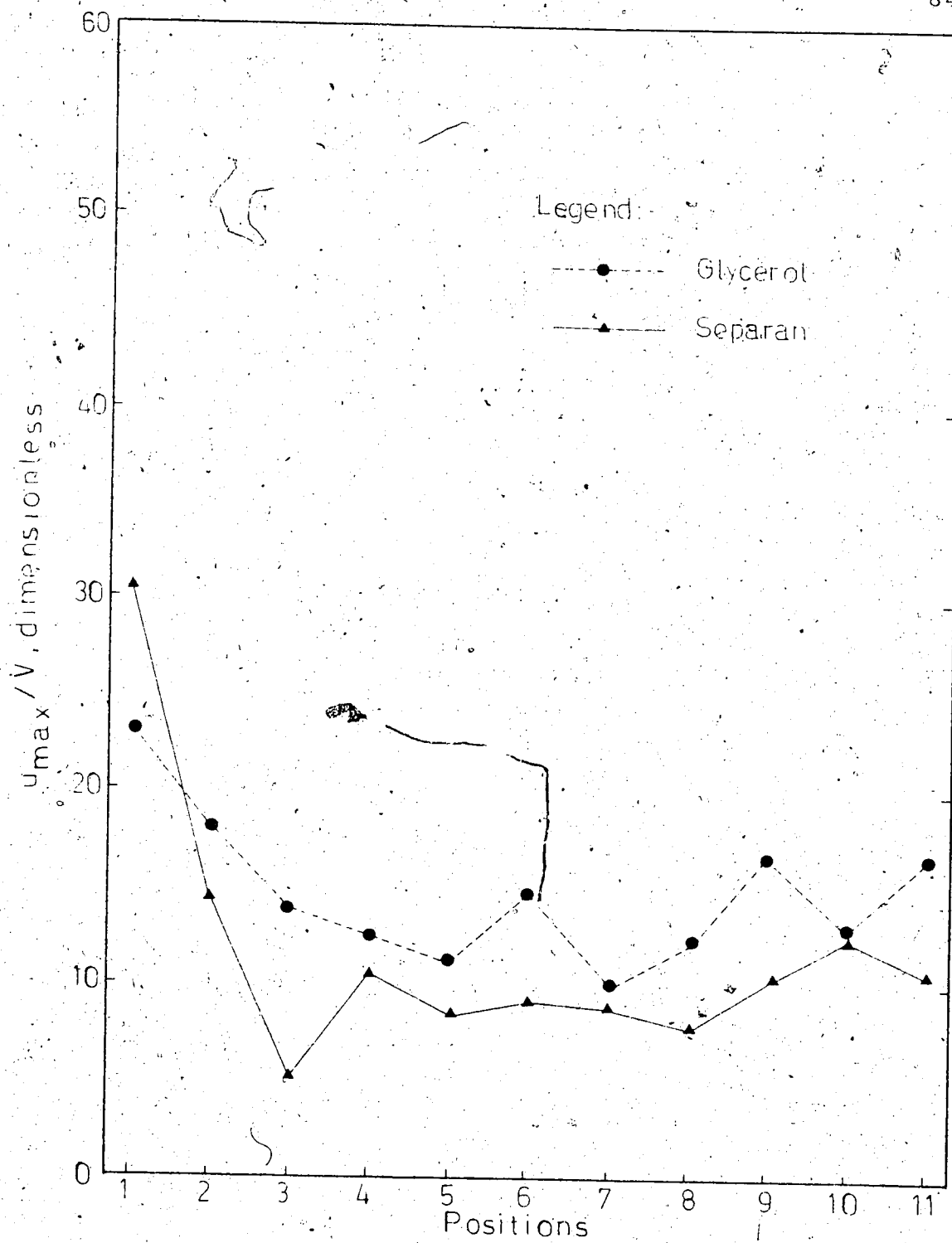


FIGURE 11.5. MAXIMUM VELOCITY

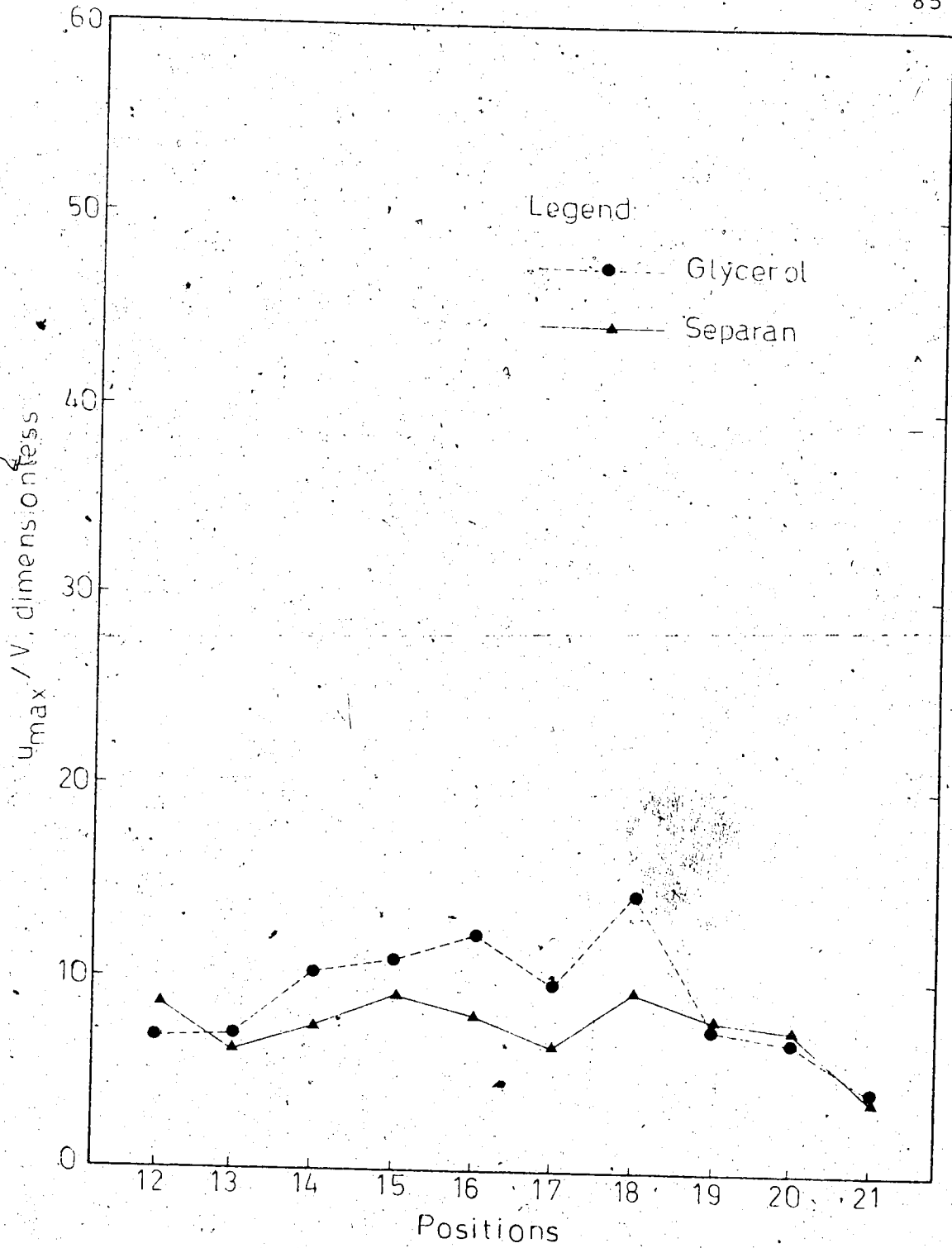


FIGURE V-6 MAXIMUM CENTER-LINE VELOCITIES
ROW NO.21

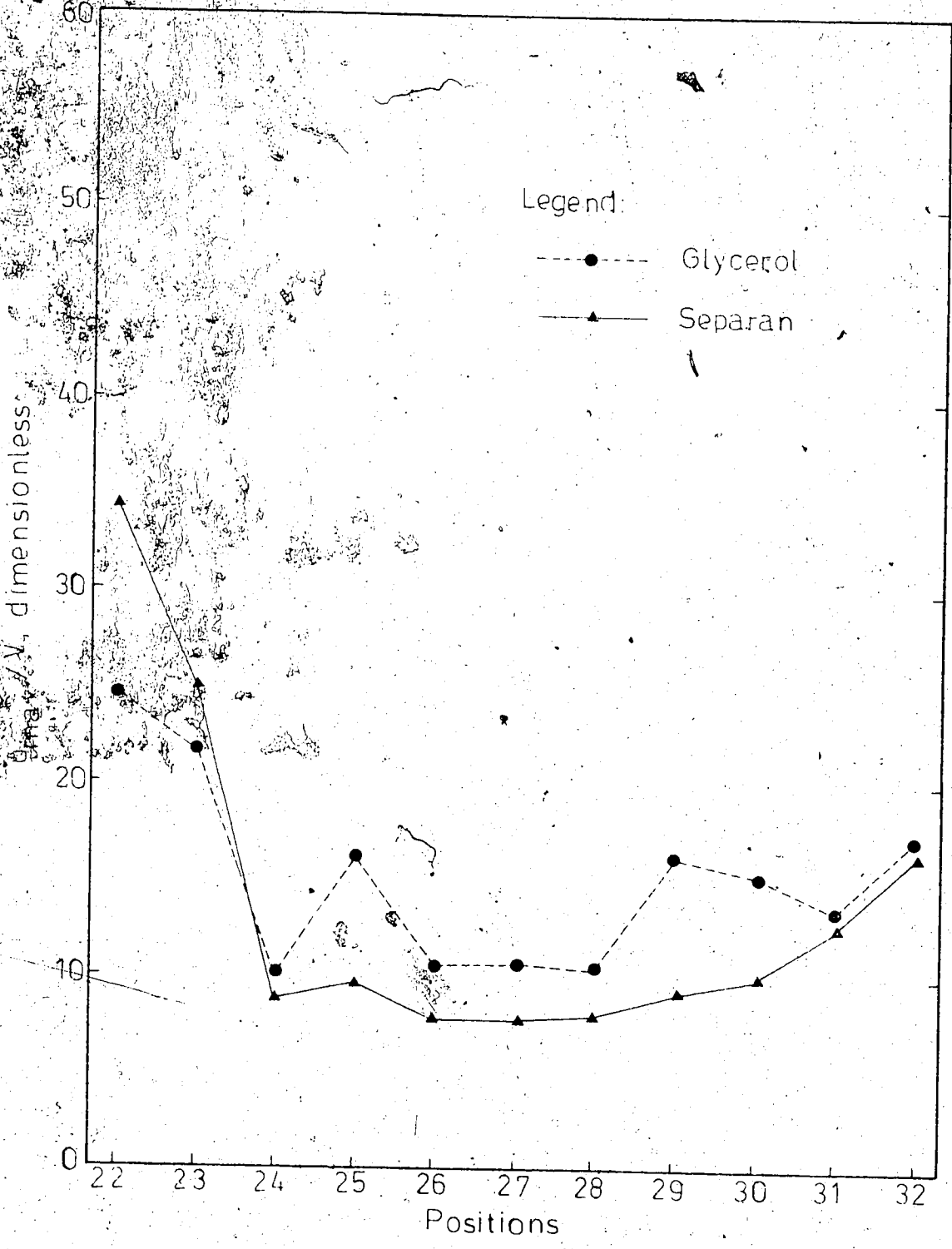


FIGURE V-7 MAXIMUM CENTER LINE VELOCITIES ROW NO.22

mentioned before is uncertain. Also, as was mentioned before, the openings of some positions have changed from Glycerol runs to Separan which makes a detailed position by position comparison without accounting for the openings invalid.

The three curves of maximum velocities were added together to find the final resultant. They are presented in Figures (V-8, 9). Again, same kind of behavior observed for the single row in Figures (V-5, 6, 7) is noticed. The resultant curve for Separan in Figure (V-9) is much smoother than that for Glycerol in Figure (V-8). To clarify the qualitative conclusion derivable from Figures (V-8, 9), let us assume a straight undisturbed line of fluid particles before row No. 20. The shape of this line of fluid particles after passing through rows No. 20, 21 and 22 would be, roughly, the resultant curve--assuming that the major disturbances were at the minimum center line openings.

It is also shown from Figures (V-5, 6, 7) that the flow rate passing through positions 1, 12 and 22, which are next to the wall, are significantly larger for the case of Separan than those of Glycerol. The increase in by-pass flow should not only be attributed to the wall effect, but the relative magnitude of the openings next

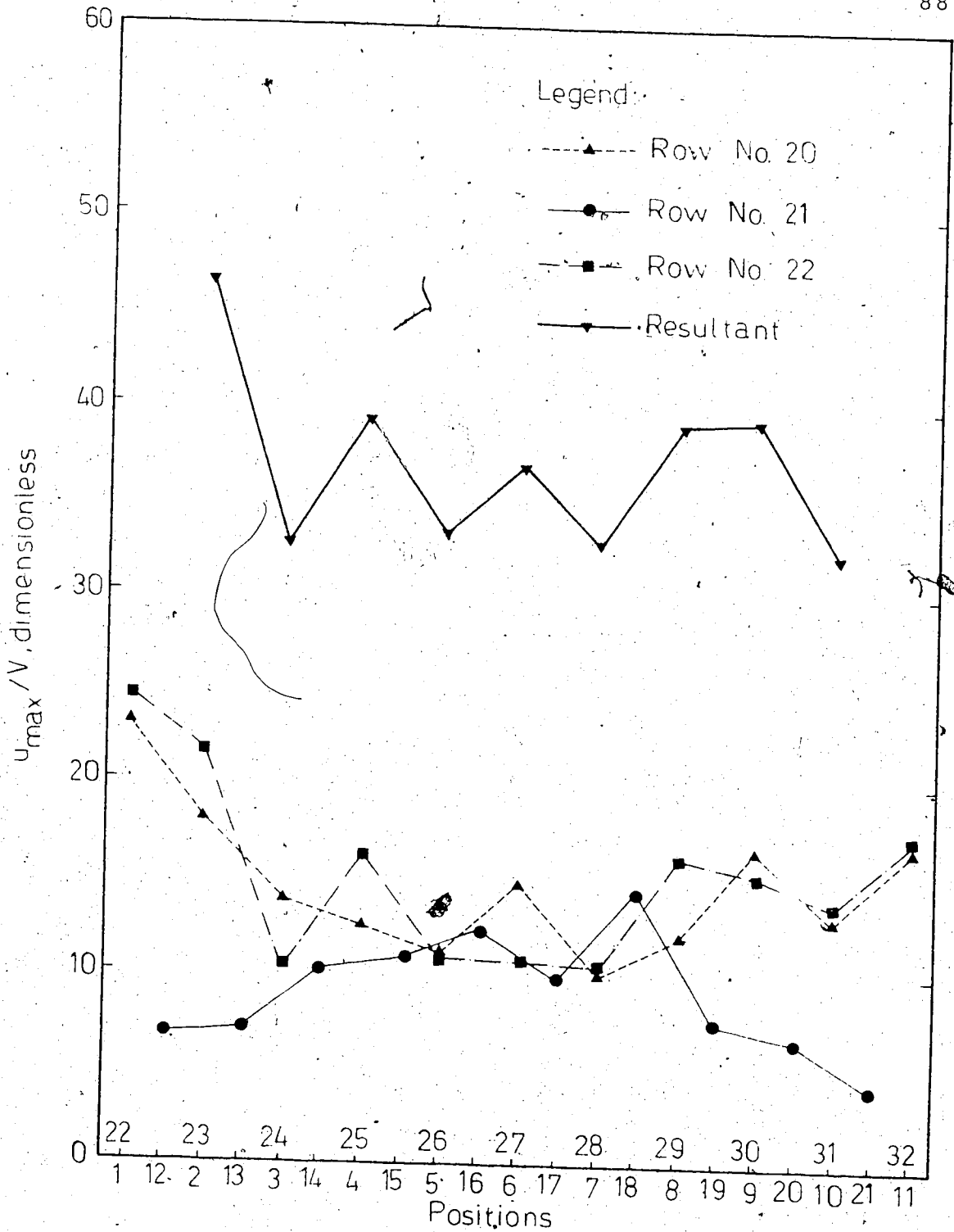


FIGURE V-8 RESULTANT OF MAXIMUM CENTER LINE VELOCITIES OF THREE ROWS - GLYCEROL

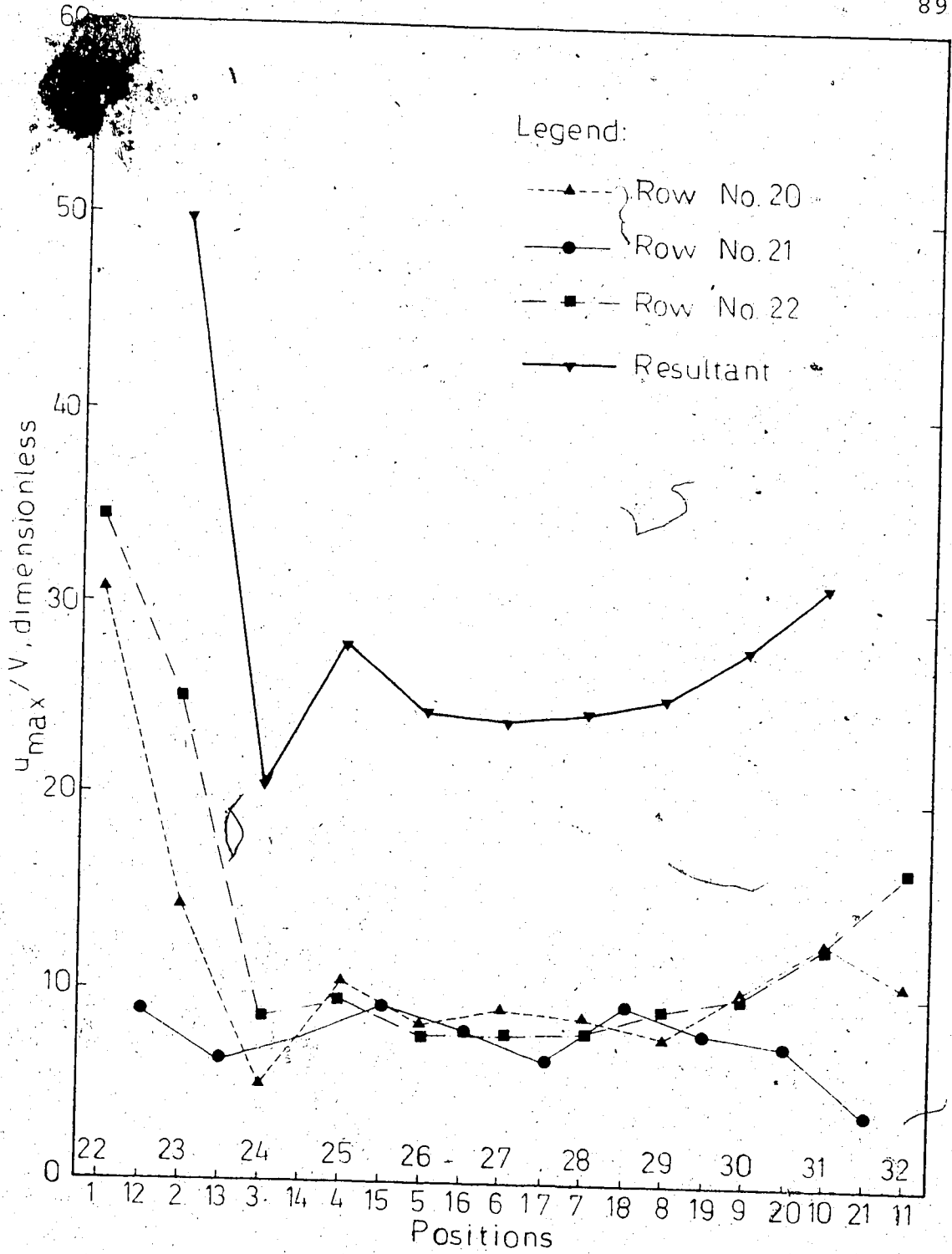


FIGURE V-9 RESULTANT OF MAXIMUM CENTER LINE VELOCITIES OF THREE ROWS - SEPARAN

to the walls and also the effect of the other neighborhood openings.

To eliminate the effect of by-pass flow, the following procedure was undertaken. Positions 1, 2, 10, 11, 12, 13, 21, 22, 23, 31 and 32 which were near the walls were ignored. The flow rates of the remaining openings of each row were added together. Then the percentage of this total flow rate passing through each opening of a row was calculated. These values will be referred to as "corrected fractional flow rates", f . This procedure makes it also possible to compare, quantitatively, the flow rates of the individual openings in different rows. Since every alternate row has two by-pass openings and more flow rate will pass from these openings, therefore, less flow would be available for the openings far from the walls comparing with the openings of those rows without by-pass channel. However, by applying the above procedure, all the remaining openings of the three rows are scaled up on the same basis. Corrected fractional flow rates are recorded in Table (V-3), but fractional flow rates without applying by-pass correction are presented in Table (C-1).

An attempt was made to find the behavior of flow

TABLE (V-3)

CORRECTED FRACTIONAL FLOW RATES

Position No.	d_G/d_{min} Dimensionless	d_S/d_{min} Dimensionless	f_G Dimensionless	f_S Dimensionless
3	1.54	1.54	12.7	?
4	1.74	1.38	12.8	15.14
5	1.71	1.48	11.32	12.9
6	2.03	2.03	17.5	17.1
7	1.66	1.66	10.2	13.65
8	1.73	1.73	12.1	12.77
9	2.38	2.01	23.4	20
14	2	2	15.5	17.1
15	1.84	1.67	12.9	15.9
16	1.85	1.69	15.27	12.6
17	1.59	1.5	10.83	10.73
18	2.04	2.04	21.6	18.7
19	1.575	1.575	12.2	12.2

TABLE (V-3) (continued)

Position No.	d_G/d_{min} Dimensionless	d_G/d_{min} Dimensionless	f_G Dimensionless	f_S Dimensionless
20	1.645	1.645	11.6	12.77
24	1.69	1.69	10.5	12.6
25	2.03	2.03	20.8	19.3
26	1.64	1.54	11.57	10.57
27	1.71	1.58	11.07	12.78
28	1.54	1.54	10.23	11.3
29	2.04	2.04	20.36	18.1
30	1.65	1.65	15.44	15.3

distribution with respect to pore openings. Equation (D-8) predicts that the flow rate varies with opening to the power $(1 + 2n)/n$. Since $n < 1$, it is expected that the effect of openings is aggravated for pseudoplastic fluid compared to Newtonian in which $n = 1$. In Figures (V-10) and (V-11), corrected fractional flow rates for Glycerol and Separan, respectively, are plotted v.s. dimensionless openings, i.e. d/d_{\min} , where $d_{\min} = 0.33\text{mm}$ is the minimum d from Table (C-1). The line with slope 3 is the theoretical equation for a Newtonian fluid through parallel plates, i.e. Equation (D-11), and the line with slope 4.5 in Figure (v-11) is presenting Equation (D-8) with $n = 0.4$. It is evident from Figures (V-10,11) that the effect of openings on polymer fractional flow rates is somewhat less than expected theoretically. Furthermore a line with slope even less than 3, probably, will fit the experimental data points of Separan.

Since the openings are coupled, i.e. the effect of the neighborhood openings can not be eliminated; therefore, the data points of Figures (V-10, 11) are expected to be scattered. However, f_G is a measure of local permeability and portrays the combined effect of the neighborhood openings. Since the fractional flow rates of Glycerol and Separan are directly proportional to local permeability, therefore, it is felt that a plot of f_G and f_S v.s. $f_G d_G$ and $f_G d_S/d_{\min}$, respectively, will be less scattered. These are presented in Figures (V-12, 13). The eye-fit line passing through the points of Figure (V-13) has less slope

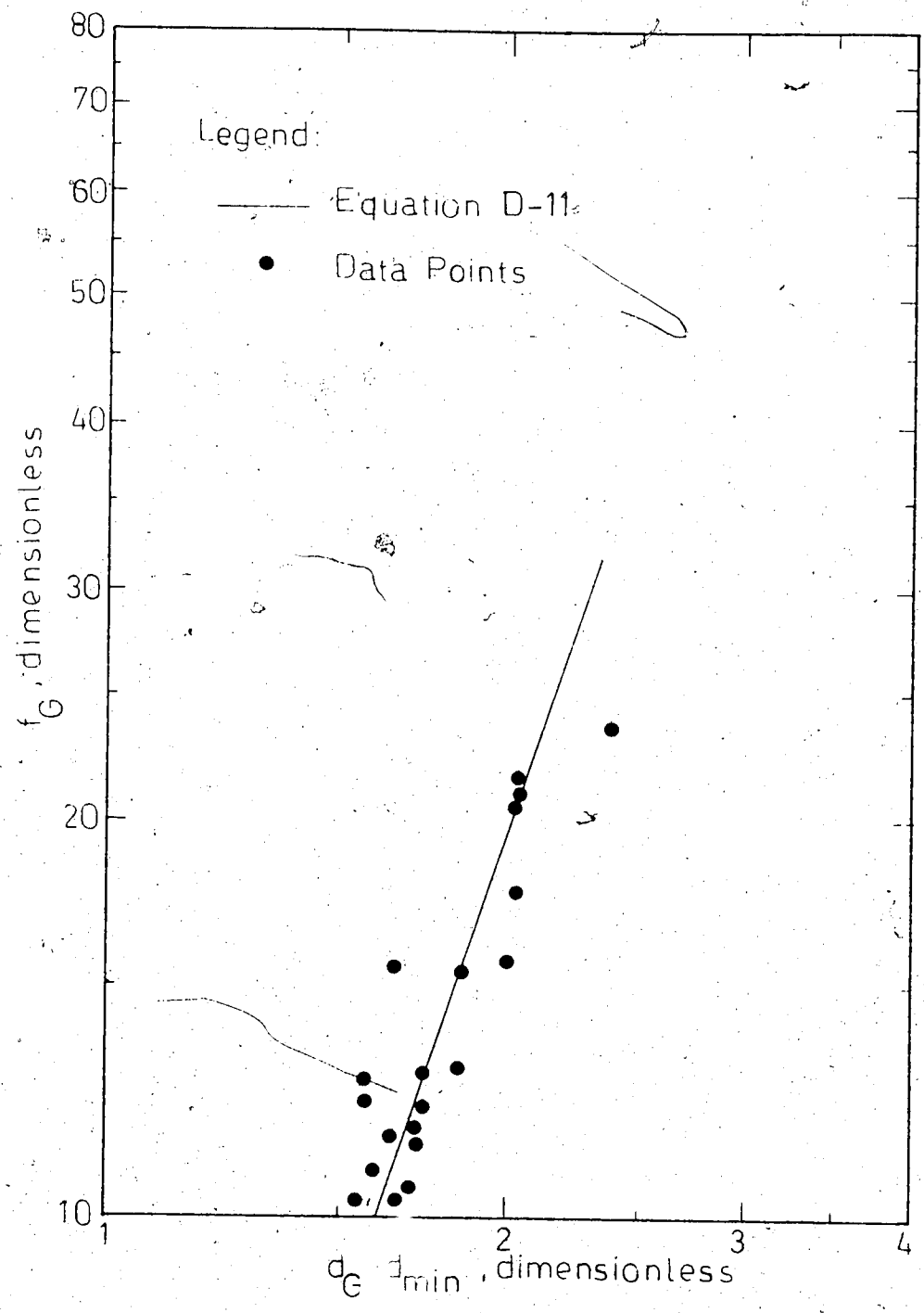


FIGURE V-10 FLOW DISTRIBUTION WITH OPENING, GLYCEROL

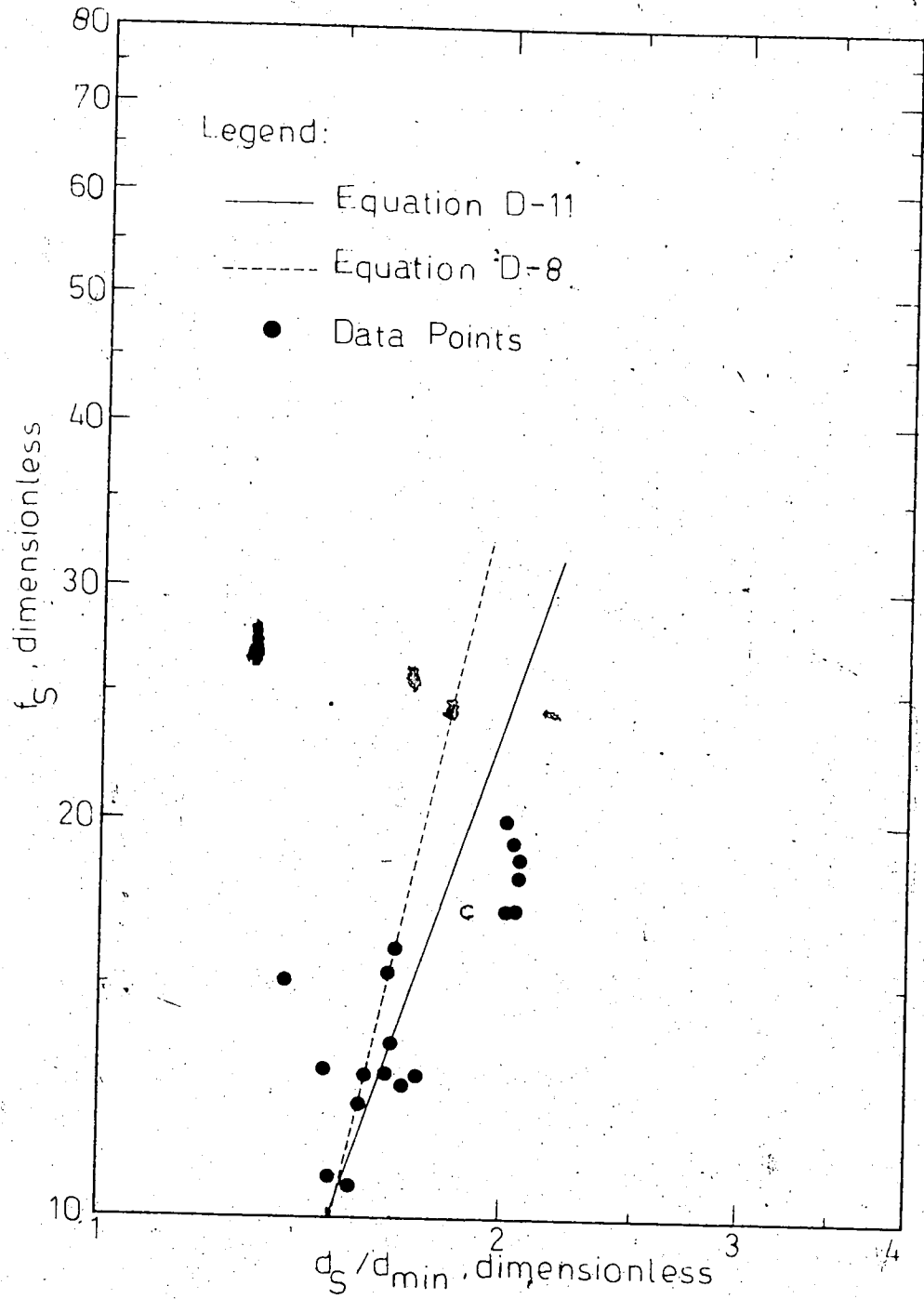


FIGURE V-11 FLOW DISTRIBUTION WITH OPENING, SEPARAN

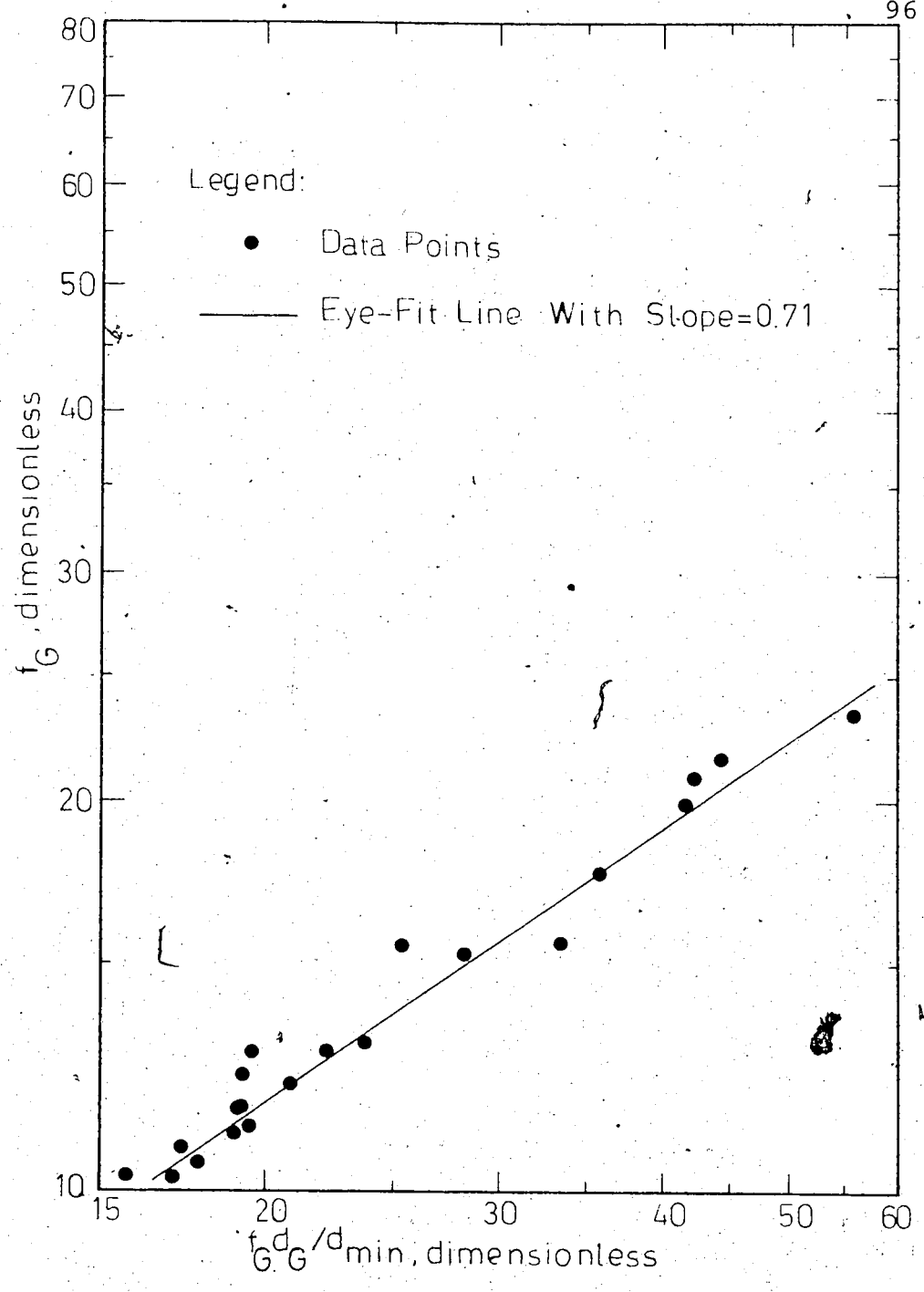


FIGURE V-12 FLOW DISTRIBUTION WITH OPENING, GLYCEROL

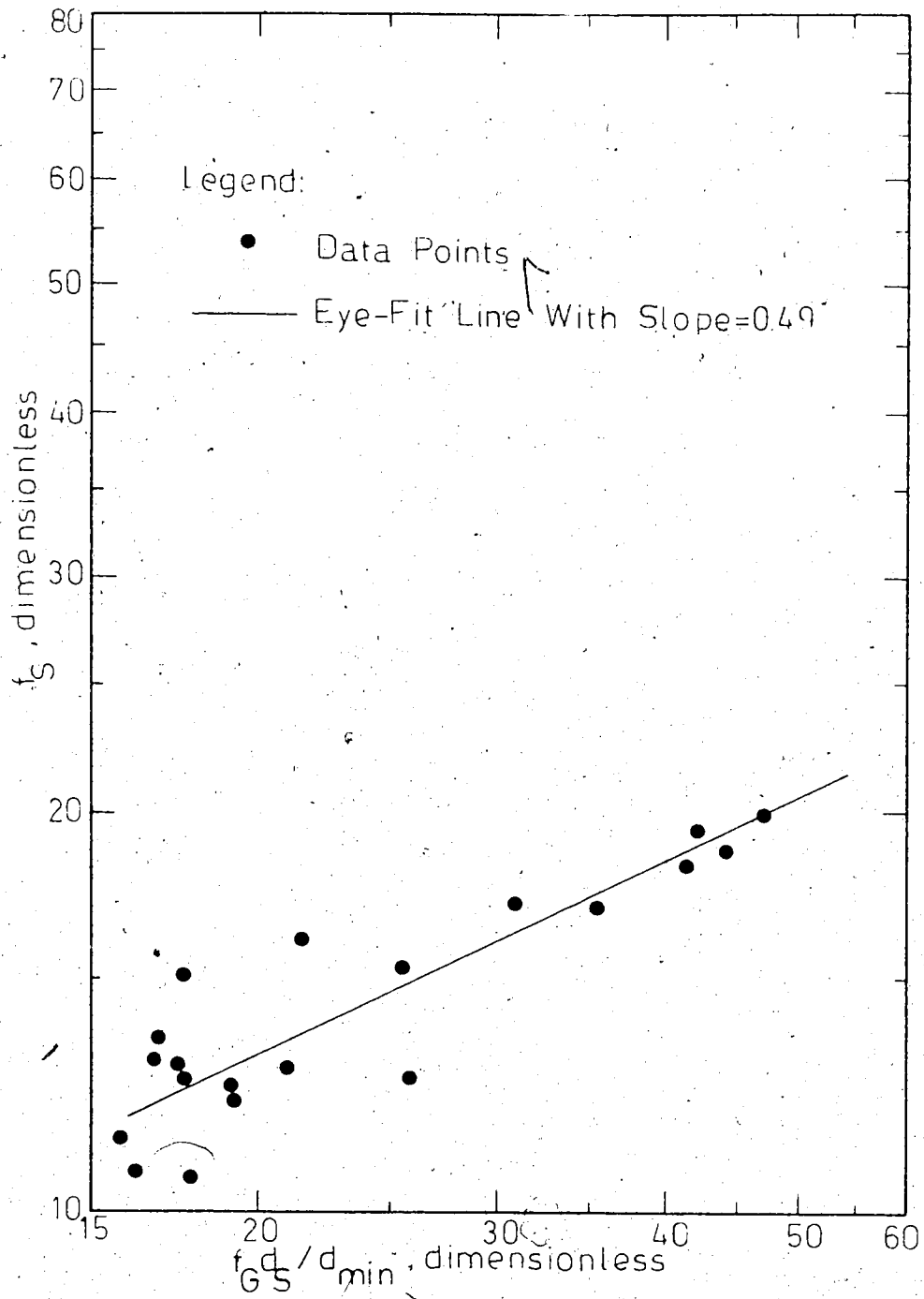


FIGURE V-13 FLOW DISTRIBUTION WITH OPENING,
SEPARAN

than that of Figure (V-12) which confirms the former discussion. From Figure (V-12) one can conclude,

$$f_G \sim (f_G d_G)^{0.71} \quad (V-15)$$

or, approximately,

$$f_G \sim d^3 \quad (V-16)$$

And from Figure (V-13),

$$f_S \sim (f_G d_S)^{0.5} \quad (V-17)$$

or, substituting for f_G from (V-16),

$$f_S \sim d^2 \quad (V-18)$$

That is the fractional flow rates of the Glycerol solution is proportional with the openings to the power three, while those of Separan solution is proportional with the openings to the power two.

The fact that the effect of openings is suppressed due to the use of polymer solution may have major effects on the stability of a displacement front: one via conventional dispersion and the other via dispersion coefficient.

According to Scheidegger (14a), the most conservative dependency of dispersion coefficient on interstitial velocity is,

$$C_D = b_1 u \quad (V-19)$$

where C_D is dispersion coefficient, b_1 , a constant, and u , interstitial velocity. This implies that by adding some little amount of polymer to the water not only the nonuniform interstitial velocities will tend to be more uniform, but the

effect of non-homogeneity of the bed on dispersion coefficient would, also, be damped out.

The above experimental observation reveals that the flow distribution of polymer solution in the bed can not be predicted simply by power-law model and some other effects such as elasticity have a significant influence. The failure of the power-law model in prediction of the flow behavior of polymer solution is also shown by direct comparison of the experimental data with predicted velocity profiles. The experimental data and predicted velocity profiles by power-law were given for positions No. 13, 15 and 16 in Figure (IV-13). As it is noticed from the Figure (IV-13), the experimental data of Glycerol solution is fairly close to the parabola obtained from flow of Newtonian fluid through parallel plates. In contrast, although not shown vividly by the particular profiles plotted, predicted power-law profiles are significantly flatter than the polymer solution data. This feature is best shown by Table (V-2) where the calculated values of \bar{u}_{\max}/V , which are based on power-law fluid flow through parallel plates, are, without exception, less than the experimental values.

CHAPTER VI.

CONCLUSIONS AND RECOMMENDATIONS

VI. 1 Conclusions

The following are the main conclusions of this study.

1. Nonhomogeneity of the bed affected the flow distribution significantly. The effect of polymer solution was to suppress variations in velocity with pore opening to levels even below those for Newtonian fluids.

2. The experimental velocity profiles for Glycerol solution were consistent with prediction for Newtonian fluid flow through parallel plates. On the other hand those of the polymer solution were much more rounded than the predicted velocity profiles for a power-law fluid.

3. Consistent with earlier studies, increased pressure drop because of elasticity were observed. However, these occurred at flow rates in excess of those at which velocity measurements were made. Therefore, the elasticity of the fluid affects the flow distribution before it affects the pressure drop.

4. Qualitative visual observations revealed that the number of the dead zones or nearly dead zones and recirculation regions for polymer solution were reduced relative to

the Newtonian case. This implies the possibility of enhanced displacement efficiency in a microscopic sense.

VI. 2 Recommendations

1. Two-phase flow, i.e. displacing oil with Newtonian and also polymer solution in the present bed, could be useful in visualizing fingering which, hopefully, could be related to the present single phase behavior. It is recommended that the by-pass channels be eliminated in the future model design.

2. A study of local velocity profiles and flow distribution should be undertaken using the same kind of model with more diversified pore size distributions.

BIBLIOGRAPHY

1. Sandiford, B. B. "Laboratory and Field Studies of Water Floods Using Polymer Solutions to Increase Oil Recoveries." J. Pet. Tech., (August, 1964), p. 917.
2. "History of Petroleum Engineering." A Publication of the American Petroleum Inst., (1961), p. 850.
3. Muskat, M. "Physical Principles of Oil Production." McGraw-Hill Book Co. Inc., (1949), p. 648.
4. Aronofsky, J. S. "Mobility Ratio-Its Influence on Flood Patterns During Water Encroachment." Trans. AIME, 195 (1952), p. 15.
5. Aronofsky, J. S., and Ramey, H. J., Jr. "Mobility Ratio--Its Influence on Injection or production Histories in Five-Spot Water Flood." Trans., AIME, 207 (1956), p. 205.
6. Hurst, W. "Determination of Performance Curve in Five-Spot Water Flood." Petroleum Engineer, 25, P.B.-40 (April 1953).
7. Craig, F. F., Jr., Geffen, T. M., and Morse, K. A. "Oil Recovery Performance of Pattern Gas or Water Injection Operations from Model Tests." Trans., AIME, 204, (1955), p. 7.
8. Dyes, A. B., Candle, B. H., and Erickson, R. A. "Oil Production After Breakthrough as Influenced by Mobility Ratio." Trans. AIME, 201, (1954), p. 81.
9. Mahaffey, J. L., Rutherford, W. M., and Mathews, C. S. "Sweep Efficiency of Miscible Displacement in a Five-Spot." Soc. Pet. Eng. J., 6 (March 1966), p. 73.
10. Slobod, R. L., and Candle, B. H. "X-Ray Shadowgraph Studies of Areal Sweepout Efficiencies." Trans. AIME, 195 (1952), p. 265.
11. Slobod, R. L., and Thomas, R. A. "Effect of Transverse Diffusion on Fingering in Miscible-Phase Displacement." Soc. Pet. Eng. J. (March 1963), p. 9.

12. Caudle, B. H., and White, M. S. "Production Potential Changes During Sweep-Out in a Five-Spot System." *Trans., AIME*, 216 (1959), p. 446.
13. Collins, R. E. "Flow of Fluids Through Porous Materials." Reinhold Publishing Corporation, New York: (1961), p. 174.
14. Scheidegger, A. E. "The Physics of Flow Through Porous Media." University of Toronto Press, (a) p. 69, (b) p. 160, (c) p. 259 (1963).
15. Christopher, R. H., and Middleman, S. "Power-Law Flow Through a Packed Tube." *I & EC Fundamentals*, 4, No. 4 (November 1965), p. 422.
16. Pirson, S. J. "Oil Reservoir Engineering." McGraw-Hill Book Co. Inc., (a) p. 558, (b) p. 560, (1958).
17. Welge, H. J. "A Simplified Method for Computing Oil Recovery by Gas or Water Drive." *Trans., AIME*, 195, (1952), p. 91.
18. Jones, M. A. "Waterflood Mobility Control: A Case History." *J. Pet. Tech.* 18 (September 1966), p. 1151.
19. Mungan, N. "Improved Waterflooding Through Mobility Control." Paper prepared for the 19th Canadian Chemical Engineering Conference and 3rd Symposium on Catalysis, Edmonton, Alberta (October 1969).
20. Mungan, N., Smith, F. W., and Thompson, J. L. "Some Aspects of Polymer Floods." *J. Pet. Tech.*, 18 (September 1966), p. 1143.
21. Stiles, W. E. "Use of Permeability Distribution in Water-Flood Calculations." *Trans., AIME*, 186 (1949), p. 9.
22. Dykstra, H., and Parsons, R. L. "The Prediction of Oil Recovery by Water Flood." *Secondary Recovery of Oil in the United States*, API, New York: (1950), p. 160.
23. Pye, D. J. "Improved Secondary Recovery by Control of Water Mobility." *J. Pet. Tech.* (August 1964), p. 911.
24. Gogarty, W.B. "Mobility Control with Polymer Solutions." *Soc. Pet. Eng. J.*, 7 (June 1967), p. 161.
25. Dauben, D. L., Menzie, D. E. "Flow of Polymer Solutions Through Porous Media." *J. Pet. Tech.* (August 1967), p. 1065.

26. Slater, G. E., and Farough Ali, S. M. "Prediction of Sweep Efficiency in Polymer Flooding." *Prod. Monthly*, 32, No. 10 (October 1968), p. 22.
27. Lee, K. S., and Claridge, E. L. "Areal Sweep Efficiency of Pseudoplastic Fluids in a Five-Spot Hele-Shaw Model." *Soc. Pet. Eng. J.* (March 1968), p. 52.
28. Smith, F. W. "The Behavior of Partially Hydrolyzed Polyacrylamide Solutions in Porous Media." *J. Pet. Tech.* (February 19), p. 148.
29. McCartney, J. A., and Sloat, B. "Polymer Reduce Risk in Waterflooding." *Pet. Eng.*, (December 1970), p. 74.
30. Lozanski, W. R., and Martin, I. "Taber South-Canada's First Polymer Flood." Paper prepared for the 21st Annual Technical Meeting of the Petroleum Society of CIM in Calgary, Alberta (May 1970).
31. White, J. L., Goddard, J. E., and Phillips, H. M. "Use of Polymers to Control Water Production in Oil Wells." *J. Pet. Tech.* (February 1973), p. 143.
32. Jewett, R. L., and Schurz, G. F. "Polymer Flooding --A Current Appraisal." Paper prepared for the 44th Annual Fall Meeting of the Society of Petroleum Engineers of AIME, Denver, Colorado: September 28-October 1, 1969.
33. Ustick, R. E., and Hillhouse, J. D. "Comparison of Polymer Flooding and Water-Flooding at Huntington Beach, California." *J. Pet. Tech.*, 19 (September 1967), p. 1103.
34. Jennings, R. R., Rogers, J. H., and West, T. J. "Factors Influencing Mobility Control by Polymer Solutions." *J. Pet. Tech.* (March 1971), p. 391.
35. Burcik, E. J. "A Note on the Flow Behavior of Polyacrylamide Solutions in Porous Media." *Prod. Monthly*, 29 No. 6, (June 1965), p. 14.
36. _____. "Pseudo Dilatant Flow of Polyacrylamide Solutions in Porous Media." *Prod. Monthly*, 31, No. 3 (March 1967), p. 27.
37. Burcik, E. J., and Ferrer, J. "The Mechanism of Pseudo Dilatant Flow." *Prod. Monthly*, 32, No. 3 (March 1968), p. 7.

38. Burcik, E. J. "What, Why and How of Polymers for Waterflooding." *Pet. Eng.* (August 1968), p. 60.
39. _____, and Walrond, K. W. "Microgel in Polyacrylamide Solutions and Its Role in Mobility Control." *Prod. Monthly*, 32, No. 9, (September 1968), p. 12.
40. Lynch, E. J., and MacWilliams, D. C. "Mobility Control with Partially Hydrolyzed Polyacrylamide--A Reply to Emil Burcik." *J. Pet. Tech.*, 21 (October 1969), p. 1247.
41. Patton, J. T., Coats, K. H., and Colegrave, G. T. "Prediction of Polymer Flood Performance." *Soc. Pet. Eng. J.*, (March 1971), p. 72.
42. Ultman, J. S. "Viscoelastic Uniform Streaming Flow Past Submerged Obstacles." Ph.D. dissertation, University of Delaware, Newark: (1970).
43. Harvey, A. H. "An Investigation of the Flow of Polymer Solutions Through Porous Media." Ph.D. dissertation, University of Oklahoma, Norman (1967).
44. Sadowski, T. J., and Bird, R. B. "Non-Newtonian Flow Through Porous Media." *Trans. Soc. Rheol.*, 9 (2), (1965), p. 243.
45. Marshall, R. J., and Metzner, A. B. "Flow of Viscoelastic Fluids Through Porous Media." SPE paper 1687, prepared for the Society of Petroleum Engineers Symposium on Mechanics of Rheologically Complex Fluids, Houston, Texas: December 15-16, 1966.
47. Astarita, G. "Two Dimensionless Groups Relevant in the Analysis of Steady Flows of Viscoelastic Materials." *I & EC Fundamentals*, 6, No. 2 (May 1967), p. 257.
48. Gaitonde, N. Y., and Middleman, S. "Flow of Viscoelastic Fluids Through Porous Media." SPE Paper 1685, prepared for the Society of Petroleum Engineers Symposium on Mechanics of Rheologically Complex Fluids, Houston, Texas: December 15-16, 1966.
49. Harrington, R. E., and Zimm, B. H. "Anomalous Plugging of Sintered Glass Filters by High Molecular Weight Polymers." *J. Polymer Science, Part A-2*, 6 (1968), p. 294.
50. Jones, W. M., and Maddock, J. L. "Flow of Viscoelastic Liquids: Comparison of Departures from Laminar Flow in Porous Beds and in Tubes." SPE Paper 1686, (ont.)

prepared for the Society of Petroleum Engineers
symposium on Mechanics of Rheologically Complex
Fluids, Houston, Texas: December 15-16, 1966.

51. Savins, J. G. "Non-Newtonian Flow Through Porous Media." I & EC, 16, No. 10 (October 1969), p. 18.
52. Ford, R. B., Stewart, W. E., and Lightfoot, E. N. "Transport Phenomena." John Wiley & Sons, Inc. (a) p. 62, (b) p. 79, (c) p. 197 (1966).
53. McKelvey, J. M. "Polymer Processing." John Wiley & Sons, Inc. (1962), p. 100.
54. Ergun, S. "Fluid Flow Through Packed Columns." Chem. Eng. Prog., 48, No. 2 (1952), p. 89.
55. Kyle, C. R., and Perrine, R. L. "An Experimental Model for Visual Studies of Turbulent Flow in Porous Materials." C. J. Ch. E., 49 (February 1971), p. 19.
56. Rollin, A. L. "Similarity Laws and Turbulence Structure of Drag Reducing Fluids." Ph.D. dissertation, University of Alberta, Edmonton (1971).
57. Catania, P. Ph.D. dissertation, under print, University of Alberta, Edmonton (1973).
58. Bergelin, O. P., Bell, K. J., and Leighton, M. D. "Heat Transfer and Fluid Friction During Flow Across Banks of Tubes." VII "By-passing Between Tube Bundle and Shell." Chem. Eng. Prog. Symposium Series, 55, No. 29 (1959), p. 45.
59. Ishihara, K. "Incompressible Viscous Flow Across Banks of Tubes at Low Reynolds Numbers." Ph.D. dissertation, Oklahoma State University (1971).
60. Boger, D. V., and Rama Murthy, A. V. "Normal Stress Measurement and Evaporation Effects on the Weissenberg Rheogoniometer." Trans. Soc. Rheol., 13 (1969), p. 405.
61. The Weissenberg Rheogoniometer, Instruction Manual, Model R. 18, Sagamo Controls limited, Section D, Theory.
62. Seyer, F. A., and Metzner, A. B. "Turbulence Phenomena in Drag Reducing Systems." AIChE J., 15, No. 3 (May 1969), p. 426.
63. Middleman, S. "The Flow of High Polymers." Interscience Publishers (1968), p. 148.

APPENDIX A

RHEOLOGICAL PROPERTIES OF THE SOLUTIONS

A WEISSENBERG Rheogoniometer was used to measure viscosity of the Glycerol and polymer solutions. It was calibrated with a standard oil. Also, normal forces were measured for polymer solution to estimate relaxation time of the solutions. To eliminate the surface evaporation of the solution at the edge of the platen a thin film of a light nonvolatile oil was used as recommended in reference (60). However, inconsistency in the different sets of the measurements for the same fluid forced us to change the procedure and diameter-correction method, which will be discussed later, was performed to correct for evaporation.

Plots of shear stress and viscosity v.s. shear rate are given in Figure (A-2) and (A-3). Figure (A-2) includes standard oil, pure Glycerol and 90% Glycerol, while the viscometric behavior of polymer solution is presented in Figure (A-3). The straight lines of shear stress v.s. shear rate with slope unity obtained for standard oil and Glycerol solution indicate the Newtonian behavior of these fluids. It is also checked by constant viscosity horizontal lines obtained for these fluids. The curve of 0.2% (by weight) polymer solution indicated pseudoplastic behavior in the range of shear rates studied. The flow behavior index varied from 0.8 to 0.346 for low shear rate region and from 0.346 to 0.443 for high shear

rate region. The apparent viscosity varied from 0.2 to 42 poise at the lowest shear rate. Table (A-2) represents the viscometric data and the results obtained from the Rheogoniometer for all the fluids used in the present study.

I. Rheogoniometer Parameters

From (61), the shear stress is given by,

$$\tau = \frac{3T_r}{2\pi R_{pl}^3} = \frac{3.82T_r}{d_{pl}^3} \quad (A-1)$$

where,

τ = shear stress, dynes/cm²

T_r = torque = $S_1 \Delta t K_t$

S_1 = torque transducer sensitivity, micron/volt

Δt = movement of torsion head transducer, volts

K_t = torsion bar constant in dyne cm per micron movement of the transducer,

R_{pl} = radius of the platen, cm.

d_{pl} = diameter of the platen cm.

The shear rate is given by,

$$\sigma = \frac{360}{\alpha t} ; \quad (A-2)$$

where,

σ = shear rate, sec⁻¹

α = angle of cone, degrees,

t = $2\pi/\beta$, second/revolution

β = angular rotation of the platen, rad./sec.

The normal force is calculated by,

$$P_{11} - P_{22} = \frac{4F}{\pi d_{p1}^2} \quad (A-3)$$

where,

$$P_{11} - P_{22} = \text{primary normal stress difference,} \\ \text{dyne/cm}^2$$

$$F = S_2 g v_t, \text{ normal force, dyne,}$$

$$S_2 = \text{sensitivity of the normal force trans-} \\ \text{ducer, gr/volt}$$

$$g = \text{acceleration of gravity, cm/sec}^2$$

$$v_t = \text{output of transducer, volt.}$$

The normal force transducer was calibrated by placing analytic weights on the plate while rotating and the sensitivity was found to be $S_2 = 0.2$ gr/volt. The calibration curve is presented in Figure (A-1) and the data in Table (A-1).

Apparent viscosity was calculated by,

$$\mu = \frac{\tau}{\sigma} \quad (A-4)$$

and relaxation time (62) by,

$$\theta_0 = \frac{P_{11} - P_{22}}{2 \tau \sigma} \quad (A-5)$$

The plot of relaxation time v.s. shear rate is given in Figure (A-4). The maximum relaxation time was estimated by Bueche's theory (63),

$$\theta_0 = \frac{12(\mu_0 - \mu_s) M}{\pi^2 C R_g T} \quad (A-6)$$

where,

μ_0 = viscosity of the solvent, poise,

M = solute molecular weight, g-mole

C = solute concentration, gr/cm^3

R_g = gas constant, $\text{gr cm}^2/\text{sec}^2$ g-mole ok

T = absolute temperature, ok

The above parameters for 0.2% (by weight) Separan AP-273 solution are,

$$\mu_0 = 42 \text{ poise}$$

$$\mu_s = 0.013 \text{ poise}$$

$$M = 3 \times 10^6 \text{ g-mole}$$

$$C = 0.2/100 = 0.002 \text{ gr}/\text{cm}^3$$

$$R_g = 8.3 \times 10^7 \text{ gr cm}^2/\text{sec}^2 \text{ g-mole ok}$$

$$T = 292 \text{ ok}$$

Therefore,

$$\theta_0 = 3.126 \text{ sec.} \quad (\text{A-7})$$

For the entire set of runs two different platens but only one torsion bar was used.

Runs with small platen,

$$d_{pl} = 5 \text{ cm}$$

$$\alpha = 2^\circ - 0' - 53''$$

$$K_t = 106.6 \text{ dynes cm/micron.}$$

$$S_1 = 1.008 \text{ micron/volt.}$$

$$S_2 = 0.2 \text{ gr/volt.}$$

Therefore, Equations (A-1, 2, 3) becomes,

$$\tau = 3.285 \Delta t, \quad (\text{A-8})$$

$$\sigma = \frac{180}{t}, \quad (\text{A-9})$$

$$P_{11} - P_{22} = 10 v_t. \quad (A-10)$$

Runs with Large Platen,

$$d = 7.5 \text{ cm}$$

$$\alpha = 55', 10''$$

$$K_t = 106.6 \text{ dyne cm/micron,}$$

$$S_1 = 1.008 \text{ micron/volt.}$$

Therefore, Equations (A-1, 2, 3) become,

$$\tau = 0.974 \Delta t, \quad (A-11)$$

$$\sigma = \frac{392}{t}, \quad (A-12)$$

$$P_{11} - P_{22} = 4.443 v_t. \quad (A-13)$$

II. Evaporation Correction

Care should be taken that the fluid covers the whole area of the platens. However, due to the evaporation at the edges of the platens, the area covered by the liquid would always be less than the platen's area. Therefore, the platen's diameter in former calculation should be replaced by the exact diameter of the portion of the platen which is covered with liquid.

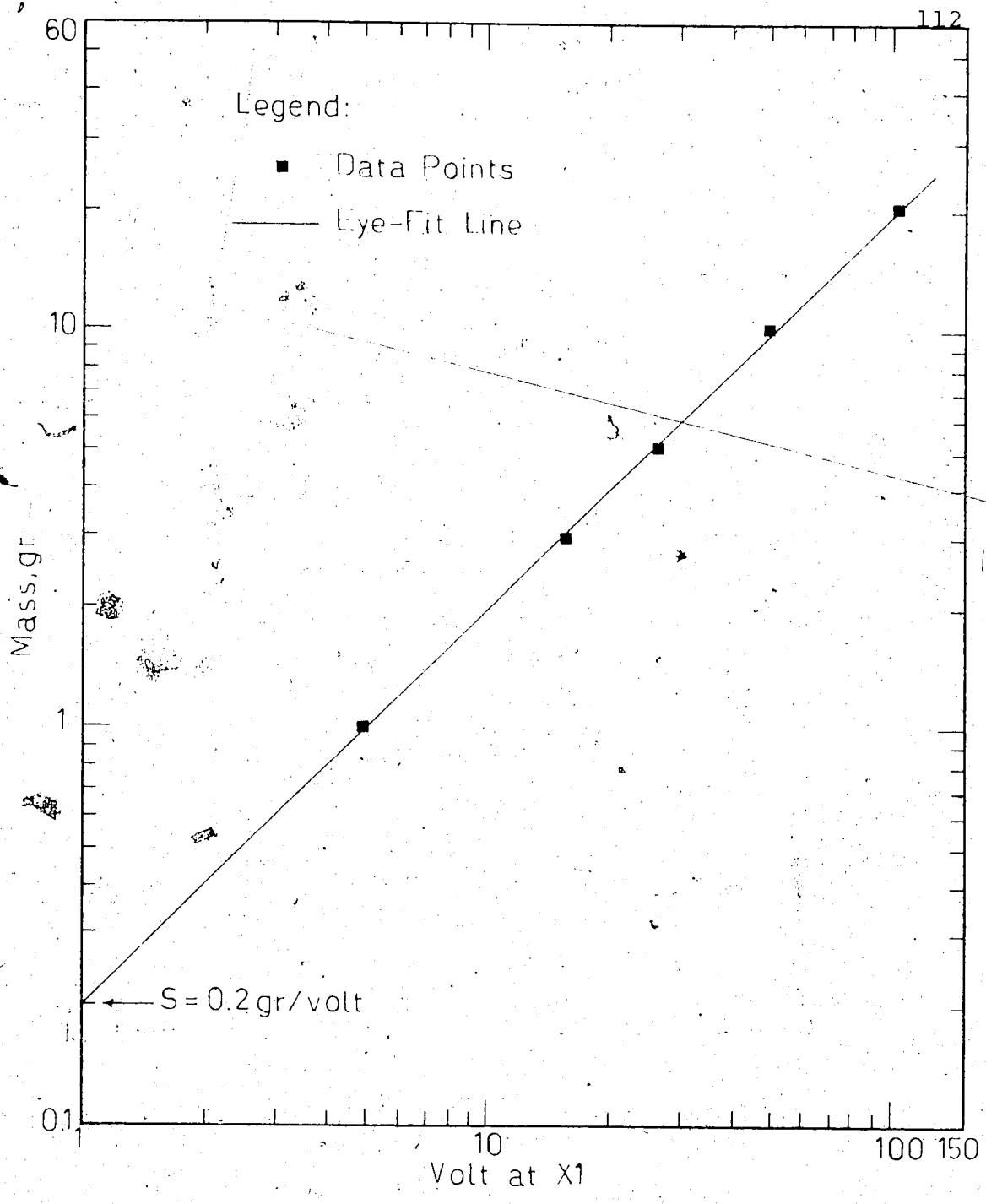


FIGURE A-1 NORMAL FORCE TRANSDUCER CALIBRATION

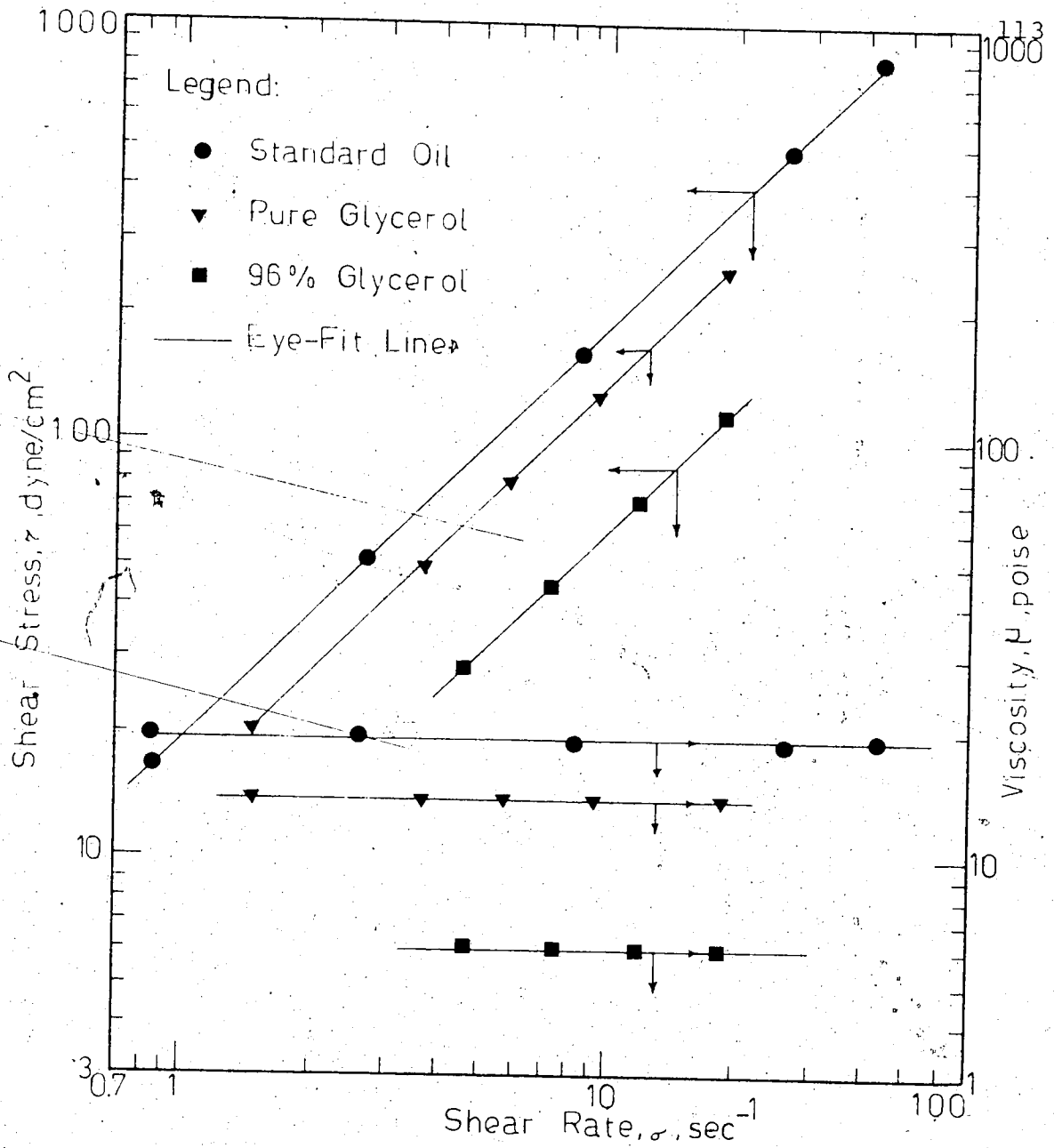


FIGURE A-2 VISCOMETRIC BEHAVIOR OF NEWTONIAN FLUIDS

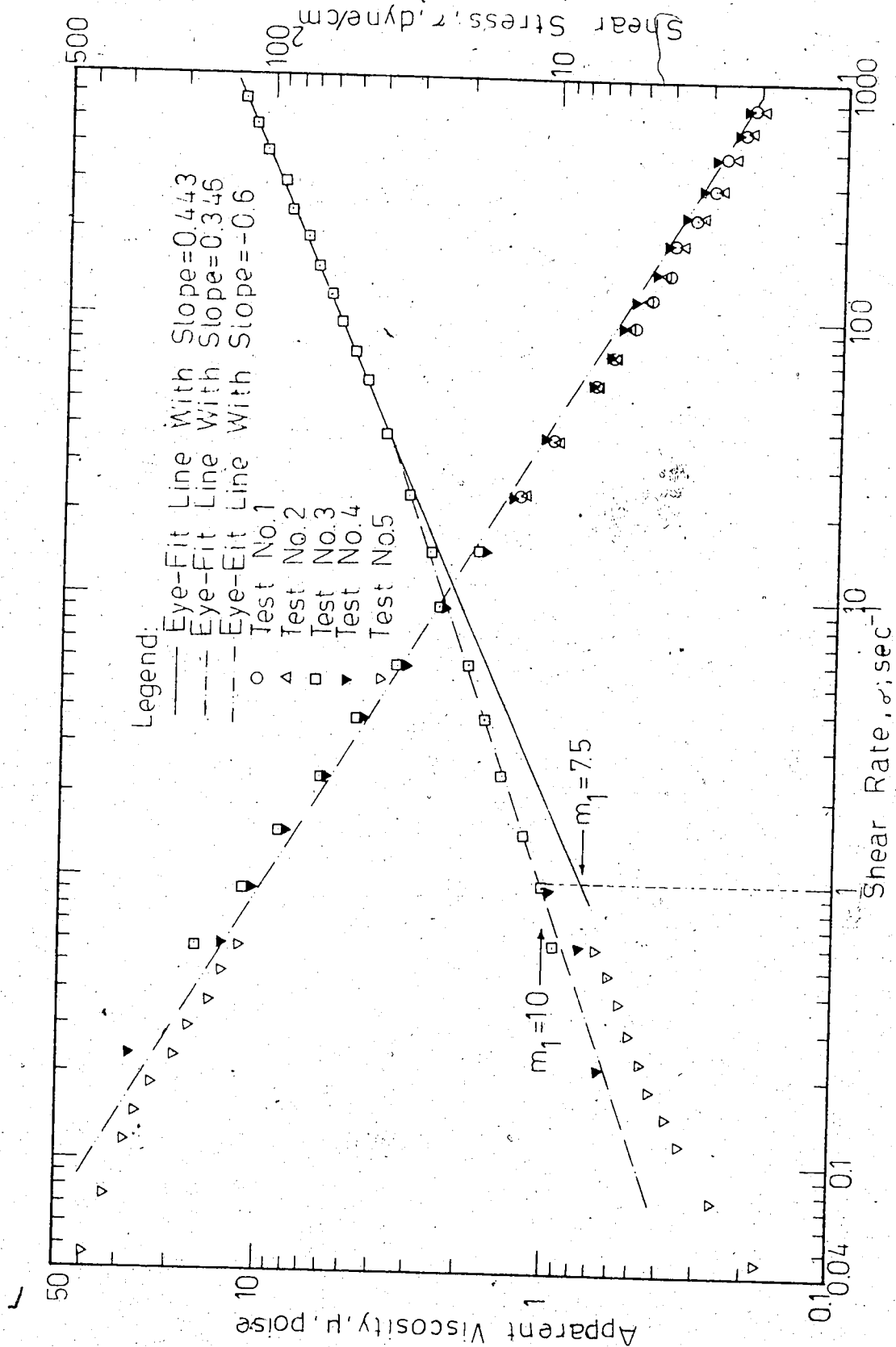


FIGURE A-3 VISCOMETRIC BEHAVIOR OF SEPARAN AP-273, 0.2% (by weight)

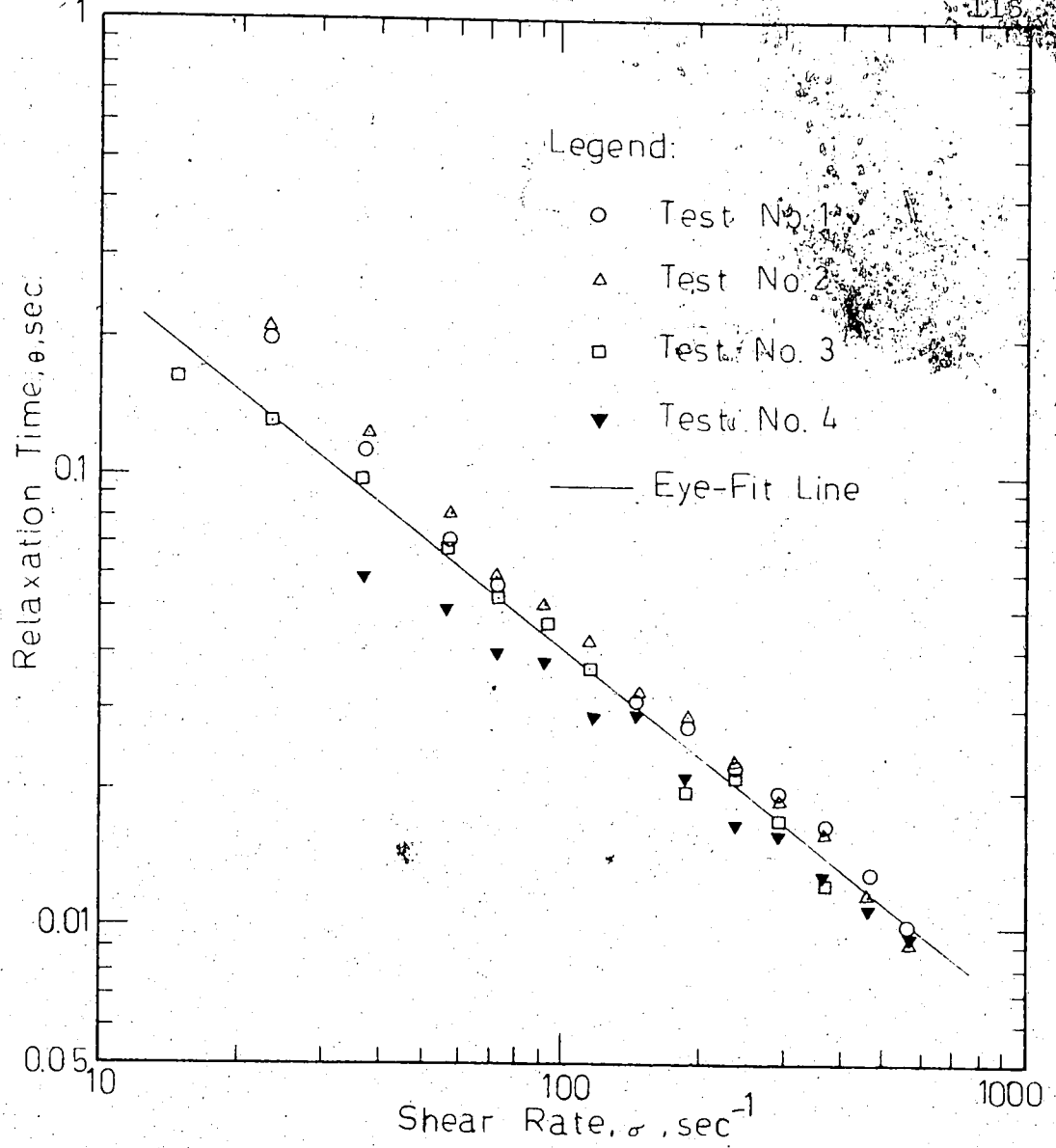


FIGURE A-4 RELAXATION TIME OF SEPARAN AP-273, 0.2% (by weight)

TABLE A-1
CALIBRATION OF NORMAL FORCE TRANSDUCER

Run No.	Mass (gr.)	Volt (at XI)
1	1	4.9
2	3	15.4
3	5	26
4	10	49.4
5	20	101.5
6	30	150
7	50	247

TABLE A-2
VISCOMETRIC MEASUREMENTS FOR STANDARD OIL, GLYCEROL,
AND POLYMER SOLUTION

1. Standard Oil

VISC. No. S-600-68-1h was used as standard oil, which had viscosity of 1974 C.P. at 20°C. and 1294 C.P. at 25°C.

The temperature of this experiment was 21°C.

Run No.	σ sec ⁻¹	Δt Volt	τ dyne/cm ²	μ C.P.
1	26.5	150	493	1861
2	42.6	248	815	1915
3	84.6	490	1610	1900
4	8.48	48	157.7	1860

TABLE A-2 (continued)

Run No.	σ sec ⁻¹	Δt Volt	τ dyne/cm ²	μ C.P.
5	2.65	15.5	50.9	1922
6	0.848	5	16.42	1934
7	0.265	1.6	5.26	1982
8	0.0848	0.55	1.808	2130

2. Pure Glycerol, T = 21°C

1	9.23	130	126.7	1373
2	18.4	260	253.5	1377
3	5.75	80	78	1356
4	1.464	20.8	20.25	1382
5	3.68	51	49.7	1350
6	9.23	128	124.8	1350

NOTE: Run No.'s 1-3 are for the pure Glycerol before being used, while runs 4-6 are for the same solution after being used in the system.

3. 96% Glycerol, T = 21°C

1	18.4	115	112	609
2	4.62	29	28.25	611
3	7.35	45	43.8	596
4	11.6	72.5	70.6	608

4. 81% Glycerol, T = 20°C

1	35.5	65	26.65	75
2	22.4	42	172	76.8

TABLE A-2 (continued)

Run No.	σ sec ⁻¹	Δt Volt	τ dyne/cm ²	μ C.P.
3	14.13	27	11.08	78.3
4	55.5	105	43.1	77.5
5	89	165	67.5	75.8
6	141.3	260	106.6	75.3

5. 58% Glycerol, T = 20°C

1	44.6	10.5	4.31	9.66
2	71	17	6.98	9.83
3	112	26	10.67	9.6
4	177.5	41	16.8	9.47

6. Domestic Tap Water

1	71	1.8	0.739	1.04
2	112	2.8	1.148	1.025
3	177.5	4.5	1.844	1.039
4	112	2.8	1.148	1.025
5	224	5.75	2.36	1.053
6	355	9.2	3.77	1.061

7. 0.2% Separan AP-273 Solution, Test No. 1, T = 20°C

Run No.	σ sec ⁻¹	Δt Volt	τ dyne/cm ²	μ C.P.	V_t Volt	$P_{11} - P_{22}$ dyne/cm ²	θ sec.
1	23.24	26	28.55	122.6	57.5	277	0.209
2	36.8	31.2	34.25	93.1	61.5	296.5	0.1177

Run No.	σ sec ⁻¹	Δt Volt	τ dyne/cm ²	μ C.P.	V_t Volt	$P_{11}-P_{22}$ dyne/cm ²	t_0 sec.
3.	57.5	36.5	40.1	69.6	86	414	0.0897
4	73.5	40.5	44.4	60.4	80	385.5	0.059
5	92.3	44.5	48.8	52.9	91	439	0.0486
6	116	49	53.8	46.3	110	531	0.0426
7	146.4	54.5	59.8	40.8	120	579	0.033
8	184	59.5	65.3	35.5	144	694	0.0289
9	232.4	65	71.4	30.7	160	771	0.0232
10	292.5	72.5	79.6	27.2	188	906	0.0194
11	368	80	87.8	23.9	220	1061	0.01645
12	462	89	97.7	21.1	240	1158	0.0128
13	575	100	109.8	19.1	240	1158	0.00916

NOTE: The sample was taken from a freshly prepared solution before being used for the experiment and the period between the time of solution preparation and the time of performing viscometric measurements was 15 days.

Test No. 2, T = 19.5°C

1	23.24	27.2	29.85	128.3	64.5	311	0.224
2	36.8	32.6	35.8	97.3	65	313.5	0.1189
3	57.5	39	42.8	74.4	73.5	354.5	0.072
4	73.5	42	46.1	62.7	88	424	0.0625
5	92.3	46.5	51	55.3	95	458	0.0486
6	116	50.5	55.4	47.8	100	482	0.03745
7	146.4	55.5	60.9	41.6	118	569	0.0319
8	184	61	66.9	36.4	146	704	0.0286

Run No.	σ sec ⁻¹	Δt Volt	τ dyne/cm ²	μ C.P.	V_t Volt	$P_{11} - P_{22}$ dyne/cm ²	θ sec.
9	232.4	68.5	75.2	32.4	169	815	0.0233
10	292.5	75	82.4	28.2	204	984	0.0203
11	368	84.5	96.6	26.2	240	1188	0.0167
12	462	94	107.5	23.2	262	1298	0.01306
13	575	105	120	20.9	282	1395	0.0101

NOTE: The sample was taken from the same solution as Test No. 1 but after experimental runs and viscometric measurements were performed same day as Test No. 1.

Test No. 3, T = 19.5°C

1	0.575	8	9.16	1159	-	-	-
2	0.923	9	10.3	1117	-	-	-
3	1.464	10.5	12.02	821	-	-	-
4	2.324	12.5	14.3	615	-	-	-
5	3.68	14.5	16.6	451	-	-	-
6	5.75	16.5	18.9	328.5	-	-	-
7	9.23	19.5	22.3	241.5	-	-	-
8	14.64	23	26.35	180	22.6	111.9	0.1455
9	23.24	27	30.9	133	37.2	184.2	0.1282
10	36.8	32	38.25	104	53.5	273	0.097
11	57.5	37.5	44.8	77.8	70	357	0.0693
12	73.5	41.5	49.6	67.4	75	382.5	0.0525
13	92.3	45	56.1	60.8	94	494	0.0477
14	116	49	61.1	52.4	100	525	0.037
15	146.4	54	67.4	46.1	120	630	0.0319

Run. No.	σ sec ⁻¹	Δt Volt	τ dyne/cm ²	μ C.P.	v_t Volt	$P_{11}-P_{22}$ dyne/cm ²	t sec.
16	184	59	73.6	40	100	525	0.01938
17	232.4	67	83.6	36	153	803	0.0206
18	292.5	72.5	90.5	30.95	170	893	0.01686
19	368	82	102.3	27.8	180	945	0.01252
20	462	90	112.3	24.3	220	1156	0.01113
21	575	100	124.8	21.7	262	1375	0.0958

Test No. 4, T = 19.5°C

1	0.232	6	6.23	2730	-	-	-
2	0.575	6.8	7.47	1300	-	-	-
3	0.923	8.9	9.77	1060	-	-	-
4	1.464	10.9	11.98	817	-	-	-
5	2.324	12.2	13.4	576	-	-	-
6	3.68	14.8	16.25	442	-	-	-
7	5.75	16.8	18.44	321	-	-	-
8	9.23	19.0	20.85	226	-	-	-
9	14.64	22.4	24.6	168	-	-	-
10	23.24	27.6	31.6	136	-	-	-
11	36.8	32.5	38.83	105.5	34	173.4	0.0607
12	57.5	37	44.2	76.9	50	255	0.0501
13	73.5	40	47.8	65	55	280.5	0.0399
14	92.3	45	53.8	58.3	75	382.5	0.0385
15	116	50	59.8	51.6	80	408	0.0294
16	146.4	54	67.4	46.1	90	472	0.02395
17	184	60	74.8	40.7	111	583	0.0212

Run No.	σ sec ⁻¹	Δt Volt	τ dyne/cm ²	μ C.P.	v_t Volt	$P_{11}-P_{22}$ dyne/cm ²	θ sec.
18	232.4	68	84.8	36.5	125	656	0.01664
19	292.5	72	89.8	30.7	158	830	0.0158
20	368	82	102.2	27.8	184	966	0.01283
21	462	90	112.2	24.3	213	1118	0.01082
22	575	101	126	21.9	260	1365	0.00942

Test No. 5, T = 20°C

Run No.	σ sec ⁻¹	Δt Volt	τ dyne/c ²	μ C.P.
1	0.02925	0.9	1.228	4200
2	0.0462	1.3	1.774	3840
3	0.0735	1.8	2.46	3345
4	0.116	2.4	3.275	2820
5	0.1464	3.0	3.74	2555
6	0.184	3.4	4.24	2310
7	0.2324	3.6	4.49	1930
8	0.2925	4	4.99	1706
9	0.368	4.5	5.38	1462
10	0.462	5.5	6.04	1308
11	0.575	6	6.59	1146

NOTE: Tests No. 3, 4, and 5 were performed on the samples of the same solution which was different from that of tests No. 1 and 2. However, the sample of test No. 3 was one day old and was taken from the freshly prepared solution, while the samples of tests No. 4 and 5 were 10 and 17 days old, respectively, and were taken after the experimental runs. The results of the different tests indicate the lack of major degradation of the samples.

APPENDIX B

PRESSURE DROP AND RELATED CORRELATIONS

Bergelin, et al. (58) suggested the following empirical correlation to predict pressure drop of the flow across an ideal bank of tubes,

$$\Delta P_B = \frac{4K_1 \mu W_B N}{2 \rho S_B D} \left(\frac{\mu}{\mu_w}\right)^m \quad (B-1)$$

For isothermal flow the viscosity correction need not be considered; therefore,

$$\Delta P_B = \frac{4K_1 \mu W_B N}{2 \rho S_B D} \quad (B-2)$$

where,

$W_B = \rho q =$ mass flow rate, gr/sec.

$S_B = d_x l_x N_m =$ minimum free flow area, cm^2

$N_m =$ number of the minimum openings in one row,

$N =$ number of major restriction encountered in flow through the bank,

$B =$ indicates an ideal bundle of tubes, i.e. without by-pass flow.

$K_1 =$ dimensionless constant which is determined by the following procedure,

$$f_B = \frac{K_1}{Re_t} \quad (B-3)$$

where f_B is friction factor and Re_t is tube bank Reynolds

number, defined as,

$$Re_t = \frac{D W_B}{\mu S_B} \quad (B-4)$$

In general, for tube banks (59),

$$f_B = \frac{6}{Re_t} \frac{P_t^{-1}}{P_t^3} F(P_t) \quad (B-5)$$

This is obtained (59) by integrating the Hagen-Poiseuille equation for a creeping flow between two tubes and using the tube bank friction factor defined as,

$$f_B = \frac{2 \Delta P \rho S_B^2}{4 W_B^2 N_t} \quad (B-6)$$

In Equation (B-5), $F(P_t)$ is equal to,

$$F(P_t) = \int_0^1 \frac{dx}{[P_t - \sqrt{2x-x^2}]^3} \quad (B-7)$$

P_t is pitch ratio and is defined as,

$$P_t = \frac{S_T}{D} \quad (B-8)$$

where S_T is transverse pitch as shown in Figure (III-1). It is worthwhile to mention that in staggered configuration the smaller pitch (i.e. S_L or S_T whichever is smaller) should be taken to calculate pitch ratio. For the present model,

$$S_T = 0.65 \text{ cm} \quad (B-9)$$

Therefore,

$$P_t = 1.08 \quad (B-10)$$

By graphical integration, $F(P_t)$ from Equation (B-7) was determined to be,

$$F(P_t) = F(1.08) = 462.8. \quad (B-11)$$

Hence, by substituting into Equation (B-5),

$$f_B = \frac{176}{Re_t}. \quad (B-12)$$

comparing (B-12) with (B-3),

$$K_1 = 176. \quad (B-13)$$

As mentioned before, the Equation (B-1) was for an ideal bundle of tubes, i.e. without by-pass flow. To apply this equation to the present model, the by-pass flow should be eliminated. That is according to Figure (III-3), only the flow passing through the positions 13 to 20 should be considered. Hence, an imaginary wall is assumed to pass through the centers of the outermost cylinders which was shown by dashed-line in Figure (III-3). Therefore, ideal bundle volumetric flow rate, q_B , is,

$$q_B = \frac{\sum_{i=13}^{20} A_i}{\sum_{i=12}^{21} A_i} q. \quad (B-14)$$

From Table (C-1), q_B for Glycerol is,

$$q_B = \frac{3.405}{6.128} q = 0.556 q. \quad (B-15)$$

That is approximately 50% of the flow passes between the cylinders in row No. 21. For Separan,

$$q_B = \frac{2.465}{5.654} q = 0.436 q. \quad (B-16)$$

In the above calculations, the flow rate passing through the imaginary wall and the outermost cylinders of row No. 21 was

neglected. A further assumption made is that the flow distribution would remain the same for the whole range of flow rates studied in pressure drop measurement.

Considering the above assumptions, the Equation (B-2) can be used for the present model with the following known parameters,

$$K_1 = 176$$

$$W_B = 0.556 \text{ } \rho g$$

$$N = 35 \text{ (i.e. the number of rows between the two pressure taps)}$$

$$S_B = dx \times x N_m = (0.05)(5.2)(9) = 2.34 \text{ cm}^2$$

$$D = 0.6 \text{ cm}$$

$$\mu = 13.6 \text{ poise (pure Glycerol solution)}$$

$$\mu = 6.06 \text{ poise (96\% Glycerol solution)}$$

$$\mu = 0.765 \text{ poise (81\% Glycerol solution)}$$

$$\mu = 0.0964 \text{ poise (58\% Glycerol solution)}$$

$$\mu = 0.0104 \text{ poise (Domestic Tap Water)}$$

Substituting into Equation (B-2) and performing the necessary algebraic operations,

$$\Delta P_B = 6.63 \times 10^4 q \text{ dyne/cm}^2 \text{ (pure Glycerol) (B-17)}$$

$$\Delta P_B = 2.96 \times 10^4 q \text{ dyne/cm}^2 \text{ (96\% Glycerol) (B-18)}$$

$$\Delta P_B = 3.75 \times 10^3 q \text{ dyne/cm}^2 \text{ (81\% Glycerol) (B-19)}$$

$$\Delta P_B = 4.7 \times 10^2 q \text{ dyne/cm}^2 \text{ (58\% Glycerol) (B-20)}$$

$$\Delta P_B = 50.6 q \text{ dyne/cm}^2 \text{ (Dom. Tap W.) (B-21)}$$

In terms of superficial velocity, one can write,

$$v = \frac{q}{A} \text{ (B-22)}$$

where $A = 33.8 \text{ cm}^2$ is the cross sectional area of the box, therefore,

$$\Delta P_B = 2.24 \times 10^6 \text{ V dyne/cm}^2 \text{ (pure Glycerol)} \quad (\text{B-23})$$

$$\Delta P_B = 1.0 \times 10^6 \text{ V dyne/cm}^2 \text{ (91\% Glycerol)} \quad (\text{B-24})$$

$$\Delta P_B = 1.27 \times 10^5 \text{ V dyne/cm}^2 \text{ (81\% Glycerol)} \quad (\text{B-25})$$

$$\Delta P_B = 1.59 \times 10^4 \text{ V dyne/cm}^2 \text{ (58\% Glycerol)} \quad (\text{B-26})$$

$$\Delta P_B = 1.71 \times 10^3 \text{ V dyne/cm}^2 \text{ (Dom. Tap W.)} \quad (\text{B-27})$$

Equations (B-23) to (B-27) together with the experimental data points were presented in Figure (IV-1).

To apply Bergelin's correlation, i.e. Equation (B-2), to the polymer solution, an apparent viscosity must be defined for each flow rate, which the flow behavior indices, i.e. m_1 and n , can be considered constant. As a first approximation, these parameters are estimated directly from the experimental curve of pressure drop v.s. superficial velocity in Figure (IV-2). According to the figure (IV-2), the whole region of flow rates studied can be divided into four parts,

Region of flow rate cc/sec.	n	m_1
0.431 - 1.717	0.346	10
2.13 - 6.84	0.443	7.5
8.53 - 21.52	0.632	2.93
27.25 - 34.35	0.917	0.778

n is the slope of the eye-fit line through the data points in Figure (IV-2). These lines have not been shown. m_1 was calculated by assuming power-law

$$m_1 = \mu \sigma^{1-n} \quad (\text{B-28})$$

To estimate the apparent viscosity, the following procedure was undertaken.

The wall shear rate for flow through parallel plates is given by,

$$\sigma_w = \frac{2n+1}{n} \frac{\bar{V}}{d/2} \quad (\text{B-29})$$

where σ_w is wall shear rate, \bar{V} , average velocity and d is shown in Figure (II-2). Equation (B-29) can be easily derived from equation of motion for power-law fluid flow through parallel plates (53). To modify Equation (B-29) for the present model, \bar{V} should be replaced by average interstitial velocity, i.e.

$$\bar{V} \equiv \frac{V}{\epsilon} \quad (\text{B-30})$$

and $d/2$ should be replaced by volumetric hydraulic radius of the bed. Therefore,

$$\sigma_w = \frac{2n+1}{n} \frac{V}{\epsilon R_H} \quad (\text{B-31})$$

on the other hand, R_H can be calculated as follows (52c),

$$R_H = \frac{\text{volume of voids}}{\text{wetted surface}} = \frac{\text{volume of voids}}{\text{volume of bed}} \frac{\text{volume of bed}}{\text{wetted surface}} = \frac{\epsilon}{s_v} \quad (\text{B-32})$$

where s_v represents the wetted surface per volume of bed.

Specific surface, s_s , is defined as,

$$s_s = \frac{\text{wetted surface}}{\text{solid volume}} \quad (\text{B-33})$$

For the present bed,

$$S_s = \frac{(\pi D \ell) N_T}{(\pi D^2 \ell / 4) N_T} = \frac{4}{D} \quad (\text{B-34})$$

In calculation of s_s , the area of the surrounding walls has been neglected. One can also write,

$$S_v = S_s (1 - \epsilon). \quad (\text{B-35})$$

From Equations (B-32, 34, 35),

$$R_H = \frac{\epsilon D}{4(1 - \epsilon)}. \quad (\text{B-36})$$

Substituting (B-22, 36) into (B-31),

$$\sigma_w = \frac{4(1 - \epsilon)}{A \epsilon^2 D} \frac{2n + 1}{n} q. \quad (\text{B-37})$$

Knowing the following parameters,

$$A = 33.8 \text{ cm}^2$$

$$\epsilon = 0.357$$

$$D = 0.6 \text{ cm.}$$

Equation (B-37) becomes,

$$\sigma_w = 0.995 \frac{2n + 1}{n} q. \quad (\text{B-38})$$

The estimated σ_w from Equation (B-38) laid in the region of 2.1 to 100.5 sec^{-1} . Over this range of shear rates Figure A-4 shows n to be approximately .346 to .443. After the initial estimate of shear rate using (B-38) by n estimated from the pressure drop measurements, these new values of flow behavior indices were used in apparent viscosity calculation. Therefore, the calculated apparent viscosity, consequently, the predicted pressure drops were based on the viscometric measurement of the fluid.

The calculated values of wall shear rate, apparent viscosity, and pressure drop are recorded in Table (B-3) and the predicted curve of pressure drop v.s. superficial velocity by Equation (B-2) is presented in Figure (IV-2).

TABLE B-1

FLOW BEHAVIOR PARAMETERS OF 96% GLYCEROL SOLUTION

Run No.	q cc/sec.	V cm/sec.	$\Delta P \times 10^{-4}$ dyne/cm ²	$K \times 10^4$ cm ²	$f_K \times 10^{-2}$ Dimensionless	$N_{Re} \times 10^4$ Dimensionless	$f_K^{0.8} Re$
1	0.835	0.0248	2.785	1.198	48.9	2.057	1.005
2	1.49	0.443	4.36	1.369	25.3	3.65	0.924
3	2.13	0.0633	6.75	1.261	19.2	5.23	1.004
4	3.39	0.1007	10.36	1.308	11.62	8.32	0.967
5	3.39	0.1007	10.5	1.291	11.8	8.32	0.982
6	4.28	0.127	13.04	1.31	9.21	10.5	0.966
7	5.38	0.1598	16.19	1.328	7.23	13.2	0.955
8	6.76	0.201	19.68	1.372	5.54	16.64	0.921
9	8.53	0.2535	25.4	1.342	4.51	20.95	0.944
10	8.53	0.2535	21.8	1.564	3.87	20.95	0.81
11	10.76	0.3195	29.05	1.481	3.24	27	0.875
12	13.6	0.404	32.5	1.672	2.27	33.4	0.757
13	17.06	0.507	40.2	1.698	1.79	41.9	0.75
PURE GLYCEROL							
14	0.431	0.0128	3.6	1.07	251	0.471	1.18
15	0.685	0.02037	5.27	1.165	145	0.748	1.085
16	1.07	0.0318	7.69	1.25	86.6	1.17	1.01
17	1.717	0.0511	11.78	1.311	51.6	1.88	0.97

TABLE B-1 (continued)

Run No.	q cc/sec.	V cm/sec.	$\Delta P \times 10^{-4}$ dyne/cm ²	$K \times 10^4$ cm ²	$f_K \times 10^{-2}$ Dimensionless	$N_{Re} \times 10^4$ Dimensionless	$f_{KN} Re$
18	2.17	0.0645	14.63	1.332	40.2	2.37	0.954
19	2.725	0.081	18	1.37	31.35	2.98	0.934
20	3.42	0.1017	22.3	1.379	24.55	3.75	0.92
PURE GLYCEROL							
1	0.431	0.0128	3.6	1.07	251	0.471	1.18
2	0.685	0.02037	5.27	1.165	145	0.748	1.085
3	1.07	0.0318	7.69	1.25	86.6	1.17	1.01
4	1.717	0.0511	11.78	1.311	51.6	1.88	0.97
5	2.17	0.0645	14.63	1.332	40.2	2.37	0.954
6	2.725	0.081	18	1.37	31.35	2.98	0.934
7	3.42	0.1017	22.3	1.379	24.55	3.75	0.92
96% GLYCEROL SOLUTION							
8	0.835	0.0248	2.785	1.198	48.9	2.057	1.005
9	1.49	0.0443	4.36	1.369	25.3	3.65	0.924
10	2.13	0.0633	6.75	1.261	19.2	5.23	1.004
11	3.39	0.1007	10.36	1.308	11.62	8.32	0.967
12	3.39	0.1007	10.5	1.291	11.8	8.32	0.982
13	4.28	0.127	13.04	1.31	9.21	10.5	0.966

TABLE B-1 (continued)

Run No.	q cc/sec.	V cm/sec.	$\Delta P \times 10^{-4}$ dyne/cm ²	$K \times 10^4$ cm ²	$f_K \times 10^{-2}$ Dimensionless	$N_{Re} \times 10^4$ Dimensionless	$\frac{K \cdot V \cdot N_{Re}}{Q}$
14	5.38	0.1598	16.19	1.328	7.23	13.2	0.955
15	6.76	0.201	19.68	1.372	5.54	16.64	0.921
16	8.53	0.2535	25.4	1.342	4.51	20.95	0.944
17	8.53	0.2535	21.8	1.564	3.87	20.95	0.81
18	10.76	0.3195	29.05	1.481	3.24	27	0.875
19	13.6	0.404	32.5	1.672	2.27	33.4	0.757
20	17.06	0.507	40.2	1.698	1.79	41.9	0.75
81% GLYCEROL SOLUTION							
21	0.835	0.0248	0.392	1.075	7.51	15.72	1.18
22	1.49	0.0443	0.597	1.258	3.59	28.1	1.008
23	2.13	0.0633	0.938	1.146	2.76	40.1	1.107
24	3.39	0.1007	1.484	1.15	1.72	63.9	1.1
25	4.28	0.127	1.86	1.16	1.358	80.5	1.093
26	5.38	0.1598	2.34	1.16	1.08	101.2	1.092
27	6.76	0.201	2.88	1.184	0.84	127.5	1.071
28	8.53	0.2535	3.58	1.2	0.656	160.7	1.054
29	10.76	0.3195	4.43	1.222	0.511	202.5	1.034
58% GLYCEROL SOLUTION							
30	2.13	0.0633	0.0882	1.53	0.275	302	0.83

TABLE B-1 (continued)

Run No.	q cc/sec.	V cm/sec.	$\Delta P \times 10^{-4}$ dyne/cm ²	Kx10 ⁴ cm ²	$f_K \times 10^{-2}$ Dimensionless	$N_{Re} \times 10^4$ Dimensionless	$f_K \times N_{Re}$
31	3.39	0.1007	0.1588	1.356	0.1935	483	0.934
32	4.28	0.1262	0.206	1.31	0.16	605	0.968
33	5.38	0.16	0.253	1.35	0.1222	766	0.936
34	6.76	0.2	0.3235	1.325	0.1	959	0.959
35	8.53	0.254	0.418	1.3	0.08	1218	0.974
36	10.76	0.321	0.524	1.31	1.0629	1538	0.966
37	13.6	0.403	0.676	1.3	0.0515	1930	0.994
38	17.06	0.505	0.864	1.25	0.419	2420	1.015
39	21.52	0.636	1.088	1.25	0.0333	3045	1.014
40	27.25	0.806	1.372	1.256	0.02615	3860	1.01
41	34.35	1.015	1.723	1.26	0.0207	4860	1.006
A TAP WATER							
42	10.76	0.321	0.0809	0.916	0.01118	12380	1.384
43	13.6	0.403	0.1029	0.905	0.00902	15530	1.4
44	17.06	0.505	0.1322	0.882	0.00738	19460	1.434
45	21.52	0.636	0.1983	0.74	0.00698	24500	1.71
46	27.25	0.806	0.228	0.816	0.005	31000	1.55
47	34.35	1.015	0.3015	0.779	0.00416	39100	1.625
48	42.8	1.262	0.404	0.722	0.00361	48700	1.758

TABLE B-2

FLOW BEHAVIOR PARAMETERS OF 0.2% SEPARAN

Run No.	Q , cc/sec.	V cm/sec.	$\Delta P \times 10^{-4}$ dyne/cm ²	H $\text{grcm}^{-n} \text{sec. } n^{-2}$	$f_K \times 10^{-2}$ Dimensionless	$N_{Re} \times 10^3$ Dimensionless
1	0.431	0.01272	1.049	0.202	92.6	0.1436
2	0.685	0.02025	1.186	0.202	41.3	0.318
3	0.835	0.0247	1.28	0.202	29.9	0.438
4	1.07	0.0316	1.3	0.202	18.58	0.624
5	1.49	0.0441	1.47	0.202	10.81	1.134
6	1.717	0.0508	1.586	0.202	8.8	1.436
7	2.13	0.063	1.739	0.202	6.19	2.065
8	2.17	0.0642	1.835	0.202	6.27	2.1
9	2.725	0.0805	1.911	0.202	4.21	3.06
10	3.39	0.103	2.1	0.202	2.82	4.6
11	3.42	0.1011	2.31	0.202	2.93	4.47
12	4.27	0.1262	2.43	0.202	2.18	6.45
13	4.28	0.1262	2.31	0.202	2.07	6.45
14	8	0.16	2.6	0.202	1.45	9.57
15	5.41	0.1602	2.7	0.202	1.45	9.57
16	6.76	0.2	2.87	0.202	1.02	13.9
17	6.84	0.202	3.12	0.202	1.07	14.1

TABLE B-2 (continued)

Run No.	q cc/sec.	V cm/sec.	$\Delta P \times 10^{-4}$ dyne/cm ²	H grcm ⁻ⁿ sec. n-2	$f_K \times 10^{-2}$ Dimensionless	$N_{Re} \times 10^3$ Dimensionless
18	8.53	0.254	3.265	0.276	0.72	17.58
19	8.58	0.254	3.46	0.276	0.77	17.58
20	10.76	0.321	3.82	0.276	0.53	24.8
21	10.84	0.321	4.11	8.276	0.57	24.8
22	13.6	0.403	4.37	0.276	0.38	35.3
23	13.62	0.403	4.66	0.276	0.409	35.3
24	17.06	0.505	5.28	0.276	0.295	50.1
25	17.19	0.507	5.4	0.276	0.3	50.6
26	21.52	0.636	6.28	0.276	0.221	71.8
27	27.25	0.806	7.7	0.276	0.1693	104
28	34.35	1.015	9.56	0.267	0.132	149

TABLE B-3

PREDICTED PRESSURE DROPS BY BERGELIN'S CORRELATION--0.2% SEPARAN

Run No.	q cc/sec.	n Dimensionless	$\frac{m_l}{gcm^{-1}sec^{n-2}}$	σ_w^{-1} sec ⁻¹	μ Poise	ΔP_B dyne \times cm ²
1	0.431	0.346	10	2.1	6.2	1.02
2	0.685	0.346	10	3.34	4.8	1.258
3	0.835	0.346	10	4.07	4	1.277
4	1.07	0.346	10	5.21	3.5	1.432
5	1.49	0.346	10	7.26	2.6	1.482
6	1.717	0.346	10	8.36	2.5	1.64
7	2.13	0.346	10	10.4	2.2	1.79
8	2.17	0.346	10	10.5	2.2	1.82
9	2.725	0.346	10	13.3	1.9	1.976
10	3.39	0.346	10	16.5	1.6	2.07
11	3.42	0.346	10	16.9	1.6	2.09
12	4.27	0.346	10	20.8	1.4	2.28
13	4.28	0.346	10	20.8	1.4	2.29
14	5.38	0.346	10	26.2	1.2	2.46
15	5.41	0.346	10	26.3	1.2	2.48
16	6.76	0.346	10	33	1.05	2.71
17	6.84	0.346	10	33.3	1.05	2.71

TABLE B-3 (continued)

Run No.	q cc/sec.	n Dimensionless	$\frac{m_1}{\text{grcm}^{-1}\text{sec}^{n-2}}$	σ_w^{-1} sec ⁻¹	μ Poise	ΔP_B dyne/cm ²
18	8.53	0.443	7.5	36.2	1	3.26
19	8.58	0.443	7.5	36.4	1	3.28
20	10.76	0.443	7.5	45.7	0.86	3.53
21	10.84	0.443	7.5	46	0.86	3.56
22	13.6	0.443	7.5	57.7	0.74	3.85
23	13.62	0.443	7.5	57.9	0.74	3.86
24	17.06	0.443	7.5	72.4	0.64	4.17
25	17.19	0.443	7.5	73	0.64	4.2
26	21.52	0.443	7.5	91.2	0.58	4.76
27	27.25	0.443	7.5	115.5	0.5	5.21
28	34.35	0.443	7.5	138.6	0.44	5.77

APPENDIX C

CONSTRUCTION OF VELOCITY PROFILE FROM STREAK LENGTH

As was mentioned in Section III-4-2, the length of the streaks and openings were taken from 0.1-inch division graph paper at total magnification of 100. Data points presented in Appendix E and the local velocity profile plotted in Figure (IV-7 to 12) are based on this magnified scale. However, the scale given in the plots has been chosen so that the profiles present the dimensionless interstitial velocity, i.e. u/V v.s. position. The RPM's reported in Tables (E-1, 2) are based on the chopper disk with one radial slit. That is, if the experimental RPM was 25 revolution per minute with a 4-slit chopper disk, it would be reported 100 RPM. Because the time duration of every period of opening or closing the light would be same for a 4-slit chopper at 25 RPM as for one-slit at 100 RPM. For every rotating disk, one can write,

$$t = \frac{60}{\text{RPM}} \quad \text{sec/rev.} \quad (\text{C-1})$$

where t , is the duration of one revolution. For a one-slit chopper disk,

$$t_p = \frac{60}{\text{RPM}} \times \frac{1}{2} = \frac{30}{\text{RPM}} \quad \text{sec.} \quad (\text{C-2})$$

where t_p is the time of every period of opening or closing

the light. Therefore, taking s as the length of streak, the velocity is calculated by,

$$u = \frac{s}{t_p} = \frac{\text{RPM}}{30} s. \quad (\text{C-3})$$

The flow rate passing through each opening is obtained by,

$$q_i = \ell \int_0^d u dx, \quad (\text{C-4})$$

where x -direction is shown in Figure (V-1). Substituting (C-3) into (C-4),

$$q_i = \frac{\text{RPM}}{30} \ell \int_0^d s dx. \quad (\text{C-5})$$

The area under the velocity profiles, A_V , is obtained by,

$$A_V = \int_0^d u dx = \frac{\text{RPM}}{30} \int_0^d s dx. \quad (\text{C-6})$$

However, the plots in Figures (IV-7 to 12) are u/V v.s. x . Therefore, the area under the profiles, A_i , which have been presented for three positions in Figures (IV-7 to 12), is given by,

$$A_i = \frac{A_V}{V} = \frac{\text{RPM}}{30V} \int_0^d s dx. \quad (\text{C-7})$$

A_i 's are recorded in Table (C-1). Comparing (C-5) with (C-7), q_i can be obtained in terms of A_i ,

$$q_i = A_i \ell V. \quad (\text{C-8})$$

It is understood from Tables (E-1, 2) that all the lengths are reported in inches, i.e.

$$d = 2.54 d_M,$$

$$s = 2.54 S,$$

$$x = 2.54 X.$$

Total volumetric flow rate can be obtained by using sum of the A_i 's for each row in place of A_i in Equation (C-8). These values were in a good agreement with the flow rates measured by the formerly calibrated pump. For instance, for the Glycerol solution,

$$\text{row No. 20 } \rightarrow \rightarrow \rightarrow \rightarrow \Sigma A_i = 6.632 \text{ cm.}$$

$$\text{row No. 21 } \rightarrow \rightarrow \rightarrow \rightarrow \Sigma A_i = 6.497 \text{ cm.}$$

$$\text{row No. 22 } \rightarrow \rightarrow \rightarrow \rightarrow \Sigma A_i = 6.567 \text{ cm.}$$

Therefore, the calculated flow rate from Equation (C-8) in the case of minimum flow rate, i.e. $q = 0.685 \text{ cc/sec.}$ or $V = (0.685/33.8) \text{ cm/sec.}$

$$\text{row No. 20 } \rightarrow \rightarrow \rightarrow \rightarrow q = 0.698 \text{ cc/sec.}$$

$$\text{row No. 21 } \rightarrow \rightarrow \rightarrow \rightarrow q = 0.684 \text{ cc/sec.}$$

$$\text{row No. 22 } \rightarrow \rightarrow \rightarrow \rightarrow q = 0.691 \text{ cc/sec.}$$

and for the Separan solution,

$$\text{row No. 21 } \rightarrow \rightarrow \rightarrow \rightarrow \Sigma A_i = 5.956 \text{ cm.}$$

$$\text{row No. 22 } \rightarrow \rightarrow \rightarrow \rightarrow \Sigma A_i = 6.142 \text{ cm.}$$

Therefore, the calculated flow rate,

$$\text{row No. 21 } \rightarrow \rightarrow \rightarrow \rightarrow q = 0.628 \text{ cc/sec.}$$

$$\text{row No. 22 } \rightarrow \rightarrow \rightarrow \rightarrow q = 0.648 \text{ cc/sec.}$$

TABLE C-1

OPENINGS, d , AREA UNDER THE DIMENSIONLESS VELOCITY
 PROFILES, A_i , AND FRACTIONAL FLOW RATES, $q\%$

Position No.	$d \times 10^2$, cm.		$A_i \times 10^3$, cm.		$q\%$	
	Glycerol	Separan	Glycerol	Separan	Glycerol	Separan
ROW NO. 20						
1	7.5	7.5	1193	1891	18.4	31.3
2	5.69	5.21	720	562	11.1	9.29
3	5.08	5.08	488	?	7.51	?
4	5.74	4.57	493	400	7.39	6.61
5	5.54	4.87	437	340	6.73	5.63
6	6.7	6.7	673	451	10.37	7.45
7	5.49	5.49	392	337	6.04	5.57
8	5.71	5.71	467	312	7.18	5.16
9	7.87	6.66	901	528	13.89	8.74
10	4.9	4.9	446	512	6.86	8.46
11	3.68	3.68	422	440	6.5	7.27
ROW NO. 21						
12	40	37.1	1877	2380	28.9	39.25
13	6.35	6.35	326	249	5.03	4.9
14	6.6	6.6	509	402	7.84	6.82
15	6.1	5.51	424	374	6.53	6.17
16	6.12	5.59	502	297	7.72	4.91
17	5.26	4.96	356	252	5.49	4.17
18	6.76	6.76	710	418	10.93	6.19
19	5.21	5.21	401	288	6.17	4.75
20	5.44	5.44	382	286	5.88	4.73
21	32.8	32.8	1010	1010	15.56	16.64
ROW NO. 22						
22	5.94	5.94	986	1660	15.2	27.45

TABLE C-1 (continued)

Position No1	$dx \times 10^2$, cm.		$A_i \times 10^3$, cm.		q%	
	Glycerol	Separan	Glycerol	Separan	Glycerol	Separan
23	6.99	5.14	991	1038	15.27	17.13
24	5.59	5.59	378	300	5.83	4.96
25	6.7	6.7	790	461	12.16	7.61
26	5.41	5.08	417	301	6.41	4.98
27	5.67	5.21	399	318	6.14	5.26
28	5.11	5.11	369	258	5.69	4.26
29	6.76	6.76	734	451	11.3	7.45
30	5.46	5.46	557	381	8.57	6.29
31	4.96	4.96	509	510	7.84	8.42
32	3.3	3.3	437	464	6.73	7.67

NOTE: q% for Separan are based on average ΣA_i of row No. 21 and 22, while q% for Glycerol are based on the minimum total flow rate, i.e. $q = 0.685$ which is equivalent to $A_i = 6.49$ cm.

APPENDIX D

FLOW THROUGH PARALLEL PLATES--POWER LAW MODEL

The equation of motion can be, easily, solved for a power-law fluid flow through two parallel plates to obtain the velocity profile. The direction of the coordinates are given in Figure (II-2)

$$u_z = m_1^{-\frac{1}{n}} \frac{n}{1+n} \left(\frac{\Delta P}{\Delta L}\right)^{\frac{1}{n}} R^{\frac{1+n}{n}} \left[1 - \left(\frac{x}{R}\right)^{\frac{1+n}{n}}\right] \quad (D-1)$$

where m_1 and n are power-law model parameters and $R = d/2$ shown in Figure (II-2). Also,

$$\frac{q_i}{\ell} = 2 \int_0^R u_z dx. \quad (D-2)$$

After integrating with Equation (D-1)

$$\frac{q_i}{\ell} = 2m_1^{-\frac{1}{n}} \frac{n}{1+2n} \left(\frac{\Delta P}{\Delta L}\right)^{\frac{1}{n}} R^{\frac{1+2n}{n}}. \quad (D-3)$$

Equations (D-1) and (D-3) may approximate the rectilinear flow through the bundle of glass rods, assuming that the minimum center line opening between two contiguous rods of the same row, with length ℓ , is d and the flow rate passing through that opening is q_i . Therefore,

$$u_z = m_1^{-\frac{1}{n}} \frac{n}{1+n} \left(\frac{\Delta P}{\Delta L}\right)^{\frac{1}{n}} \left(\frac{d}{2}\right)^{\frac{1+n}{n}} \left[1 - \left(\frac{2x}{d}\right)^{\frac{1+n}{n}}\right], \quad (D-4)$$

$$\frac{q_i}{\ell} = 2m_1^{-\frac{1}{n}} \frac{n}{1+n} \left(\frac{\Delta P}{\Delta L}\right)^{\frac{1}{n}} \left(\frac{d}{2}\right)^{\frac{1+n}{n}}. \quad (D-5)$$

where $\frac{\Delta P}{\Delta L}$ is unknown, but can be eliminated by dividing Equation (D-4) by (D-5). Hence,

$$u_z = \frac{1+2n}{1+n} \frac{q_i}{\ell d} \left[1 - \left(\frac{2x}{d} \right)^{\frac{1+n}{n}} \right], \quad (D-6)$$

where q_i is known experimentally. Therefore, the velocity profile can be established for each opening. Also, by setting $x = 0$, the maximum velocity at center line opening can be obtained, i.e.

$$u_{\max} = \frac{1+2n}{1+n} \frac{q_i}{\ell d} \quad (D-7)$$

From Equation (D-5) one can write,

$$q_i = C_5 d^{(1+2n)/n} \quad (D-8)$$

where C_5 is a constant. Equation (D-8) is based on the fact that $\Delta P/\Delta L$ is the same for all the openings.

Equations (D-6, 7, 8) can be applied to a Newtonian fluid by setting $n = 1$, i.e.

$$u_z = \frac{3}{2} \frac{q_i}{\ell d} \left[1 - \left(\frac{2x}{d} \right)^2 \right], \quad (D-9)$$

$$u_{\max} = \frac{3}{2} \frac{q_i}{\ell d} \quad (D-10)$$

$$q_i = C_6 d^3 \quad (D-11)$$

Equations (D-6, 7) can, also, be written in terms of the dimensionless velocity,

$$\frac{u_z}{V} = \frac{1+2n}{1+n} \frac{q_i}{\ell d V} \left[1 - \left(\frac{2x}{d} \right)^{\frac{1+n}{n}} \right], \quad (D-12)$$

$$\tau = \frac{1+2n}{1+n} \frac{q_i}{d} \quad (D-13)$$

Using Equation (C-8),

$$\frac{u_z}{V} = \frac{1+2n}{1+n} \frac{A_i}{d} \left[1 - \left(\frac{2x}{d} \right)^{\frac{1+n}{n}} \right], \quad (D-14)$$

$$\frac{u_{\max}}{V} = \frac{1+2n}{1+n} \frac{A_i}{d} \quad (D-15)$$

For Newtonian fluids,

$$\frac{u_z}{V} = \frac{3}{2} \frac{A_i}{d} \left[1 - \left(\frac{2x}{d} \right)^2 \right], \quad (D-16)$$

$$\frac{u_{\max}}{V} = \frac{3}{2} \frac{A_i}{d} \quad (D-17)$$

The calculated values of u_{\max}/V by Equations (D-15, 17) are recorded in Table (V-2) and the velocity profiles obtained from Equations (D-14, 16) have been shown in Figure (IV-13) for three positions.

APPENDIX E

EXPERIMENTAL DATA POINTS

The complete data points of row No. 21 for the volumetric flow rate of 0.685 cc/sec, and the complete data points of one arbitrary position in each row will be presented. For the other rows and other flow rates only a few necessary points to show the shape of the profiles will be given. The RPM reported in the following tables are based on the chopper disk with one radial slit--refer to Appendix C for more details. The pictures are labeled by the number of rolls and the number of exposure, E. The reported data in the following tables have already been converted to the same RPM. The necessary correction due to the error of the stroboscope reading mentioned in Section (III-4-1 b) is also included in the reported data.

The length of the streaks, S , position X , and the openings, d_M , were read directly from the 0.1 - inch division graph paper on which the pictures were projected and the total magnification was 100 in all cases. The procedure to analyze the data points was discussed in Appendix C. The position numbers are presented in Figure (III-3) and the direction of X and the origin with respect to the light and flow direction is given in Figure (E-1).

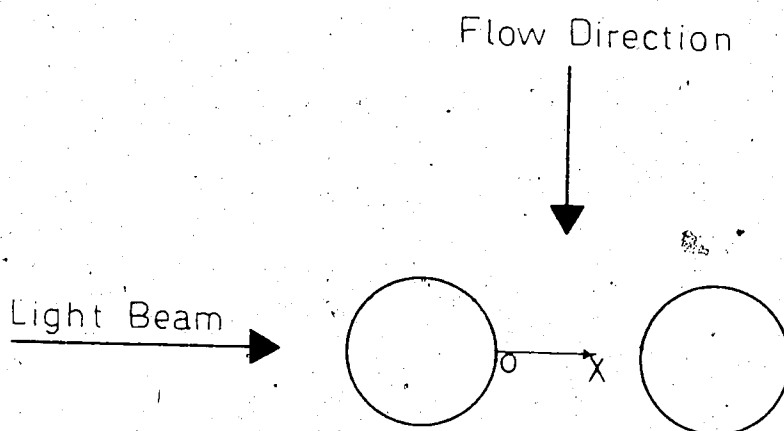


FIGURE E-1 DIRECTION OF x AND THE POSITION OF ORIGIN WITH RESPECT TO THE LIGHT AND FLOW DIRECTION.

TABLE E-1
STREAK LENGTH DATA OF GLYCEROL

$X \times 10^3$ Inch	$S \times 10^3$ Inch	$X \times 10^3$ Inch	$S \times 10^3$ Inch	$X \times 10^3$ Inch	$S \times 10^3$ Inch	$X \times 10^3$ Inch	$S \times 10^3$ Inch
Position No. 1		55	15.5	E19		NCL=62x10 ⁻³ in.	
Roll No. 238		73	15.1	7.5	42.6	4.8	5.8
NCL=91x10 ⁻³ in.		79	15.1	NCL=40x10 ⁻³ in.		23	19.5
q=0.685cc/sec.		86	14.6	E17		32	20.7
RPM=100				10.5	18.5	44.6	11.8
E1		q=3.42cc/sec.		22	22.2	48.2	5
12	6.3	RPM=500		31	17.8	E12	
29	11.1	E11				3	3.1
37	12.9	10	6.4	25	22.2	4.5	9
42	14.8	32	12.6	E19		12.5	12.4
47	15.5	37	13.5	16	22.2	19.5	17
58	15.9	47	14.2	E20		23.5	18.2
61	15.9	63	15.4	32	18.5	43.6	13.3
82	14.8	71	15.2	NCL=62x10 ⁻³ in.		50	7.4
91	14.8	86	15.2	E18		55	3.8
E2				26.7	19.6	E13	
25	11.1	q=6.82cc/sec.		27.1	20	12	12.4
44	14.8	RPM=1000		33.6	18.5	24	16
51	15.5	E16		35	18.1	29	19.2
64	14.8	77	15.6	E19		35.8	17
74	15.5	50	15.6	19.5	14.8	38.7	15.4
83	15.5	E17		21.8	18.5	44.3	12.6
		50	15.6	36.5	17.4	E14	
		55	15.6	58.3	2.96	9	10.1
q=1.717cc/sec.		82	15.2			25	16.7
RPM=250		E18		q=1.717cc/sec.		E15	
E6		40	15.2	RPM=250		3.4	3.1
12	6.9	53	15.2	d=20.5x10 ⁻³ in.		21.5	17.8
34	13.3			E11		50	9.6
44	14.1	Position No. 2		1.1	12.6		
54	15.2	Roll No. 239		NCL=40x10 ⁻³ in.		q=3.42cc/sec.	
57	15.5	d=20.5x10 ⁻³ in.		E11		RPM=500	
66	16.1	q=0.685cc/sec.		2.5	5.9	NCL=40x10 ⁻³ in.	
76	15.5	RPM=100		35.4	13	E6	
79	15.5	E16		E12		7	11.5
91	14	5.2		1.6	3.7	37	6.2
E7		33.3		6	10.1	NCL=62x10 ⁻³ in.	
22	9.9	40.7		E15		E6	
35	13.5	E18		3.7	6.2	3.4	3.9
51	15.5	12.4	44.4	17	22.2	7.4	8.5

TABLE E-1 (continued)

Xx10 ³ Inch	Sx10 ³ Inch	Xx10 ³ Inch	Sx10 ³ Inch	Xx10 ³ Inch	Sx10 ³ Inch	Xx10 ³ Inch	Sx10 ³ Inch
10.2	10.9	41	12.6				
18	16.2	44.4	10.9	q=6.82cc/sec.		E1	15.8
22.5	15.5	48	8.6	RPM=1000			2.4
33.4	18.5	52.2	5.4	NCL=62x10 ⁻³ in.		E2	
35	17.7	54.2	3.7	E1		9.9	9.9
39.5	12.8		E18.	7.6	8.4	15.8	14
45.5	10.1	4.5	5.4	E2		42	13.1
52.8	4.7	15	15.4	6.2	7.7	43.3	11.8
56.4	2.7	18.6	18.7	10.2	10.9	47	9.6
	E7	22	17.7	30.7	17.7		E3
9.2	10.3	27.6	19.8	56	3.3	27.5	16.8
12	12.8	30.5	19.4		E3	51	7.2
14	13.5	39	16.8	37	15.2		E5
45	9.6	50.5	7.6	55.6	3.5	7	6.9
49	7.2	NCL=40x10 ⁻³ in.		E4		12.8	9.1
56	2.6	E11		5.4	6.1	43.5	42
	E8	14.8	18.8	50	6.7		
3.6	5.7	24	24		E5		Position No. 3
18.1	18.5	35	8.8	2	3		
32	15.8		E13	6.2	7.8		Roll No. 263
33.3	16.8	4.6	10.9	49	8.4		NCL=58x10 ⁻³ in.
37.5	14.5	16	22.8	54.5	3.8		q=0.685cc/sec.
39	13.5		E14		E6		RPM=100
46	9.9	3.8	8.3	40	14.3		E16
55.8	3	34	10.1	53	5.3	20	11
	E9		E15	56.3	3	22	12.4
8	8.5	11.8	16.8		E7	33	13.2
21.8	16.5	28	19.4	4	4.4	35.8	9.9
34.4	19.4	34.4	12.6		E8	41	8
38	14.5		E16	7	8.6	47	6.2
41	14.5	1.6	3.9	30	16.9	50.5	4
	E10	8.5	15.2	51	6.7		E17
5	4.9	17.2	23.6		E9	10.4	5.9
17.8	14.2	31.3	16.1	9	12.2	14.8	9.1
36.5	16.1		E17	21	15	24.2	12.8
52.5	6.2	29.5	17.7	24	14.7	31.8	12.1
Roll No. 262			E18	32.5	15.2	35	12.1
	E11	11.8	23.4	34.3	14.7	36.8	12.1
3	5.9	14	22.4		E10	47.4	6.6
19	18.9	28.3	20.2	30.5	16.4		
21.7	19.4		E19	50.7	6.2		q=1.717cc/sec.
25.5	22.8	31.6	18.5	52.5	5.6		RPM=250
31.6	18.5		E20	55.5	3.4		E11
33.8	17.7	16	21.1	Roll No. 239		3.4	2.5

TABLE E-1 (continued)

$X \times 10^3$ Inch	$S \times 10^3$ Inch	$X \times 10^3$ Inch	$S \times 10^3$ Inch	$X \times 10^3$ Inch	$S \times 10^3$ Inch	$X \times 10^3$ Inch	$S \times 10^3$ Inch
8.8	5.1	q=0.685cc/sec.				15	9.9
29.4	13.2	RPM=100				22	14.1
39.4	9.4	NCL=57x10 ⁻³ in.			q=3.42cc/sec.	38	6.2
44.8	7	E1			RPM=500		
48	5.1	15.2	10.2	30	E9	E13	
53	2.2	18.8	11.7	44		7.2	5.9
	E12	24.4	13.2		E10	9.8	7.4
5	3.7	32.5	13.9	5		16	10.4
7.8	4.7	37.5	12.4	34		40.5	6.1
11	6.6	43.7	8	44.2			
27	11.7	48	5.5	49.5		q=3.42cc/sec.	
38	10.7	NCL=37x10 ⁻³ in.			E11	RPM=500	
47	5.9	10.8	15.4	9		E6	
49.5	4	27.3	15.7	49		17.4	11.8
55	1.76	30	9.1			30.4	12.9
		32	8.8		q=6.82cc/sec.	5	4.2
q=3.42cc/sec		34.3	5.5		RPM=100	26	11.3
RPM=500		E2			E15	31.5	11.8
	E1	17.4	18.3	28		E8	
11.5	6.2	25.8	14.6	32.4	13.5		
19.3	10.3	28.3	11		13.7	15	9.9
35.5	11.3	NCL=57x10 ⁻³ in.		Position No. 5		24.6	12.6
46.8	5.7	25.5	14.3				
	E2	38.2	11		Roll No. 265	q=6.82cc/sec.	
8	4.2	41.5	8.8		q=0.685cc/sec.	RPM=1000	
20	12.3	46	5.9		RPM=100	E1	
48	5.4	49	3.7		NCL=48.2x10 ⁻³ in.	29.4	11.8
51.5	3.3				E16	E3	
		q=1.717cc/sec.		13.4		8.9	5.9
		RPM=250		17	10	29	9.7
		E5		24.5	12.2	39	6.7
	E6	NCL=37x10 ⁻³ in.		40.5	14	E4	
7.4	5.4	12	17.9	43	7.4		12.2
	E7	NCL=57x10 ⁻³ in.			5.5		
11	6.2	11	8.8	20.5	E17	Position No. 6	
44	7.2	19	12.5	27		Roll No. 243	
	E8	35.3	12.9	43.5	13.3	q=0.685cc/sec.	
21.2	11.2	45	6.4		4.4	RPM=100	
	E9					NCL=43x10 ⁻³ in.	
5	3.5	10.5	7.2		q=1.717cc/sec.	E16	
		13	7.9		RPM=250		
		24	13.9	23	E11	6.6	11.3
Position No. 4		31	13.6	42		11.2	15.7
Roll No. 264		45	6.6		E12	18.7	22
						20	23.8

TABLE E-1 (continued)

$X \times 10^3$ Inch	$S \times 10^3$ Inch	$S \times 10^3$ Inch	$X \times 10^3$ Inch	$S \times 10^3$ Inch	$X \times 10^3$ Inch	$S \times 10^3$ Inch	$X \times 10^3$ Inch
21.5	24.2		E14			5	25.2
28	22.3	32.7		17.5	8	12.6	31
32	18.3		E15		17	18.3	26.3
38	11	14		8.1	17.9	18.7	
	E17		E16		21.4	16.8	
8.6	12.8	8.8		6.2			$q=1.717\text{cc/sec.}$
34.8	12.4	48		10.9			RPM=250
					$q=3.42\text{cc/sec.}$		E11
					RPM=500		
						1	6.8
$q=1.717\text{cc/sec.}$		$q=6.82\text{cc/sec.}$			E11	4.1	19.3
RPM=250		RPM=1000		2.2		6.1	25.5
			E2	5	3.6	12.4	29.1
7	12.3	16		13.1	11.8		
16.6	21		E3		16.5	1.2	12.1
23.3	22.7	7		4.6	21.3	3	17.6
32	16.3	11.8		8.8		5.4	23.8
	E12				E12	12.2	28.8
7.3	11.6		<u>Position No. 7</u>	6.3	8.5	14	25.9
16.5	19.5			12.5	10.1	17.7	14.5
26	20.5		<u>Roll No. 244</u>	22.1	16.8		
	E13				12.6		
10	12		$q=0.685\text{cc/sec.}$				$q=3.42\text{cc/sec.}$
11	14.6		RPM=100				RPM=500
20.6	23.4		$NCL=32.8 \times 10^{-3}\text{in.}$		$q=6.822\text{cc/sec.}$		E6
					RPM=1000		
			E1			2.1	13.5
		5.2		9.1	4.8	3.8	18.5
$q=3.42\text{cc/sec.}$		10		14.3	23	4.8	22.3
RPM=500		13		16.5			
	E6	17.7		16.5	E17		E7
4.5	8.1	27.2		9.9	1.2	2.6	8.3
15	18.5		E2		24.5	10.5	18.5
31.4	16.8	8		12.4	1	2.1	26.3
35	12.9	16		18.6	26.8	7.4	
37	10.1						$q=6.82\text{cc/sec.}$
	E7						RPM=1000
3.4	6.6		$q=1.717\text{cc/sec.}$		<u>Position No. 8</u>		E3
			RPM=250			11.4	26.7
Roll No. 266			E6		Roll No. 245	8	25.3
$NCL=63 \times 10^{-3}\text{in.}$		5		8.8	$q=0.685\text{cc/sec.}$	17.5	20.4
	E11	13.8		16.1	RPM=100		E5
13	6.9	18		22	$d=22.5 \times 10^{-3}\text{in.}$	3.4	16
	E12	23		16.1		17.3	17.1
11.5	7.8		$d=21.6 \times 10^{-3}\text{in.}$	3			
35	19.9	12		24.9	7		
	E13		$NCL=32.8 \times 10^{-3}\text{in.}$	14.4			<u>Position No. 9</u>
35.2	16.8						
47.3	11.8	6	E7	19			<u>Roll No. 246</u>
				8.1	E17		$q=0.685\text{cc/sec.}$

TABLE E-1 (continued)

$X \times 10^3$ Inch	$S \times 10^3$ Inch	$X \times 10^3$ Inch	$S \times 10^3$ Inch	$X \times 10^3$ Inch	$S \times 10^3$ Inch	$X \times 10^3$ Inch	$S \times 10^3$ Inch
RPM=100 $d=31 \times 10^{-3}$ in.		Roll No. 247 $q=0.685$ cc/sec.		$NCL=64 \times 10^{-3}$ in.		45	4.6
E1		RPM=100		E1			
11.6	43.2	$d=19.3 \times 10^{-3}$ in.		2.7	9.2	$q=6.82$ cc/sec.	
14	43.2	E19		5.7	9.2	RPM=1000	
15.3	43.2	10.8	29.6	12.5	9.2	E16	
21.5	35.3	E20		40	4.8	9	8.8
24.5	23.8	14	26.2	4.4	9.2	38	6.1
E2		E21		5.3	9.2	47	4.2
7	32.4	8.9	34	10	9.2	56	2.2
11.4	39.6	10.3	29.6	34	4.5	60	1.1
21	37.8	15.2	23.2	40	4.5	E17	
				45.5	4.1	28	7.4
$q=1.717$ cc/sec.		$q=1.717$ cc/sec.				33	6.5
RPM=250		RPM=250		$q=1.717$ cc/sec.		46	4.6
E6		E11		RPM=250		59	1.7
4.5	21.6	13.8	22.2	E6		<u>Position No. 12</u>	
16.2	40.3	E13		2.5	9.6		
21	33.1	12	28	4	9.6	Roll No. 228	
26	22			11	9.6	$q=0.685$ cc/sec.	
E7		$q=3.42$ cc/sec.		19	8.1	RPM=100	
20	36	RPM=500		36	6.2	$d=157.5 \times 10^{-3}$ in.	
23.2	27	E6		42	5.2	E16	
		16	12.6	50	3.7	17.6	6.98
$q=3.42$ cc/sec.		E7				36	11.76
RPM=500		14	20.6	1	9.7	39.5	12.85
E11		E8		3	9.7	42.3	12.85
1.2	9.8	10	32.2	17	8.7	76.6	15.8
28	8.1	12.4	19.1	23	8		E17
E13		E9		44	4.7	41.5	13.22
2	9.3	13.8	22	53	3	58	14.7
22.2	30.3	E10				70.4	16.52
E14		15	10.9	$q=3.42$ cc/sec.			E18
6	29			RPM=500		41	13.22
15.5	40.5	$q=6.82$ cc/sec.		E11		44.4	13.22
3.7	22	RPM=1000		0	9.8	61.8	16.15
		E1		10.5	9.5		E19
$q=6.82$ cc/sec.		4.5	26.1	28	6.7	17	6.24
RPM=1000						42	13.6
E17		<u>Position No. 11</u>		E12		9.6	63.8
16.2	38.3	0				9.5	74
		Roll No. 248		13	9.5	92	16.52
<u>Position No. 10</u>		$q=0.685$ cc/sec.		21	8.5	97.4	15.42
		RPM=100		38	5.9	138.4	8.45

TABLE E-1 (continued)

$X \times 10^3$ Inch	$S \times 10^3$ Inch	$X \times 10^3$ Inch	$S \times 10^3$ Inch	$X \times 10^3$ Inch	$S \times 10^3$ Inch	$X \times 10^3$ Inch	$S \times 10^3$ Inch	
	E20	90	16.1	27.7		7.35	9.4	17.8
11.5		6.24	E3		E2		E7	
15		6.24	28	10.6	5.6	9.2	24	3.68
43		13.22	139	7.1	8.2	11		E8
66.7		15.8			12.6	12.1	10.6	18.8
80.6		16.52	Position No. 13		15.3	14.7		E9
				18.3		13.2	4.4	11.7
q=1.717cc/sec.		Roll No. 229		22.5		11.75	7.5	16.4
RPM=250		q=0.685cc/sec.		29		4.77	14.6	16.1
	E11	RPM=100			E3		22.3	3.08
21		8.1	d=25x10 ⁻³ in.		7.4	11		
58		15.7	E1		12.7	12.8	q=3.42cc/sec.	
71.5		16.6	7.4	16.2	14.6	14.3	RPM=500	
74		16.2	9.8	17.3	17.6	13.6	E11	
79		16.9	10.9	19.1	24.4	9.55	13.7	17.1
	E12		17.8	16.2	27.5	7.35		E13
10		4.4	20.6	8.8		9.55	5.1	12.6
16		5.7			3	4.5	9	16.8
19		6.6	7	15.4	9	11	NCL=32.9x10 ⁻³ in.	
31		10.3	13.6	19.8	14.7	12.8		E11
			17	16.5	20.5	12.5	10.2	12.8
q=3.42cc/sec.		23.8		2.94	23.6	7.6	18.1	15.2
RPM=500					25	7.6		E13
	E6		5.1	14.3	29	5.9	6.5	10.5
16.7		6.3	6.1	14.3			11.4	13.8
27		9.1	13.4	18.7	3.3	5.14		E14
33		11.8	21.1	10.3	8	11.7	27.2	6.6
	E7				11	13.6		
9		4.3	7	13.6	18.8	14	q=6.82cc/sec.	
23		8.8	14.8	17.6	28	6.24	RPM=1000	
29.5		10.5	21	11			d=25x10 ⁻³ in.	
44		13.5						E16
68		15	2.6	6.25	q=1.717cc/sec.		4.8	9.6
103		15.2	3.6	6.6	RPM=250		NCL=70.8x10 ⁻³ in.	
124		12.2	7	14.7	6.1	7.3	8	1.6
			14.6	18.4	12	13.6	13.4	2.8
q=6.82cc/sec.		19.3		14.7			20	4.8
RPM=1000		NCL=32.9x10 ⁻³ in.		8		9.5	38.2	7
	E1		E1	29.5		2.1	57.5	4.2
19.5		7.6	5.1	8.45		E8	64.4	2.2
23		8.5	8.8	11.4	14.3	13.6		E17
32		10.9	12	13.6	19.6	12.6	24.3	5.5
	E2		14	15.1	d=25x10 ⁻³ in.		31	6.6
20		7.1	23.5	11		E6	40.6	6.4

TABLE E-1 (continued)

$X \times 10^3$ Inch	$S \times 10^3$ Inch	$X \times 10^3$ Inch	$S \times 10^3$ Inch	$X \times 10^3$ Inch	$S \times 10^3$ Inch	$X \times 10^3$ Inch	$S \times 10^3$ Inch
25	11.8	28	13.2			23	14.7
28	10.5	36.6	11	Position No. 17		30	8.7
	E14	41.3	7.35				E7
30.4	9.3	47	4.4	Roll No. 233		7	7.3
				q=0.685cc/sec.		10.5	10.3
Position No. 16		q=1.717cc/sec.		RPM=100		20	14.7
		RPM=250		d=19.5x10 ⁻³ in.		27	11
Roll No. 232			E11		E2		E8
q=0.685cc/sec.		20	12.5	2.2	7.3	12.7	13.2
RPM=100		23.8	15.3	5.5	20.6	20	14
d=24.1x10 ⁻³ in.		27	14.3	11.5	22.4	25	13.2
	E17	30	12.8	13.5	22		E9
20	11.4	31.6	13.2		E4	4	7.8
21	12.1	38	9.1	15	18.4	11.8	11.7
	E18	46.4	3.7	17	18.4	17.3	14.7
21.8	6.6	d=24.1x10 ⁻³ in.			E5		E10
	E19	E11	10	24.6	2.8	4.7	
9.5	31.2	19.6	11.5	NCL=35.2x10 ⁻³ in.		4	6.6
15.5	24.2	E13	E1		8	8.8	
21.3	9.18	17	20.6	8.8	10.6	10.8	12.2
	E20	E14	23		11.7	20	12.6
16.5	19.8	18.2	12.5	26	10.6	31	4.4
NCL=52x10 ⁻³ in.		E15	E2			d=19.5x10 ⁻³ in.	
	E16	15.3	23.1	4.8	6.24		E6
29	14.7	19.8	15.7	8.5	11.4	10.8	24.2
45.3	5.5			11.8	14.3		E7
	E17	q=3.42cc/sec.		22.5	14.7	12.8	22.3
28.5	15.06	RPM=500		25.5	11	11	23.5
30.6	12.5	NCL=52x10 ⁻³ in.		27.4	8.45		E9
39	8.44	E7	E3			2	11.5
45.3	5.5	16.4	13.5	29	7.3		
	E18	23.5	14.5		E4	q=3.42cc/sec.	
31.3	12.8	42	5.9	23	14	RPM=500	
33	12.8	48.5	2.3	26.5	11	NCL=35.2x10 ⁻³ in.	
45	4.8			31	5.5		E11
	E19	q=6.82cc/sec.			E5	14.6	12.9
20	13.6	RPM=1000		10.3	14.3	16.4	12.2
22	14.3	E1		18.2	15.1	20	16.1
26	15.4	23	13.2			25	12.5
32.6	12.5	26	12	q=1.717cc/sec.		31.3	4.2
41	8.1	35	10.9	RPM=250			E12
45.6	4.04	42	7.5		E6	8	8.6
	E20	d=24.1x10 ⁻³ in.		15	13.2	13	11.8
14.7	13.2	15.5	22	19	15.4	16.4	14.8

TABLE E-1 (continued)

$X \times 10^3$ Inch	$S \times 10^3$ Inch	$X \times 10^3$ Inch	$S \times 10^3$ Inch	$X \times 10^3$ Inch	$S \times 10^3$ Inch	$X \times 10^3$ Inch	$S \times 10^3$ Inch
<u>Position No. 21</u>		78	10.3	32.5	8	E6	
Roll No. 237		85.5	10.3	34	8.4	13.2	5
q=0.685cc/sec.		95	9.2	36.1	9	19	7.2
RPM=100		q=1.717cc/sec.		61.2	10.1	24	9.6
d=129x10 ⁻³ in.		RPM=250		70	9.5	44.3	14.2
E16		E11		80.4	9.5	53.2	14.2
59.8	9.2	99.2	3.1	102	7.9	66.5	15.8
64.2	10	11.8	3.7	107	6.8	81.1	17.2
68	10	13.4	4.7	120.3	4.7	E7	
70	10	11	7.8	<u>Position No. 22</u>		25.5	9.5
81.2	9.2	15	8.4	Roll No. 249		78.8	16.7
85	9.2	q=0.685cc/sec.		q=6.82cc/sec.		84	16.5
109.5	6.7	47.3	9.2	RPM=100		RPM=1000	
127.2	3.3	47.5	9.3	NCL=84x10 ⁻³ in.		E3	
E17		67	10.1	E16		7	3.3
34.4	8.1	72	9.8	7.2	2.22	11.7	4.7
39.2	9.2	87	9.6	25	8.1	15.4	6.9
48.3	8.9	93	9	39	11.1	18.4	7.6
52.4	10	97	8.4	64	14.8	21	8.1
55	10	109	6.7	84	14	E4	
57	10.3	q=3.42cc/sec.		E17		5.6	2.3
72	10	RPM=500		44	12.2	27.3	10.1
86.5	9.2	E6		53.8	13.7	32.7	10.8
105.8	7.4	41.2	8.9	q=1.717cc/sec.		84	13.5
114.3	7	45	9.6	RPM=250		<u>Position No. 23</u>	
E18		53.4	9.5	E11		Roll No. 250	
30.4	8.1	66	9.9	E12		q=0.685cc/sec.	
35.2	9.2	72.3	10.1	12.5	5.5	RPM=100	
58	11.5	80.3	9.1	24.7	8.9	NCL=60x10 ⁻³ in.	
68	10	85.5	9.3	35.6	12.3	E1	
84.5	10	92	8.6	54	9.9	E1	
E19		98.8	7.8	65	15.2	8.3	11.1
41	8.9	107.8	6.6	79	16	26.5	25.5
46.2	10.3	111.7	6.6	E12		31	25.1
53	10.3	q=6.82cc/sec.		13	5.5	39.4	19.6
58.5	10.3	RPM=1000		22	8.9	44	16.6
76.2	10	E1		27.4	10.2	56.4	4.06
82.5	9.2	11.2	4.2	78	15.5	E2	
90	8.9	23.2	6.9	82	15.7	29.7	24.8
94	8.1	25	6.7	q=3.42cc/sec.		37.3	22.2
107.8	7.4	27.6	7.7	RPM=500		39.4	21.4
E20		q=3.42cc/sec.		RPM=500		21.4	

TABLE E1 (continued)

$X \times 10^3$ Inch	$S \times 10^3$ Inch	$X \times 10^3$ Inch	$S \times 10^3$ Inch	$X \times 10^3$ Inch	$S \times 10^3$ Inch	$X \times 10^3$ Inch	$S \times 10^3$ Inch
50	10.7	1.5	10.7	52.4	1.7	7.4	7.3
		5.5	20.5		E12	17.2	14.7
$q=1.717\text{cc/sec.}$		8	23.7	21.5		20	16.2
RPM=250		10	23.2	44		21.5	16.9
E6		17	22.7	50		2.8	25.3
22	24.4		E18		E13	28.9	20.2
29	24.5	10.8	25.3	21.5		7.7	35
42	17	17	14.7	12.3		4.6	39.3
	E7	$NCL=59 \times 10^{-3}\text{in.}$					42
24.6	25.1		E11	$q=6.82\text{cc/sec.}$		49	16.9
	E10	6.8	3.2	RPM=1000		52.4	12.8
14	15.2	16.2	7.7	E1		57.5	9.9
39.3	22.2	19.1	9.3	7.6		3.5	6.2
52.2	8.9	25	9.6	15.8		6.6	60
		32.5	8.3	19.2		6.8	
$q=3.42\text{cc/sec.}$		41	6.4		E2		$q=1.717\text{cc/sec.}$
RPM=500		45	4.5	6		3.1	RPM=250
E11		49.5	2.9	18.4		6.5	E15
35	17.1		26.3	52.5		7.2	13.8
	E12	$q=1.717\text{cc/sec.}$				2	17.2
44.4	12.2	RPM=250			E3		19
52	6.1		E1	6		3.1	30.5
	E13	11.1	5	45		3	41.5
44.4	12.7	16	6.1				45.5
55.8	4	20.2	7.4	<u>Position No. 25</u>			50
	E14	41.6	6.2				61.5
38.5	16.2	43.5	6.7	Roll No. 253			$d=26.4 \times 10^{-3}\text{in.}$
40	13.8	51.3	3.3	$q=0.685\text{cc/sec.}$			18.5
53	5	54	2.3	RPM=100			E16
		$d=22 \times 10^{-3}\text{in.}$		$d=26.4 \times 10^{-3}\text{in.}$			6.5
<u>Position No. 24</u>			E2		E18		20
		0.9	7.3	7.8		34.2	E17
Roll No. 252		7.2	8.3	13		39.3	6
$q=0.685\text{cc/sec.}$			E7	24.8		12.8	15.1
RPM=100		5	17.1		E19		19.5
$d=22 \times 10^{-3}\text{in.}$		11.5	20	7		33.1	24
E12				15		40.4	
7.7	24	$q=3.42\text{cc/sec.}$			E20		$q=3.42\text{cc/sec.}$
13	23.7	RPM=500		8		36	RPM=500
	E13	Roll No. 251		10.6		39.6	E8
4.8	15.7	$NCL=59 \times 10^{-3}\text{in.}$		13.2		40	3.3
9	23.5		E11	$NCL=66 \times 10^{-3}\text{in.}$			5.4
11.6	22.7	21.3	7.9		E18		E9
	E14	27.5	8.6	5.4		5.5	1.8
							$NCL=66 \times 10^{-3}\text{in.}$

TABLE E-1 (continued)

$X \times 10^3$ Inch	$S \times 10^3$ Inch	$X \times 10^3$ Inch	$S \times 10^3$ Inch	$X \times 10^3$ Inch	$S \times 10^3$ Inch	$X \times 10^3$ Inch	$S \times 10^3$ Inch
	E8		E1				
2	1.7	7.4	5.9	9.8	26.4	5.5	20.5
8.2	7.2	10.5	7.3	19.5	5.7	11.8	27.3
13.5	11.8	13.4	9.9	9	E11	16	18
27.2	19.9	29.6	13.2		E12		E4
37	19.9	32	12.5	5.3		13.4	24.1
47.7	10.1	33.4	11	7.2	20.7	19.4	9.3
55.5	9.1	35.8	9.9	NCL=49.5x10 ⁻³ in.	22.8		E5
57.3	7.6	37.6	8.4	E9		2.6	12.6
		42	5.5	2.4	2	6.2	21.9
q=6.82cc/sec.		44	4.8	10	7.7	11.1	25.4
RPM=1000		45.7	3.3	14	8.5		E6
	E1			22.2	12.8	1.4	10
16.5	12.3	q=1.717cc/sec.		31.4	12.3	14	25.9
32	14.3	RPM=250		37	10.1		21.2
	E2		E5	46	2.3		E7
1.2	3.2	11	9.8			2.3	10
8.8	9.1	15	12.9	q=6.82cc/sec.		6	21.6
35.5	14.3	16.8	12.9	RPM=1000		16.3	15.4
	E3	20.5	12.9	E13		6	E8
15	11.5	22.3	13.2	8.2	6.8	14.5	22.3
16.5	11.1	24	13.2	30	12.3		21.6
	E4	26	13.1		E14	11	E9
2	2.6	27.2	12.3	8.7	7.1	12.6	24.4
59.1	5	28.8	13.2	25.5	11.8		24.1
63.3	1.9	35	10.3		E15	7.2	E10
		37.7	8.5	8	6.7		22.6
<u>Position No. 26</u>		40	7	28	10.9	13.6	25.2
		42	4.4	39	7.9	17.2	12.6
Roll No. 254		d=20x10 ⁻³ in.		47	2.2	NCL=44.7x10 ⁻³ in.	
q=0.685cc/sec.		5	19.1			7.8	E1
RPM=100		7	24.2	<u>Position No. 27</u>		9.2	7.2
d=20x10 ⁻³ in.		10.5	27.9			12	6.5
	E1	18	13.2	Roll No. 256		14.4	9.7
16.5	18.7		E6	q=0.685cc/sec.		17.5	11.5
	E2	6	21	RPM=100		18.2	11.5
6.3	22	8	25	d=20.5x10 ⁻³ in.		22	12.6
9.8	28.6	12	24.2	E1		24.5	14.4
17.5	17.2	16.4	19.1	10.3	25.2	32.5	14.4
	E3	18	13.2		E2	37	11.1
16.5	18.3			8.8		40	8.3
	E4	q=3.42cc/sec.		11.6	26.6	43	5.4
15.2	20.9	RPM=500		19.2	27.3		3.6
NCL=49.5x10 ⁻³ in.		E9			6.1		E2
				E3		12.8	9.7

TABLE E-1 (continued)

$X \times 10^3$ Inch	$S \times 10^3$ Inch	$X \times 10^3$ Inch	$S \times 10^3$ Inch	$X \times 10^3$ Inch	$S \times 10^3$ Inch	$X \times 10^3$ Inch	$S \times 10^3$ Inch
22.4	12.1	12.3	10.8			8	6.9
25.5	14.1	15	12.9	q=3.42cc/sec.		11.4	9.1
28.5	13.6	19.2	13.5	RPM=500		15.3	11.6
30.2	12.8	23	14.4	Roll No. 255		17	11.8
35.5	9.2	25	15.1	E11		19.7	12.6
41.5	4.3	29	12.2	5.8	20.3	22.3	13.9
	E17	d=20.5x10 ⁻³ in.	NCL=44.7x10 ⁻³ in.			24.8	12.8
2	1.7		E11	6	6.6	34.3	10.1
4.4	4.5	2		9.5	7.8	36.5	6.2
9.1	9.9	12.7	12.9	10.3	8.5		E16
11.4	10.2	16	15.2	12.6	11.5	7.4	
23.2	15.4	18	9.3	15	13.2	9	5.9
27.8	11.4		E12	21.5	12.3	14	7.4
29.4	11.6	1		30.8	11.5	23.8	10.9
39.3	3.9	11	6.6	36	8.3	28.5	11.6
41	2.2		E13	42	3.3	36	11.3
	E18	10.8	24.4		E12	43.5	8.6
1.6	0.7		E14	3	3.3		2.6
5	4.3	5	21.3	5.6	5.7	6.7	E17
6.5	5	10	25.9	10	8.8	9	5.4
9	7.9	17.8	9.5	12	9.3	17.4	7.5
12	10.3		E15	16.5	10.9	18.4	12.6
20	11.9	3.2		28	12.2	30.6	10.8
26	16.1	9	13.9	26	10.1	38.4	9.8
32.5	10.3		E16	37	7.6	42.5	6.2
33.5	10.3	4	17	42.3	3.6		3.3
42	3	13	21.8		E13	5.6	E18
	E19	18	9.3	6.5		11.3	5
5.2	4.7		E17	10.3	6.6	15	9.1
14	12.2	3.2		13	8.9	17.2	11.1
18	13.2	5.5	18.4	21.2	10.9	23.5	11.8
20.5	14.4	9.5	19.4	25.5	13.5	38.5	12.6
23	14.4	18	23.2	33	14.4	43.4	6.2
25	12.9		7.3	36.3	9.3		2
29	12.2	1.3	E18	38.5	7.6		E19
30.5	11.1	7		41.5	5.4	10	7
31.5	10.5	14	9.2	23	3	10.8	8.8
35	8.9		20.8		E14	13	10.1
35.6	7.2	3.2	E19	6	4.2	17	11.3
39.6	3.6	10.5		9.6	12.5	19.6	11.5
	E20		E20	25.9	13.5	43	3.3
4.4	4.5	3		31.5	11.8		E20
6.2	5.5	6.6	13.6	43.5	3.2	5	4.2
7.6	7.2	10	23.4		E15	6.2	5.2
			23.7	6.4		9	7

TABLE E-1 (continued)

$X \times 10^3$ Inch	$S \times 10^3$ Inch	$X \times 10^3$ Inch	$S \times 10^3$ Inch	$X \times 10^3$ Inch	$S \times 10^3$ Inch	$X \times 10^3$ Inch	$S \times 10^3$ Inch
39	6.6	4	17.6	16	15.8	RPM=250	
		9.1	24.8	17.2	10.5	E11	
q=26.82cc/sec. RPM=1000		14.2	20.2		E8	8	15.4
E1		16.6	12.6	5	19.4	10	19.2
13	8.8	1.4	7.56	16.3	22.8	22.7	24
17	10.5	NCL=35x10 ⁻³ in.		NCL=35x10 ⁻³ in.		25.8	23.6
19.3	12.6	E1		E7		42	6.6
		5.8	8.3	2.5	3.7	12	18.7
4	3.1	7.3	10.8	7.7	10.1	16	18.9
40.3	4.7	9	10.8	14	13.5	19.5	19.5
43.5	2.9	11	12.6	19.5	11.8	23	21
		12	13.3	29	10.1	30	15.5
8	5	24	13.3	32.2	5.9	36	14.3
39	4.3	29.3	9.4			37	13.6
		33	2.9	q=6.82cc/sec. RPM=1000		40.5	6.2
10	8			E11			
40	5.4	q=1.717cc/sec. RPM=250		3	4.7	q=3.42cc/sec. RPM=500	
6.4	4.7	E4		4.2	6.4	E6	
22.6	12.3	3.6	5.8	13.7	14	12	18.3
43	2.6	4.8	7.2	22.1	14.6	14	17.5
		6	7.9	25	11.8	24.4	21.6
11.4	8	7	10.1	27.2	10.1	36	18.7
43	2.8	8.5	10.7	29	6.9		E7
		10.4	13			16	24.6
25.3	13.5	15	13.4	Position No. 29		22	23
		16.8	15.4				
11.5	9.1	21	14.8	Roll No. 223			
37	7.6	27	11.5	q=0.685cc/sec. RPM=100		q=6.82cc/sec. RPM=1000	
		29	9.2	RPM=100		E1	
Position No. 28		34	2.4	NCL=45x10 ⁻³ in.		18	20
		d=20.1x10 ⁻³ in.		E16		22.4	23.4
Roll No. 257		2.2	12.5	13	21	30	17.8
q=0.685cc/sec. RPM=100		4.4	18	15	24	32.6	17.7
d=20.1x10 ⁻³ in.		6	21.6	19	25.5		E2
E1		9.5	25.5	23	25.8	15	18.7
		12	23.8			22.5	26.4
0.6	3.96	16.5	15.4	7.2	13	34.5	17.1
6.4	21.2			12.8	22.5		
13.3	21.6	q=3.42cc/sec. RPM=500		26	24.4	Position No. 30	
17	16.2	E7		30	22.2		
1.8	10.4		16.7	q=1.717cc/sec.		Roll No. 224	q=0.685cc/sec.

TABLE E-1 (continued)

$X \times 10^3$ Inch	$S \times 10^3$ Inch
-------------------------	-------------------------

5	8.8
---	-----

$q=6.82\text{cc/sec}$

RPM=1000

Roll No. 227

E2

1.4	9.3
-----	-----

E3

19.6	7.5
------	-----

25	7.2
----	-----

E4

1.5	8.1
-----	-----

12	8
----	---

25	7.2
----	-----

TABLE E-2

STREAK LENGTH DATA OF SEPARAN

Xx10 ³ Inch	Sx10 ³ Inch	Xx10 ³ Inch	Sx10 ³ Inch	Xx10 ³ Inch	Sx10 ³ Inch	Xx10 ³ Inch	Sx10 ³ Inch
<u>Position No. 1</u>		102	17.8	d=20.5x10 ⁻³ in.		14.2	15.7
		111	13.5	E18		E18	
Roll No. 205				14	28.2	21.7	13.3
NCL=118x10 ⁻³ in.		30	14.5	E20		E20	
q=0.685cc/sec.		55	13.9	10.4	35.6	22	10.4
RPM=100				E18			
39	E6	36	14.5	q=3.42cc/sec.		q=3.42cc/sec.	
42		72	17.8	RPM=500		RPM=500	
	E7			E1		NCL=37x10 ⁻³ in.	
43				2	17.2	E1	
42				RPM=1000		29.9	9.4
85		113	9.6	19	24.8	E3	
110				E4		27.5	11.4
113		109	11.1	21.5	25.6	E5	
	E8					19.4	16.1
41		104	11.9	q=6.82cc/sec.		q=6.82cc/sec.	
62				RPM=1000		RPM=1000	
72		30	11.9	E6	16.2	E7	
74		108	10.6	E8		10	8.5
95				29	8.5	13.5	16.1
97		<u>Position No. 2</u>		E10			
				26	10.5	<u>Position No. 5</u>	
q=1.717cc/sec.		Roll No. 206		<u>Position No. 4</u>		Roll No. 209	
RPM=250		q=0.685cc/sec.		Roll No. 208		q=0.685cc/sec.	
65	E1	RPM=100		q=0.685cc/sec.		RPM=100	
86		NCL=40x10 ⁻³ in.		RPM=100		NCL=58x10 ⁻³ in.	
	E2	20.5	21.3	NCL=29.5x10 ⁻³ in.		41	5.9
38		31.7	12.8	E11		E7	
94				6	11.5	31.5	7.4
	E3	q=1.717cc/sec.		E12		E8	
30		RPM=250		21.3	14.8	13.4	5.5
74				E16		40.5	6.7
115		11.8	19.3	E14			
				4	8.1	E9	
		12	21.6			27	10
		29	12.9	q=1.717cc/sec.		37.6	7.4
	E16			RPM=250			
57		27	18.6	E18		E10	
				E16		41	6.7

TABLE E-2 (continued)

$X \times 10^3$ Inch	$S \times 10^3$ Inch	$X \times 10^3$ Inch	$S \times 10^3$ Inch	$X \times 10^3$ Inch	$S \times 10^3$ Inch	$X \times 10^3$ Inch	$S \times 10^3$ Inch
NCL=44.5x10 ⁻³ in.		E12		q=6.82cc/sec.			
28	E7	11.5	7.3	RPM=1000		q=6.82cc/sec.	
23.7	E9	12.2	6.6	NCL=43x10 ⁻³ in.		RPM=1000	
q=1.717cc/sec.		Position No. 6		24.3	16.2	3.4	16.5
RPM=250		Roll No. 210		32.2	10.6	9.8	17.8
19	E4	9.3	9.5	5.7	5.5	14	21.2
NCL=58x10 ⁻³ in.		q=0.685cc/sec.		E8		E15	
50.5	E2	3.8	12.8	11	10.2	8.7	
19.5	E3	5.9	14.7	24	11.9	22.8	
32.5	E4	8.6	12.8	Position No. 7		Position No. 8	
17.5	E4	7.4	14.7	Roll No. 211		Roll No. 212	
20.6	E4	7.7	12.8	q=0.685cc/sec.		q=0.685cc/sec.	
30.3	E4	9.6	14.7	RPM=100		RPM=100	
45	E5	4.9	9.2	d=21.6x10 ⁻³ in.		d=22.5x10 ⁻³ in.	
30	E5	9.5	9.2	2	6.6	3.8	12.1
33.5	E5	9.6	9.2	3.6	14.7	9.5	22.4
q=3.42cc/sec.		E15		10.2	23.1	4.2	14.7
RPM=500		E16		10.3	23.1	17.2	16.5
45.8	E16	4.9	14.5	4.6	16.9	11	18.7
13	E17	4.2	12.5	3.5	14.7	E2	22
12.2	E20	4.1	12.5	16	20.2	E3	16.5
NCL=44.5x10 ⁻³ in.		q=3.42cc/sec.		E7		E3	
14	E17	7.7	14.7	E8		E4	
q=6.82cc/sec.		RPM=500		E9		E5	
RPM=1000		E1		E8		E4	
NCL=58x10 ⁻³ in.		E2		E9		E5	
20.6	E11	6.4	7.4	10.3	23.1	16.2	14.7
37	E11	7.1	12.3	4.6	16.9	11	22
40	E11	5.4	15.5	3.5	14.7	E1	14.7
q=6.82cc/sec.		E4		16	20.2	E2	14.7
RPM=1000		E5		q=1.717cc/sec.		q=1.717cc/sec.	
NCL=58x10 ⁻³ in.		E4		RPM=250		RPM=250	
20.6	E11	6.4	16.2	2.3	8.8	E6	12.5
37	E11	7.1	16.2	14.5	20.7	E8	16.4
40	E11	5.4	16.2	2.3	8.8	E9	16.9
q=3.42cc/sec.		E4		E5		E10	
RPM=500		E4		E5		E10	
NCL=58x10 ⁻³ in.		E4		E5		E10	
20.6	E11	6.4	22.2	11	16.9	10	17.6
37	E11	7.1	22.2	10	17.6	q=3.42cc/sec.	
40	E11	5.4	22.2	8.5	19.2	RPM=500	
q=3.42cc/sec.		E4		E19		E11	
RPM=500		E4		E19		E11	
NCL=58x10 ⁻³ in.		E4		E19		E11	
20.6	E11	6.4	22.2	8.5	19.2	E11	

TABLE E-2 (continued)

$X \times 10^3$ Inch	$S \times 10^3$ Inch	$X \times 10^3$ Inch	$S \times 10^3$ Inch	$X \times 10^3$ Inch	$S \times 10^3$ Inch	$X \times 10^3$ Inch	$S \times 10^3$ Inch
7.2	13.6			E15			
14	15.4	17	21.9		<u>Position No. 10</u>	7	E19
	E12	27	16				8.4
2	5.6	$d=26.2 \times 10^{-3}$ in.		E11	Roll No. 214		$q=1.717$ cc/sec.
					$q=0.685$ cc/sec.		RPM=250
		3.3	16.3		RPM=100		E11
		7	20.6		$NCL=51.2 \times 10^{-3}$ in.	0	
	E17			E12	E1	14	8.9
5	17.9	2.4	9.3		E2	47	9.1
		11.3	24				5
	<u>Position No. 9</u>			E15	32	13.9	E13
		13	23.5		40.5	11	10.3
					E3	20	E14
							8.2
					E6	45	E15
							4.8
	E17	6	22.9		E4		$q=3.42$ cc/sec.
5	20.8			E8	10	7.3	RPM=500
14.4	27.4	2.1	10.6		48	3.29	E6
	E18	13.2	24.3				
16.2	27.7	$NCL=34 \times 10^{-3}$ in.					9.4
	E20			E6	$q=1.717$ cc/sec.	7	9
					RPM=250	23	7.6
14.3	26.3	8	15.4		E6		E7
	$NCL=34 \times 10^{-3}$ in.	26	16.2			16.1	8.7
	E17			E8	E7	15	E8
4.8	13.1	2	7.7			47	E9
19	19.3	17.2	19.6			52	E10
24.8	15.3				E10		3.9
	E18	$q=6.82$ cc/sec.				43	E10
19.4	20.1	RPM=1000					4.8
22	18.2	E1					
	E19	6.5	16.2		<u>Position No. 11</u>		$q=6.82$ cc/sec.
10.9	19	8.2	17.2				RPM=1000
				E3	Roll No. 215		E1
		6.1	15.2		$q=0.685$	0	9.3
		12.8	16		RPM=100	10	8.5
	E11	29.2	10.2		$NCL=68 \times 10^{-3}$ in.		E2
5	12.8			E5	E16	25	6.6
8.6	15.8	18.2	18.7			7	E4
	E12	$d=26.2 \times 10^{-3}$ in.			E17	24	6.8
3	8.8			E3			E5
14.6	20.4	5.8	22.2		E18	38	6.4
	E13			E5			
3.2	7.3	16.4	29.8		6	8.8	
					38	6.2	<u>Position No. 12</u>

TABLE E-2 (continued)

$X \times 10^3$ Inch	$S \times 10^3$ Inch	$X \times 10^3$ Inch	$S \times 10^3$ Inch	$X \times 10^3$ Inch	$S \times 10^3$ Inch	$X \times 10^3$ Inch	$S \times 10^3$ Inch
43	17.2	Roll No. 160	18	19.1	17.5	17.8	17.5
		E1	7	17.1	16	21	16
Position No. 13		7.2	12.1	11	23	E7	12.5
		20.8	7	27	5.36	4	8
Roll No. 140		E2	10.6	E4	22	E8	17
$q=0.685\text{cc/sec.}$		4.4	14.1	7.3	16.3		
RPM=100		10	14.3	22.5	17.1	2	5.4
$d=25 \times 10^{-3}$ in.		14.6				23.5	14.8
E14				6.2	12.2	27	10.4
20.8	11.4	$q=3.42\text{cc/sec.}$		12.5	17.3	$q=6.82\text{cc/sec.}$	
Roll No. 158		RPM=500		21.3	16.5	RPM=1000	
E1		Roll No. 159		18	20.3	E11	
12.3	14.7	E1	5.9	23.4	17.1	18	21.4
15.4	14.7	4.1	7.6			27	4.5
		5.2					
5.6	11.8	E2		$q=1.717\text{cc/sec.}$		4	8.8
8.5	13.6	13	14.7	RPM=250			
		E5		E11		18.2	13.4
14.4	13.8	5.6	8			8.8	12.3
		7.1	8	E12			
4.5	10	E6		18	20.3		
11.2	14.1	4.4	6.8	E12			
		21	9.6				
8.8	10.7			6.3	12.3	Position No. 15	
20.5	9.17	$q=6.82\text{cc/sec.}$		17	17.4	Roll No. 165	
		RPM=1000		5	8.7	$q=0.685\text{cc/sec.}$	
17.5	12.8	E11		E14		RPM=100	
		16.8	14.4	E15	9.4	$d=24 \times 10^{-3}$ in.	
22	8.23	E14		E16		E1	
		2.5	3.9			10	21.3
12	12.9	15.4	16	12.5	17.4	E3	
24.4	1.76	E16		21.8	15.4		
		6.4	10.6	E18		11.5	22.2
6	10	E17		25	11.9	13.5	22.2
8.5	12.5	7	11.1	$q=3.42\text{cc/sec.}$		E5	
				RPM=500		17	22.4
$q=1.717\text{cc/sec.}$		Position No. 14		Roll No. 162		E6	
RPM=250				E3		18	16
E15		Roll No. 161	4.2			20.5	14.7
19	10.8	$q=0.685\text{cc/sec.}$	13	10.4		E8	
		RPM=100	17	20.5	20.9		11.6
1.1	3.4	$NCL=30 \times 10^{-3}$ in.	26.3	20.3	5		11.2
		E2		10.7		E9	
7.3	8.9	11.3	18.6	7		6.8	16.9
						$NCL=35 \times 10^{-3}$ in.	

TABLE E-2 (continued)

$X \times 10^3$ Inch		$S \times 10^3$ Inch	$X \times 10^3$ Inch	$S \times 10^3$ Inch	$X \times 10^3$ Inch		$S \times 10^3$ Inch	$X \times 10^3$ Inch	$S \times 10^3$ Inch	
9.5	E1	13.7	10	14.3	E1	6.6	Roll No. 147			
18	E3	14.7	$q=6.82\text{cc/sec.}$		11.6	7.2	E1	14	16	
6		10.1	RPM=1000		32.6		E2			
24.5	E7	11.8	E7	9.8	22.5	6.7	10	E4	19.7	
3.9	E8	8.4	5.5	E8	22.4	7.8	11	E7	18.5	
9.5	E9	13.1	8	12.5	25	7.8	6	E8	13	
			E10	44	44	3.12	$NCL=52 \times 10^{-3}\text{in.}$			
			23	13.4	40.3	4.2	21	E1	7.6	
			$d=24 \times 10^{-3}\text{in.}$		40.3	6.96	23.6	E5	6	
			5.5	11.6	24.5	4.8	37		6.8	
	E11				40.3					
21		12.2	<u>Position No. 16</u>			E9	5.4	18	E7	7.5
23	E12	13.5	Roll No. 146		38			E8		
8.5	E17	13.5	$q=0.685\text{cc/sec.}$			13.2			5.6	
19		16	RPM=100		$q=1.717\text{cc/sec.}$	19.5			7.1	
			$d=22 \times 10^{-3}\text{in.}$		RPM=250					
11	E20	13.5	E1	5	5	2.1	$q=6.82\text{cc/sec.}$			
			E2	12.6	28	8.8	RPM=1000			
							Roll No. 167			
	E12		13	18.6	3	3.2	E13			
16		19	E3	22.5	22.5	8.4	13		7.2	
18	E18	16.9	6.3	12.7	44	1.9	35		6.4	
			13	18.6	20.3	7.7	30.5	E18	8.3	
			E8	19.6	29	7.7	$d=22 \times 10^{-3}\text{in.}$			
			12	11	$d=22 \times 10^{-3}\text{in.}$			E13		
			18.5							
			E10				8.3		14.5	
	E12		2.5	8.16	21.6	2.8	17.4		17.3	
8		16.1	Roll No. 166			E12		E14		
	E16		E11	13.4		18.2	13.5		21.3	
7.2		18.7	2.2	7.34						
			E20	19.5		14.4	<u>Position No. 17</u>			
	E11		13	22.2	20	14.4				
13.5		17.2	$NCL=52 \times 10^{-3}\text{in.}$			E14		Roll No. 149		
	E12		E11	1.7		4.2	$q=0.685\text{cc/sec.}$			
7.5		12.2	4	3.14	12.9	18	RPM=100			
	E15		E15				$d=19.5 \times 10^{-3}\text{in.}$			
6.2		10.7	18.5	8	$q=3.42\text{cc/sec.}$		E12			
	E16		Roll No. 146		RPM=500		12		14.4	

TABLE E-2 (continued)

$X \times 10^3$ Inch	$S \times 10^3$ Inch	$X \times 10^3$ Inch	$S \times 10^3$ Inch	$X \times 10^3$ Inch	$S \times 10^3$ Inch	$X \times 10^3$ Inch	$S \times 10^3$ Inch
13.5	13.9			E7	14		
17	12.9	6	6.3			E15	6.5
		7.8	7.1	29			$q=6.82\text{cc/sec.}$ $\text{RPM}=1000$
8.5	16.1			E10		E17	E1
		12.5	8.1	8			30
9	15.7	24	6.7	21			19
13	15.2	31.5	4.06			E19	17.3
		Roll No. 149		3			Roll No. 168
17	13.5			E12	$d=19.5 \times 10^{-3}\text{in.}$		E1
		20	11.8			E17	19.5
16	14			E14	4		E2
		17.4	10.1	Roll No. 149			2.4
13	15.7	25	9			E3	13.5
15	12.1			E15	6.5		E4
16.4	12.4	29.5	7.1	17			19.4
Roll No. 169				E16		E6	E9
		8.5	6.7	18			10
11.6	16.6			E17			$\text{NCL}=40 \times 10^{-3}\text{in.}$
		27	7.3				E1-E9
3.9	11.4			E18	$q=3.42\text{cc/sec.}$ $\text{RPM}=500$		21
$\text{NCL}=40 \times 10^{-3}\text{in.}$		22	10.1		Roll No. 168		23.6
					$\text{NCL}=40 \times 10^{-3}\text{in.}$		3.8
6.5	4.06	$q=1.717\text{cc/sec.}$ $\text{RPM}=250$		E1		E11	18.5
17	8.5						7.5
		20.4	10.3	30.3		E12	32
12.8	6.1	23.5	8.8			E13	6
24	8.1			E3	22.5		11.2
		12	8.5			E15	21.4
8.4	4.67	29	7.5	12.8			6
20.7	7.1					E16	10.7
26.7	6.9			E6			14.3
	5.7	29	7.6	12.8		E17	20.5
	3.04	Roll No. 169					11.6
				E12	12.4		13.5
16.5	8.1	22.8	7.1	16			21.4
26	7.3			E14		E20	10
		10.3	7.3	23			11.4
17.5	9.1	32.8	2.7	$\text{NCL}=35.2 \times 10^{-3}\text{in.}$			
		$\text{NCL}=40 \times 10^{-3}\text{in.}$		E13			Position No. 18
15.5	8.1			E12	19.5		
27	6.3	26.5	6.9	Roll No. 148			Roll No. 170
$\text{NCL}=35.2 \times 10^{-3}\text{in.}$				E13		E14	$q=0.685\text{cc/sec.}$
		31	5.3	18.5			$\text{RPM}=100$
20.5	8.7			E14	27		$d=26.6 \times 10^{-3}\text{in.}$

TABLE E-2 (continued)

$X \times 10^3$ Inch	$S \times 10^3$ Inch	$X \times 10^3$ Inch	$S \times 10^3$ Inch	$X \times 10^3$ Inch	$S \times 10^3$ Inch	$X \times 10^3$ Inch	$S \times 10^3$ Inch
4.3	E11	15.2	q=1.717cc/sec.	23	12.9	5.3	12.3
20.8		17.2	RPM=250				
10	E12	22.5	E14	14.5	Position No. 19	8.3	E12
13		21.2	E18	20.8	Roll No. 173	16.5	17.5
13.5	E13	25.1	16.5	20.8	q=0.685cc/sec.	5	E14
17.7		24.3	Roll No. 170		RPM=100	11	11.9
7	E14	22.1	E1	17.1	d=20.5x10 ⁻³ in.	NCL=27x10 ⁻³ in.	E12
9.8		17.2	E2	15.2	E1	16.7	13.8
16.2	E15	22.3	E3	3	E5	10.5	E14
8.8		17.8	12	17.3	E7	12.7	13.6
18.8		23.3	20	16.8	9.5	19.8	NCL=50x10 ⁻³ in.
22.4	E17	13	21.2	17	13.4	19.8	E12
15.7	E19	22.5	E4	17.3	17.3	10.5	18
5.3	E20	15	15	21.5	E9	7.3	E14
8.7		19.2	13.5	19.5	2.1	19.8	5.2
Roll No. 150		1.3	q=3.42cc/sec.	10	E10	11.6	6.8
2.5	E2	6.3	RPM=500	16.5	E10	22.4	6.8
14		12.6	Roll No. 171	NCL=27x10 ⁻³ in.	15.9	11.6	5.2
17.5		17	E1	E9	15.9	22.4	6.8
19		24.8	4.8	12.2	NCL=50x10 ⁻³ in.	23.5	8.1
6.1	E4	23.9	17.1	15.9	8.8	37	6.2
12		22.1	17	22.5	8.8	E5	8.5
16		20.4	E4	q=1.717cc/sec.		d=20.5x10 ⁻³ in.	8.5
25	E7	20.3	E5	RPM=250		E1	18.4
20		19.4	20.3	d=20.5x10 ⁻³ in.		E5	18.4
25.2	E8	8.3	q=6.82cc/sec.	E11	16.2	9	14.7
5		16.8	RPM=1000	E12	16.7	14.3	14.1
22.5		3.03	E12	9.5	15.1	10.3	E6
11	E10	10.3	18	18	15.1	12.6	17.3
17.5		14	13.9	17	12.5		16.8
		9	E13	E14	17.6	Position No. 20	
		16.6	16	16	17.6	Roll No. 154	
		25.8	E15	q=3.42cc/sec.		q=0.685cc/sec.	
		13.6	E16	RPM=500		RPM=100	
		16.2	15.5	Roll No. 172		d=21.4x10 ⁻³ in.	
		27.9		E11		E2	
						9.3	17

TABLE E-2 (continued)

$X \times 10^3$ Inch	$S \times 10^3$ Inch	$X \times 10^3$ Inch	$S \times 10^3$ Inch	$X \times 10^3$ Inch	$S \times 10^3$ Inch	$X \times 10^3$ Inch	$S \times 10^3$ Inch
8.5	18.4	25.6	8.35	11.3	5.8	53	9.4
6.8	17	42.6	4.2	45	3.2	54.2	9.1
16	10.8	q=1.717cc/sec. RPM=250		q=6.82cc/sec. RPM=1000		56.3	9.4
7	14.8	E1-E10		E11		57.5	9.4
Roll No. 174	17.5	7.6	30	9.8	75.4	8.8	
E11	24.7	8.1	E12	85	7.6		
12	18	8.4	23	8.5	94.2	7.15	
E12	21	7.8	E13	27.3	E5		
1.1	2.92	17.7	6.8	14.1	10.6	58	9.4
6.6	15.9	2.5	1.67	E15	63.2	9.4	
17.3	14.6	14	6.7	44.6	1.2	66.6	9.1
E14	35	8	E16	69.2	8.8		
19	10.4	10.4	5.4	9	7.2	100	6.6
E15	41	4.4	27.4	9.8	105	6.2	
6.8	16.7	19.8	6	40	4.2	109.5	5.3
9.8	17.7	NCL=38.6x10 ⁻³ in. d=21.4x10 ⁻³ in.		E12		33	E6
14	16.7	12.4	9.9	5.6	19.6	36	8.3
E16	25	9.4	9.4	19.6	56	9.4	
11.3	19.4	E6	9.2	Position No. 21	90	7.4	
11.5	17.7	25	9.2	Roll No. 17	6	E7	
NCL=38.6x10 ⁻³ in. d=21.4x10 ⁻³ in.	E11	E1	17.4	q=0.685cc/sec.	15	3.5	
20.3	11.7	7	15.9	RPM=100	40	5.9	
E14	14	E2	15.9	d=129x10 ⁻³ in.	61.3	8.8	
32.4	6.3	3.2	11.5	E1	76.6	8.8	
E16	9.6	6	15.4	37	8.8	8.7	
20	9.6	6	15.4	42	9.1	94	7.15
NCL=49.2x10 ⁻³ in.	E11-E20	E3	35	85	7.6	98	6.8
29.3	8.35	8.4	18.4	89	7.6	123	3.16
38.2	6.9	q=3.42cc/sec.	30.8	E2	7.3	17.5	E9
5.1	3.34	RPM=500	98.3	7.6	9	87.3	6.3
6.6	3.76	Roll No. 175	69.5	9	9	96.5	7.5
42.4	4.6	E2	89	8.4	8.4	96.5	7
18.4	7.7	4	18.7	8.1	8.1	9.3	E10
33	3.8	NCL=49.2x10 ⁻³ in.	121	4.1	4.1	24.4	5.4
17.1	7.5	E5	37.3	E3	64	8.2	
30	7.7	12.5	6.8	37.3	67.5	9	
30	8.6	35	8.5	55.8	9	67.5	9.3
30.6	8.35	E7	110.8	E4	90	90	7.6
15	7.3	6.4	4.8	31	5.5	95.2	7.15
					3.2	98.6	6.9
						Roll No. 176	

TABLE E-2 (continued)

Xx10 ³ Inch	Sx10 ³ Inch	Xx10 ³ Inch	Sx10 ³ Inch	Xx10 ³ Inch	Sx10 ³ Inch	Xx10 ³ Inch	Sx10 ³ Inch
29.8	E16 7.5	8	E11 6	37.2	18.1	E16 30.2	10.6
32.3	7.7	10.8	6	49	19		
116	4.7	37	9.5	68	19.2		
	E17	64.3	9.5	q=1.717cc/sec. RPM=250		Position No. 23	
9.3	4.3	68.3	10.1			Roll No. 204	
27.8	6.4	90.5	9.4	E14		q=0.685cc/sec. RPM=100	
86	7.1	100	6.9	35.3	18.1	NCL=53x10 ⁻³ in.	
	E18		E12	71	17.3	E11	
45			9.1	E15			
83.6			8.7	43.3	17.9	32.5	27.6
91				74	17	42.7	18.5
			cc/sec.	98	16.2	E12	
52				E17		34.2	27.7
75.6				47.5	19.1	50	6.3
82.3			9.8	E18			
			9.7	37	18.7	7.2	15.9
60.8			8.3			51.7	5.2
66		89	8.7	q=3.42cc/sec. RPM=500			
92.4	7.5	90.2	8.9	Roll No. 178		q=1.717cc/sec. RPM=250	
112	5.35	100	7.9	E1		E16	
			E2	46	17.9	9.4	18
q=1.717cc/sec. RPM=250 Roll No. 157		61.8	9	65.5	17.9	48	11.8
		83.7	9	94.5	19.9		
		92.3	8.5	E2		11.4	22.2
69	8.9	Position No. 22		37	14.6	E18	
70	8.9			41	15.3	1.5	2.2
78.5	8.3	Roll No. 179		E3		19.5	23.6
113.2	5.6	q=0.685cc/sec. RPM=100		12.5	10.3	24	22.9
121.8	3.8	NCL=100.5x10 ⁻³ in.		28	14.3	32.5	25.4
	E12		E1	52.3	16.2	44.3	17.7
37.5	8.5			72	14.9		
43.5	9.1	5.8	6.6			q=3.42cc/sec. RPM=500	
50	9.4	79.4	19	q=6.82cc/sec. RPM=1000		Roll No. 181	
52.3	9.8		E2			E2	
69.4	9.1	23.6	14.3	E11			
74	8.8	47	21.3	32.5	13.8	13.6	14.5
87	8	64.5	18.1	80.6	16.4	E5	
91.5	7.8	31.8	17.5	E12		44	11.4
			E3	36	13.4	E8	
q=3.42cc/sec. RPM=500 Roll 156		28	16.6	69	12.4	37.8	19.4
		19	E4	20	12.9	q=6.82cc/sec.	

TABLE E-2 (continued)

$X \times 10^3$ Inch	$S \times 10^3$ Inch	$X \times 10^3$ Inch	$S \times 10^3$ Inch	$X \times 10^3$ Inch	$S \times 10^3$ Inch	$X \times 10^3$ Inch	$S \times 10^3$ Inch
RPM=1000		E20		19	9	24.8	6.5
E15		10	20.9	35	9		E3
35.4	22			45	9	2.5	
Position No. 24		q=3.42cc/sec.		E9		18.3	
Roll No. 183		RPM=500		10	5.4	22.8	
q=0.685cc/sec.		Roll No. 182		15	7.9	NCL=66x10 ⁻³ in.	
RPM=100		E17		17.7	7.9		E1
d=22x10 ⁻³ in.		12	21.2	25.5	9	27.2	9.9
E1		Roll No. 203		28.5	9	42	9.1
8.1	19.8	NCL=59x10 ⁻³ in.					E4
14	24.1	E15		q=1.717cc/sec.		31.2	10.1
10.8	17.3		6.8	RPM=250		51	6.5
16	15.8	Position No. 25		E11			E5
9	16.9	19.5			10.1	15	7.6
15.3	16.2	31.3			10.1		
E9		Roll No. 185					
14	19.8	q=0.685cc/sec.		23.5	E12	9.4	q=6.82cc/sec.
NCL=59x10 ⁻³ in.		RPM=100			E13		RPM=1000
E1		d=26.4x10 ⁻³ in.		43		7.8	E11
26.5	7.2	E1		55		5	6
34.4	7.2	14.4		29		9.4	E12
		23.8		d=26.4x10 ⁻³ in.			31
		E2		E11			16
		10.5				20.2	E14
		21.8		8		20.2	E16
		16.9		13.7		23.8	19
		E3		E12			8.7
		11					E19
		16.3		10		19	30.8
		E4		11.3		20.9	36
		2.7		13.5		21.6	d=26.4x10 ⁻³ in.
		22		E13			E14
		E5		12		22.2	7.2
		12.2		14.3		23.6	9
		E6		17.4		25	11.5
		8.3		22		15.8	17.4
		21					E15
		NCL=66x10 ⁻³ in.		19.8			4.1
		E3		19.4			6.8
		9		q=3.42cc/sec.			22.5
		9		RPM=500			9.5
		10.9		Roll No. 186			17.5
		12.2		E1			20.2
		18					E17
		E6		18.4			15
		39		21.2			12.5
		8.6		25			24.8
		10.7		E2			E19
							18.4
				18.4			4.8
				14			21.6

TABLE E-2 (continued)

Xx10 ³ Inch	Sx10 ³ Inch	Xx10 ³ Inch	Sx10 ³ Inch	Xx10 ³ Inch	Sx10 ³ Inch	Xx10 ³ Inch	Sx10 ³ Inch
17.3	18.4	Roll No. 187				8.4	17.3
		E11		Roll No. 189		11.4	17.7
Position No. 26		17	5.4	q=0.685cc/sec.		E2	
		E13		RPM=100		17	14.4
Roll No. 188		2.4	9.1	d=22.3x10 ⁻³ in.		E3	
q=0.685cc/sec.		E16		E13		8.5	17.6
RPM=100		10	21.5	19.5	12.6	E5	
d=20x10 ⁻³ in.		E18		E14		4	15.3
E1		8	18.2	14	17.3	E6	
2	8.6	15	17	E16		9.1	17.1
13	18	NCL=46.4x10 ⁻³ in.	18.8	13		E7	
E2		E11		E17		21.2	5.3
10.2	18	42	2.6	8.3	16.9	E8	
E7		E13		E20		12.5	19.2
4.3	11.5	4.6	3.7	9.6	18.7		
E9		E14		NCL=44.6x10 ⁻³ in.		q=3.42cc/sec.	
13.8	17.3	27.8	8.3	E16		RPM=500	
NCL=46.4x10 ⁻³ in.		40	5.5	22	10.1	Roll No. 190	
29.5	7.2	E15		38	5.4	E5	
30.8	7.2	10	5.4	E17		9.9	17.6
32.7	7.2	24	8.3	14.6	8.3	18	13.4
				E20		E6	
q=1.717cc/sec.		q=6.82cc/sec.		19	9	5.4	17.6
RPM=250		RPM=1000				18.4	13.4
E11		E1		q=1.717cc/sec.		E8	
23	7.2	10.5	5.2	RPM=250		14	18.2
E14		E2		E1		E9	
19.3	7.6	16.4	7.4	11.8	7.2	9.5	18
E15		E3		17	9.4	NCL=44.6x10 ⁻³ in.	
23.5	7.2	27	7.4	22.6	10.1	E2	
E16		E4		E2		23.5	9.6
7	6.9	19.8	7.4	35	6.9	E3	
E17		d=20x10 ⁻³ in.		E3		15.2	7.7
20	6.6	E1		21	8.6	23.2	7.7
E18		4.6	14.4	E5		E5	
	8.5	E2		8.8	6.5	7.8	6.4
d=20x10 ⁻³ in.		7.8	13.7	E6		18.9	7.7
E14		E4		19.5	8.2	35.5	5.2
10	18.1	5.3	12.2	E7		38.5	4.5
E18		9	14.3	28.4	9.1	E6	
11.1	18.1	E10		E8		10.5	8
		11.5	19.7	24.5	8.8	21.8	9.3
q=3.42cc/sec.				d=22.3x10 ⁻³ in.		33	8.3
RPM=500		Position No. 27		E1		37	6.8

TABLE E-2 (continued)

$X \times 10^3$ Inch		$S \times 10^3$ Inch	$X \times 10^3$ Inch	$S \times 10^3$ Inch	$X \times 10^3$ Inch	$S \times 10^3$ Inch	$X \times 10^3$ Inch	$S \times 10^3$ Inch
34.2	E7	6.8	16	15.8	18	6.3	9.4	E16 21.8
20.4	E8	9.5	Position No. 28		q=3.42cc/sec. RPM=500		1.5	6.5
23.5		8.9	Roll No. 192		Roll No. 191		13	E20 21.8
30.6		8.6	q=0.685cc/sec. RPM=100		E12		5.7	
19	E9	9.5	d=20.1x10 ⁻³ in.		8.5		18.3	RPM=250
			E1	8.8		E13	19.7	E3 21
			6.4	16.5	13.6	18.5	16.1	16.8
	E11		14.8	15.4	18.3	6.8	19.5	E4 14.5
22.6		10.1	E2	17.2	13.2	E14	20.6	E9 23.8
8.1	E12	7.6	E3	18.3	13	E15	10.5	
	E13		9.8	19.1		19.5		
23		8.5	12					q=3.42cc/sec. RPM=500
35.2		6.1	E5		q=6.82cc/sec. RPM=1000		Roll No. 202	
	E14		10.4	18.3		E2		E1 21.4
14		9.3	E7	18	11	E3	22.6	17.3 23.6
34		6.8	10.4	14.7				E5 11.3
34.8	E15	7.7	5	14.3	11		22.3	
	E16		NCL=35x10 ⁻³ in.	14	14		16.7	22.8
30.6		7.7	E8			E4		
40		4.2	14	8.4	15.7		13.4	q=6.82cc/sec. RPM=1000
24.3		8.6	E9			E5	21.2	E20 14.4
	E17		11.2	7.7	14.3		21.2	13.4
12.5		8.8				E6	17.2	Roll No. 194
21.5		9.8	q=1.717cc/sec. RPM=250		16			E5 17.3
24.5		9				E7		
35		9.8	E14	5.2	12.8		4.1	
40		4.2	25.4	8.2	10.8		19.7	
	E18		d=20.1x10 ⁻³ in.		Position No. 29		Position No. 30	
4		3.3	E11		Position No. 29		Roll No. 196	
14.5		9.5	12	17	Roll No. 193		q=0.685cc/sec. RPM=100	
32.5		9.5	E12		q=0.685cc/sec. RPM=100		d=21.5x10 ⁻³ in.	
	E19		2	6.5	d=26.6x10 ⁻³ in.		E1 14	
4.2		3.9	4	12.2	E14		18.5	
15.3	E20		10.8	17.6			E3 25.9	
		8.6	14	16.6	15.2		12	
d=22.3x10 ⁻³ in.			17	10.3	20.3		E4	
	E12		E13		E15			
6.5		22.3	11	16.9	22.5	14.5		

TABLE E-2 (continued)

Xx10 ³ Inch	Sx10 ³ Inch	Xx10 ³ Inch	Sx10 ³ Inch	Xx10 ³ Inch	Sx10 ³ Inch	Xx10 ³ Inch	Sx10 ³ Inch
6	19.8	3	13.7				
E5		16.3	19.4	15	E14	15.1	E20
4.5	16.2	E4	23.3			35.2	7.1
8.2	19.1	10.4	24.9	E15	14.4	27.4	16.1
17.4	18	NCL=44.2x10 ⁻³ in.		14.5	E16	18.3	q=6.82cc/sec.
NCL=44.2x10 ⁻³ in.		E2					RPM=1000
E1		17.4	10.9	19		19.8	E1
37.8	6.5	22.6	12	E17		12.5	13.5
E3						22.7	12.9
23	12.6	7.3	6.8	19.5		19.4	13.5
E4		34	9.5	32		14.4	E2
13.3	10.1			E18		7.5	11.8
E5		18	11.8	12		12.5	15.2
10.3	10.1	E5		36		8.3	14.7
34.3	9	10	7				E4
E6						7	10.9
35	7.2	q=6.82cc/sec.		q=1.717cc/sec.		7	16.1
		RPM=1000		RPM=250		20.5	
		E11	11	E5			
q=1.717cc/sec.		8.5	6			19.4	Position No. 32
RPM=250		17.5	10.2	E6		18.7	Roll No. 199
Roll No. 197		E17	11.1	E7		9.4	q=0.685cc/sec.
E2		19.2	34.5	E8			RPM=100
10	7.5	E18	10.9			19.4	NCL=70x10 ⁻³ in.
16.4	10.1		22	E10			E1
E4		32	10.9			8	7.7
21.2	10.4	d=21.5x10 ⁻³ in.				6.8	7.7
d=21.5x10 ⁻³ in.		E12	3			18	E2
E2		5.4	12.4	16.5		15.1	7.7
4.5	15.8	8	17.2	28.5			7.3
8	21.6	E18	19.7			20	7.3
E3		14.5	14.2	q=3.42cc/sec.		27	7.7
6.3	16.6	E20		RPM=500		34	
14.3	22.6	5.4	14.2	Roll No. 201			E3
E4				E13		6	7
10.5	21.6	Position No. 31				34	7.3
			38	E14		6.7	E4
q=3.42cc/sec.		Roll No. 197	30			15.2	6.6
RPM=500		q=0.685cc/sec.		E15		30	7.3
Roll No. 195		RPM=100	17			40	E5
E1		NCL=40x10 ⁻³ in.	32.5			17.7	7.3
2	11.5	E13		E17		10.1	7.3
E2		12	17.6			0	7.3
9	23.6	24.3	18	7.8		11.8	7.3
E3		29	18	26.2		14.5	7.7
				E18		26	7.3

TABLE E-2 (continued)

$X \times 10^3$ Inch	$S \times 10^3$ Inch	$X \times 10^3$ Inch	$S \times 10^3$ Inch
40	6.6	q=6.82cc/sec.	
45	6.6	RPM=1000	
52	5.1	E11	
		11	7.5
q=1.717cc/sec.		21	7.5
RPM=250		50	4.8
E11		58	4.8
2	7.5	62	3.3
5	7.5	E12	
16	7.5	49	5.5
22	7.5	55	5.1
26	7.5	E13	
53	6.6	10	7
57	5.9	19	7
E12		37	6.4
0	7.3	39	6.4
4	7.3	55	5.4
13	7.3	59	4.2
25	7.3	E14	
27	7.3	5	7.5
35	7.3	9	7.5
56	5.9	23	7.5
		58	5.7
q=3.42cc/sec.			
RPM=500			
Roll No. 200			
E1			
5	8.1		
10	8.1		
15	8.1		
28	8.1		
53.5	5.2		
64	3		
E2			
22	6.9		
27	6.9		
41	6.7		
57	4.9		
E3			
21	7		
39	7		
57	4.7		
60	4.2		